Dynamical Influence on the Stratospheric Ozone and Water Vapor

Vom Fachbereich für Physik und Elektrotechnik
der Universität Bremen

Zur Erlangung des akademischen Grades eines

Doktor der Naturwissenschaften (Dr. rer. nat.)

genehmigte Dissertation

von

Sandip Dhomse

Eingerich am:	31 October 2006
Tag des Promotionskolloquiums:	07 November 2006
Gutachter:	Prof. Dr. J. P. Burrows Prof. Dr. J. Notholt
Prüfer:	Prof. Dr. Rhein Prof. Dr. Bornholdt

Contents

Abstract

Influence of the some of the the most important processes contributing ozone variability (stratospheric aerosol loading, Brewer-Dobson circulation, QBO, solar variability, changes in stratospheric chlorine loading) is studied using updated meteorological and total ozone data sets. Accumulated winter eddy heat flux has been proposed as a new proxy for the attribution of dynamical influence on ozone change. A compact relationship between winter ozone gain and eddy heat flux has been demonstrated. It is shown that eddy heat flux not only controls high-latitude winter ozone gain but also chemical ozone loss due to heterogeneous chemistry. Influence of 11-year solar cycle on the stratospheric temperatures is confirmed using long term meteorological data (1958-2005) from NCEP and ECMWF. It has been observed that polar stratospheric temperatures and solar flux show strong coupling during westerly phase of QBO. Regression analysis (1979-2005) shows that mid-winter polar stratospheric temperatures are generally higher during solar maxima but lower during early winter months. The opposite is true during solar maxima. A new multivariate regression model has been used to study long term ozone trends as well changes in ozone trends due to changes in stratospheric halogen loading. Using WFDOAS GOME [1995-2003], SBUV V8 (1979-2003) and TOMS/SBUV merged (1979-2005) total ozone data sets, detailed analysis has been carried out. Largest negative ozone trends are observed at high latitudes during winter season (SH: -12 DU/decade, NH: -8 DU/decade) beyond 50° latitudes. In tropical latitudes ozone trends are quite small. Solar variability contributes up to 6-8 DU ozone change whereas QBO explains most of the ozone variability in tropical latitudes. It is also shown that the increase in planetary wave driving and solar cycle maxima contributed significantly to the observed increase in NH mid-high latitude total ozone since the late 90s. Replacing linear trend term with EESC, regression model shows that changes in ozone trends due to decline in halogen loading are up to 4 DU/decade in NH and 8 DU/decade in SH.

Influence of planetary wave driving on tropical lower stratospheric water vapor has been studied using SAGE V6.2 (1984–2005) and HALOE V19 (1991–2005) water vapor data. A compact relationship between global eddy heat flux (averaged from both hemisphere) at 50 hPa and tropical lower stratospheric water vapor (averaged between 16–20 km) have been demonstrated. Some years, such as 1991, 1997 show departure from the observed relationship indicating that water vapor variability in the tropical lower stratosphere can not be solely attributed to the strength of Brewer-Dobson circulation. It is also shown that decrease in stratospheric water vapor since 2000, is related to increase in planetary wave driving from both hemisphere. Regression analysis shows that such a increase in wave driving contributed up to 0.7 K cooling in the tropical lower stratosphere.

Publications

The work described in this thesis has been published in various journals as summarized below:

Journal Articles

1. This study was carried out as a part of EU project CANDIDOZ (Chemical and Dynamical Influences on Decadal Ozone Change). Some of the important results from this project are summerized in the following publication.
   N.R.P. Harris, E. Kyrö, J. Staehelin, D. Brunner, S-B. Andersen, S. Godin-Beekmann, S. Dhomse, P. Hadjinicolaou, G. Hansen, I. Isaksen, A. Jrrar, A. Karpetchko, R. Kivi, B. Knudsen, P. Krizan, J. Lastovicka, J. Maeder, Y. Orsolini, J.A. Pyle, M. Rex, K. Vanicek, M. Weber, I. Wohltmann, P. Zanis, and C. Zerefos (2007), **Ozone trends at northern mid- and high latitudes**, submitted to Annales Geophysicae

2. A compact relationship between planetary wave activity on stratospheric water vapor is demonstrated in the following article. This article also provides an explanation for the observed decrease in stratospheric water vapor since 2001. This is the content of Chapter 6.
   Dhomse, S., M. Weber, and J. P. Burrows (2006), **The relationship between tropospheric wave forcing and tropical lower stratospheric water vapor**, Atmos. Chem. Phys. Disc., 6, 9563-9581, 2006

3. Increase in NH mid-high latitude total ozone has been oversteered in recent years. Possible causes of increase in total zonal has been discussed in the following article and is part of Chapter 5
   S. Dhomse and M. Weber and J. Burrows and I. Wohltmann and M. Rex,(2006), **On the possible causes of recent increases in NH total ozone from a statistical analysis of satellite data from 1979 to 2003**, Atmos. Chem. Phys., 6, 1165-1180.

4. For long term trend analysis, a new proxy has been suggested in the following article. It is shown that winter eddy heat flux not only determines inter-annual ozone transport to high latitudes but also controls the chemical ozone loss due to heterogenous chemistry and these results are part of Chapter 3
   Weber, M., S. Dhomse, F. Wittrock, A. Richter, B.-M. Sinnhuber, and J. P. Burrows (2003), **Dynamical control of NH and SH winter/spring total ozone from GOME observations in 1995 -2002**, Geophys. Res. Lett., 30(11), 1583, doi:10.1029/2002GL016799.

Other Articles and Conference Proceedings

1. Weber M., S. Dhomse, F. Wittrock, A. Richter, B.-M. Sinnhuber, and J.P. Burrows (2003), **Einfluss der Dynamik auf den Ozontransport und die Ozonchemie in hohen Breiten**, Ozonbulletin des Deutschen Wetterdienstes Nr. 93, 25.

2. Sinnhuber Bjoern-Martin, Sandip Dhomse and Mark Weber (2004), **Inter-annual variability of polar stratospheric ozone loss derived from satellite observations in comparison with CTM calculations**, Quadrennial Ozone Symposium(QOS), Kos, Greece

1 Introduction

Ozone is an important greenhouse gas in the earth's atmosphere which supports life by absorbing harmful ultraviolet radiation. Ozone shows large spatial and temporal variability which is regulated by various atmospheric processes. This thesis is an attempt to understand the possible influence of some of key atmospheric processes on stratospheric ozone. This chapter provides an overview of general characteristics of the atmosphere. Vertical structure of the atmosphere is explained in Section 1.1. Zonal mean structure as well as inter-hemispheric differences (primarily stratospheric) in wind and temperature fields are discussed in Section 1.2. Important and relevant concepts such as ozone production, chemical ozone loss, and the ozone hole are briefly introduced in Section 1.3. Some of the important pathways and feedback mechanisms involved in ozone- climate interaction are assessed in Section 1.4. The objectives of this study are summarised at the end of this chapter.

1.1 Vertical structure of the atmosphere

The atmosphere is a thin layer of gases surrounding our planet that is held around the earth by gravitational attraction. Most of these gases are well mixed in the atmosphere, however the atmosphere itself varies significantly with altitude. The air pressure (p) is of the order of 1000 hPa near the surface (z_0) and decreases exponentially with height (z) as follow:

$$p(z) = p(z_0) \exp \frac{z - z_0}{H}, \tag{1.1}$$

where, the atmospheric scale height

$$H = \frac{RT}{g}, \tag{1.2}$$

is about 7 km in the stratosphere.

The atmosphere is generally divided into several vertical segments based on different criteria. Most common division is by the structure of the temperature gradient. The lowermost part of the atmosphere where temperature decreases with altitude is called the troposphere. The troposphere extends from the surface to the tropopause at an approximate altitude of 18 km in the tropics, 12 km at mid-latitudes, and 6-8 km near the poles. This layer contains about 90% of the atmospheric mass and is often dynamically active with rapid exchange of energy and mass being associated with convective overturning (hence the name "turning sphere") and an intensive water cycle. Above the

troposphere lies a stable layer called the stratosphere, where temperature increases with altitude. This layer extends up to 50 km (stratopause) and contains 90% of atmospheric ozone. In the stratosphere (from about 18-50 km), the temperature gradient is reversed, mainly due to the absorption of ultraviolet (UV) radiation by ozone (O_3) molecules. The negative temperature lapse rate suppresses vertical motion and creates a very stable dynamical environment, dominated by radiative processes (hence the name "layered sphere"). In the mesosphere (50-80 km) temperature again decreases with altitude as ozone heating diminishes. Further up, in the thermosphere, molecules are ionised by energetic solar radiation. This part of the atmosphere has a minor influence on processes lower down. Above an altitude of about 500 km lies the exosphere where air molecules collide so rarely that only the gravitational field prevents them from escaping our planet.

In some cases the atmosphere is also classified on the basis of general homogeneity of atmospheric composition. The heterosphere is characterised by variation in composition and mean molecular weight of the constituent gases. It lies roughly between 100 and 500 km where the air density is so low that transport is dominated by molecular diffusion, which creates a stratification of gases by molecular weight. In the homosphere, below about 100 km, the air is well-mixed. In some cases, the entire atmosphere above the troposphere is called the "upper atmosphere", the perspective which suggest that it is sufficient to distinguish between the part of the atmosphere that really matters for our daily weather (the troposphere) and "the rest". By now, the stratosphere and the mesosphere together are commonly referred to as "middle atmosphere", a term that reflects the recognition of the importance of this part of the atmosphere in our climate and weather. This thesis focuses mainly on the stratosphere and its coupling with the troposphere.

1.2 Zonal structure of the atmosphere

If the atmosphere would be plane-parallel, with a constant uniform influx of solar radiation, the description in the previous section would have explained much of its large scale structure. In reality, the earth is a tilted rotating sphere, that follows an annual motion around the Sun. Hence, the air motions are subjected to a Coriolis force, and the earth-atmosphere system experiences differential heating, changing with seasons. These asymmetries play a crucial role in the atmosphere's structure and dynamics. Climatological zonal mean temperature cross sections in the lower and middle atmosphere are shown in Figure 1.1. As very little solar radiation is absorbed in the troposphere, the thermal structure of the troposphere is maintained by an approximate balance between infrared radiative cooling, vertical transport of sensible and latent heat away from the surface by small scale eddies. The net result is a mean temperature structure in which maximum surface temperature is observed in equatorial region and decrease in surface temperature towards the winter as well as summer pole. Meridional heat transfer is mainly accomplished by synoptic disturbances generally in the zonal wind fields (see Figure 1.2). At low latitudes, where the Coriolis force is

weak, meridional overturning is accomplished by the Hadley circulation, with air rising near the equator and sinking at subtropical latitudes.

In addition, non-uniform solar heating responses in land-sea patterns are not only responsible for inter-hemispheric different climate systems but also drives zonal Walker circulations along the equator. El Niño /Southern Oscillation (ENSO) is an interesting example of the Walker circulation. An additional asymmetry is introduced by topography that generates several types of wave motions, from fast gravity waves to planetary scale Rossby waves.

In the stratosphere, infrared radiative cooling is on average balanced by radiative heating due to the absorption of solar ultraviolet radiation by ozone. The meridional temperature structure in the middle atmosphere is also quite different compared to the troposphere. In lower stratosphere the largest heating takes place over the summer pole and the largest cooling over the winter pole. At the equinoxes, the largest heating is over the equator while cooling at both poles. Ozone plays a crucial role in the radiation budget, creating a complex interplay between chemical composition and transport dynamics. The zonal mean temperature distribution is also affected by heat transport and adiabatic warming or cooling. A slow meridional circulation is driven by planetary and gravity waves from the extra-tropical troposphere. These waves propagate upward and break in the stratosphere and mesosphere, decelerating the wind flow and perturbing the geostrophic balance between the pressure gradient and Coriolis forces, thus causing a convergence and down-welling over the poles (accompanied by compression and adiabatic warming), and, by mass continuity, up-welling in the tropics (accompanied by expansion and adiabatic cooling) [*Haynes et al.*, 1991; *Rosenlof*, 1995].

Dobson [1930] and *Brewer* [1949] first proposed the resulting large-scale Brewer-Dobson (BD) circulation, which explains the observed distribution of stratospheric trace gases, including the dehydration of stratospheric air that enters through the cold tropical tropopause. This BD circulation also explains the fact that maximum ozone concentrations occur at high latitudes in the lower stratosphere in spring, though ozone is mainly produced in the tropical upper stratosphere (See Figure 1.3). Temperature gradient between tropics and mid-high latitudes creates a strong circumpolar jet, which isolates the air at the pole and leads to further cooling. The area inside this jet is generally referred as the polar vortex. It includes the downward branch of the BD circulation (see Figure 1.3). In fact, the planetary waves that drive the meridional overturning only reach the stratosphere during certain period in winter, when the stratospheric background winds are westerly but not too fast [*Charney and Drazin*, 1961]. The large-scale descent throughout the winter causes compression and adiabatic heating in the lower stratosphere, so that the air is warmer than it would be in radiative equilibrium. The vortex generally persists well into spring, when the returning sunlight warms the pole and reduces the latitudinal pressure gradient and thus the strength of the polar night jet. The break-up of the vortex and the transition to the summer wind regime are associated with the final

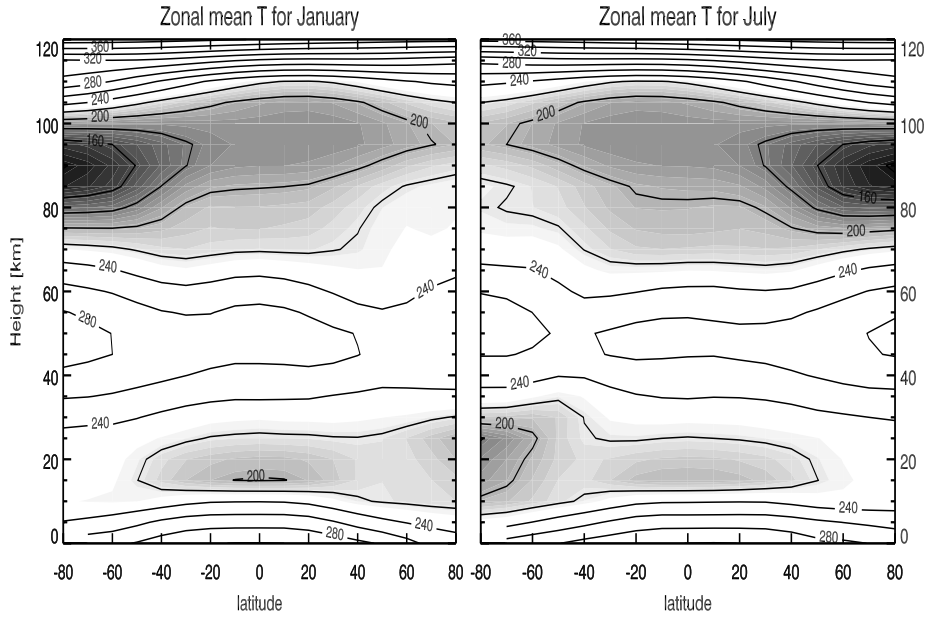

Figure 1.1: Climatological zonal temperature (in K) field for NH winter (January) and SH winter (July). Temperature and zonal wind climatology known as COSPAR International Reference Atmosphere (CIRA-86) is obtained from SPARC (Stratospheric Processes And their Role in Climate) web page http://www.sparc.sunysb.edu [*Fleming et al.*, 1988].

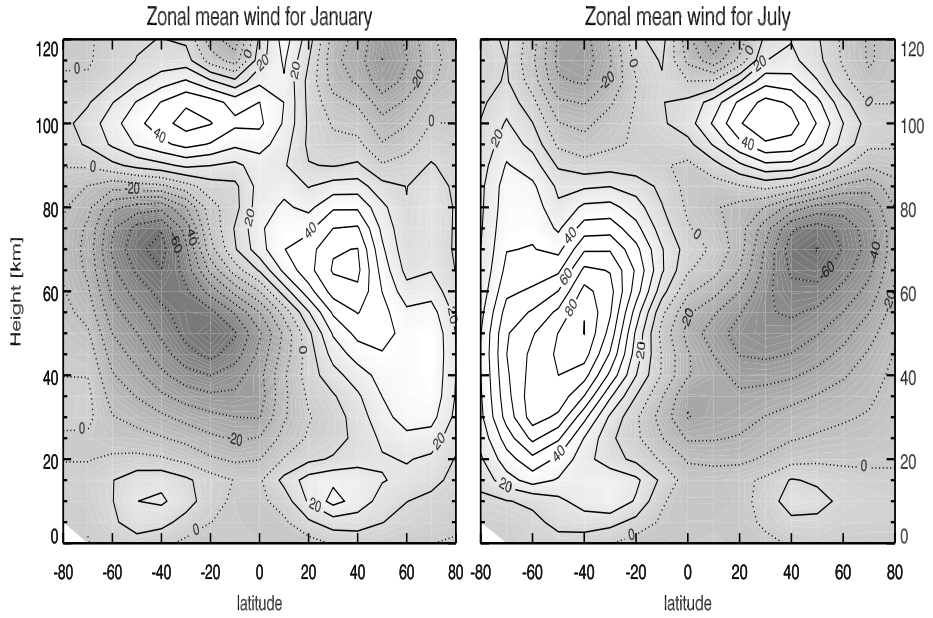

Figure 1.2: Same as Figure 1.1, but for zonal wind (in m/s) field.

major stratospheric warming. While planetary waves are the main driver of the stratospheric component of the large-scale wave driven circulation whereas the mesospheric component primarily relies on breaking gravity waves [*Holton et al.*, 1995].

1.3 Ozone chemistry

Ozone consists of three oxygen atoms bound together and can be protective or harmful to life on Earth depending on where it resides. In the stratosphere ozone acts as a shield to protect Earth's surface from the sun's harmful ultraviolet radiation. Without this shield, we would be more susceptible to skin cancer, cataracts, and impaired immune systems[*WHO*, 1995]. At ground level, ozone is a health hazard. It is a harmful pollutant that causes damage to lung tissue and plants. Most of ozone resides in the stratosphere (more than 90/the equator) and denser towards the poles (shown in Figure 1.4). The amount of ozone above a point on the earth's surface is measured in Dobson units (DU), typically $\sim$260 DU near the tropics and higher elsewhere, though there are large seasonal fluctuations. It is created when ultraviolet radiation (sunlight) strikes the stratosphere dissociating (or "splitting") oxygen molecules (O_2) to atomic oxygen (O). The atomic oxygen quickly combines with further oxygen molecules to form ozone.

Chapman mechanism

The original mechanism for atmospheric ozone formation and destruction from oxygen species was suggested by Chapman in 1930. The elementary reactions which constitute the Chapman mechanism are as follows.

Solar ultraviolet radiation of wavelength less than 242 nm slowly dissociates molecular oxygen.

$$O_2 + h\nu \rightarrow 2O \tag{1.3}$$

The oxygen atom (O) reacts rapidly with O_2 in the presence of a third molecule, denoted as M (usually O_2 or N_2) to form ozone,

$$O + O_2 + M \rightarrow O_3 + M \tag{1.4}$$

Reaction 1.4 is probably the only reaction that produces ozone in the atmosphere. The O_3 molecule formed in above reaction strongly absorbs radiation in the wavelength below 320 nm to decompose back to O and O_2.

$$O_3 + h\nu \rightarrow O + O_2 \tag{1.5}$$

Additionally O_3 can react with atomic oxygen to convert back to O_2 molecules.

$$O + O_3 \rightarrow 2O_2 \tag{1.6}$$

Combination of two atomic oxygen atoms (O) in the presence of third body also alters the concentration of O producing O_2 molecule.

$$O + O\,(+M) \rightarrow O_2\,(+M) \tag{1.7}$$

The UV absorption of O_2 in the region 175-195 nm (Shuman-Runge band) and formation of O from O_2 (reaction 1.3) are important reactions in the mesosphere where they lead to large concentrations of O. The oxygen atom concentration decreases with decreasing altitude as the intensity of light in Shuman-Runge band weakens as [M] rises, increasing speed of reaction 1.4. The ratio $[O_3]/[O]$ increases and reaction 1.4 dominates over reaction 1.5 in the stratosphere. The oxygen family can be divided into two types even oxygen (O_2) and odd oxygen (O and O_3). The odd oxygen species are quite reactive and inter-convert rapidly through 1.4 and 1.5 and hence in reality these reactions do not affect ozone production or destruction. The formation of odd oxygen in 1.3 is driven by UV radiation, which is primarily absorbed in upper stratosphere. As intensity of solar radiation is highest over tropical region, ozone formation mainly takes place in tropical stratosphere.

Homogenous chemical ozone loss

Some years after Chapman's work it was discovered that observed ozone concentrations can not be adequately explained by Chapman reactions. Estimated total ozone values from Chapman mechanism are too high in tropics and too low at higher latitudes. On global scale this mechanism predicts almost 800 DU total ozone compared to observed 300 DU (see Figure 1.4). Role of two other mechanisms in controlling ozone amount in the atmosphere (mainly in the stratosphere) was recognised. Firstly, it was noted that ozone is transported from tropics to higher latitudes through BD circulation (discussed in detail in Chapter 3). It also explains lower total ozone in the tropics although ozone production is highest there. Secondly, it was observed that both O and O_3 react with various other chemical species which alters the ozone budget significantly. It was found that ozone can be destroyed by a number of free radical catalysts. Among these the most important are hydroxyl (OH) [*Bates and Nicolet*, 1950], nitric oxide (NO) [*Crutzen*, 1970, 1974] and atomic chlorine (Cl) and bromine (Br) [*Stolarski and Cicerone*, 1974; *Molina and Rowland*, 1974]. All of these radicals have natural and anthropogenic (manmade) sources. The catalytic reactions involved can be summarised as follows,

$$X + O_2 \rightarrow XO + O_2 \tag{1.8}$$

$$O + XO \rightarrow O_2 + X, \tag{1.9}$$

where X and XO are chain carriers involving HO_x, NO_x, ClO_x and BrO_x families and X=OH, NO, Cl, Br. At present, most of OH and NO in the stratosphere is of natural origin, but human activity has dramatically increased chlorine and bromine. They are found in certain stable compounds, especially chlorofluorocarbons (CFCs), which may find their way to the stratosphere.

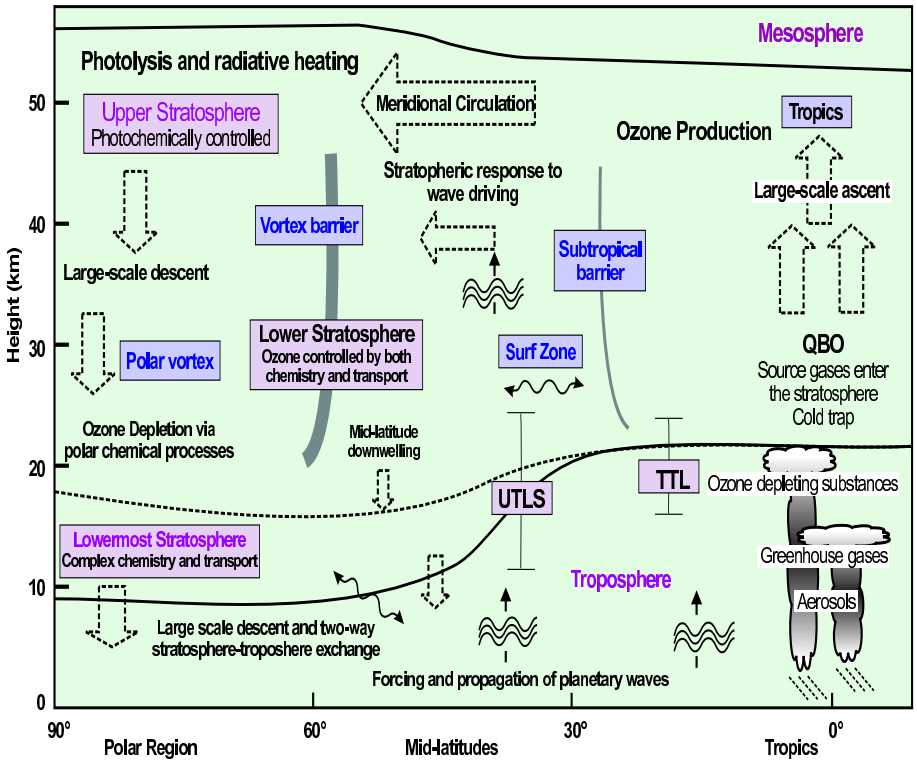

Figure 1.3: Schematic diagram of the different regions and some of the important processes in the upper troposphere and lower stratosphere. Broad arrows shows direction of BD circulation and wavy arrows denote transport along isentropic surfaces. The average position of the tropopause is shown by the lower thick-black line, the average position of the stratopause by the upper thick-black line, and the 380-K isentropic surface by the thick-black dot-dashed line. (Update from *Eyring et al.* [2005])

Polar stratospheric clouds and ozone hole

The stratosphere is very dry compared to the troposphere. Water vapor mixing ratios are generally of the order of few parts per million (ppm) in the stratosphere. But as noted earlier polar stratosphere is very cold during winter and early spring, specially in SH polar stratosphere where temperature can reach as low as 185 K. In addition due to strong polar jet, air inside the polar vortex remain isolated from the surrounding for quite long time. In such a dynamical condition even very little amount of water vapor gets condensed to form the polar stratospheric clouds (PSCs). A natural layer of aerosols (mainly sulphates) in polar lower stratosphere generally provides the required cloud condensation nuclei. PSCs are generally classified in two categories. Clouds with temperatures above and below frost point temperature are called as Type I and Type II PSCs respectively. Type I PSCs have been further subdivided into Type Ia and

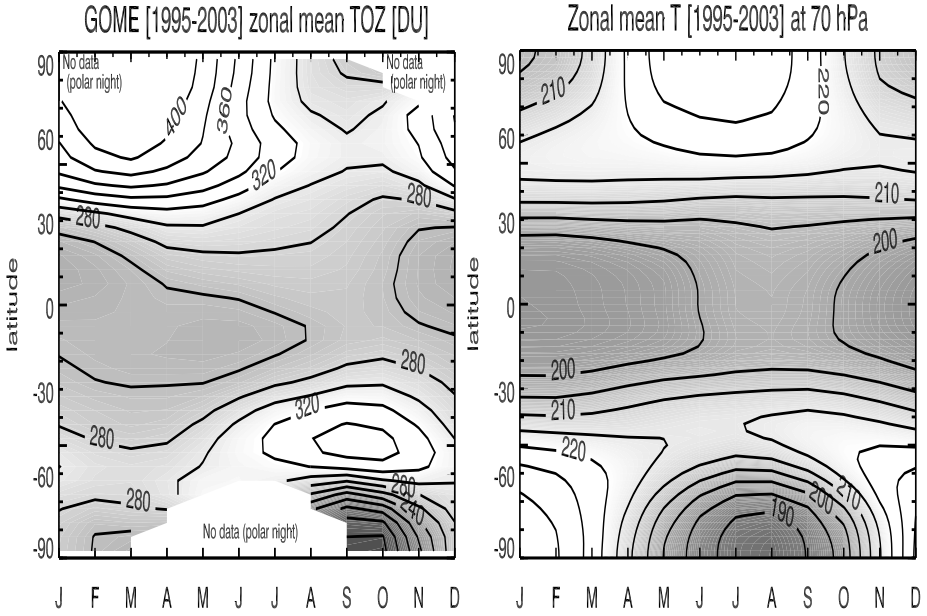

Figure 1.4: Monthly zonal mean total ozone (in DU) from GOME [1995-2003] (left panel) and 70 hPa zonal mean temperature (in K) from NCEP [1995-2003] (right panel). Note that both temperature and total ozone shows very less seasonal variation in tropical latitudes whereas in high latitude amplitude of seasonal variation is largest. During winter season satellite measurements are not possible in polar region due to lack of sunlight. Very cold stratospheric temperatures and lower total ozone values during SH winter season are clearly visible.

Type Ib. Clouds with nitric acid trihydrate ($HNO_3.3H_2O$) or NAT crystals are identified as Type Ia PSCs. Type Ia clouds are generally observed when temperatures fall below 195 K, while Type Ib occur at temperatures of about 191 K. Type Ib, PSCs consists of supercooled ternary solutions of $HNO_3/H_2SO_4/H_2O$ while Type II PSCs are mainly large frozen water ice, nonspherical crystalline particles.

Type I PSC particles are generally smaller in size ($\sim$1 micron) and hence sedimentation velocity is of the order few meters per day. Type II PSC particle are much larger ($\geq$10 micron) with sedimentation velocity of the order of 1.5 km/day. This sedimentation process in very important in polar chemistry as it transports reactive nitrogen and water out of the stratosphere. The removal of the reactive nitrogen is called as denitrification and the removal of the reactive water vapor is known as dehydration. Due to large winter-time interhemispheric temperature differences, formation of PSCs is quite different in both the hemispheric (see Figure 1.4). In SH, polar stratospheric temperatures are extremely low, PSCs form in early winter and persist till late winter. Type II PSCs are formed each year inside Antarctic polar region in large amount

leading both denitrification and dehydration in each year. Denitrification leads to decrease in reactive NO_2 which generally reacts with ClO to form reservoir (discussed in the following paragraph). This results in a maintenance of high levels of active chlorine that can continuously destroy ozone. In Arctic stratosphere, due to unstable polar vortex denitrification and dehydration are not regular phenomenon.

Large decrease in stratospheric ozone in spring over Antarctic were reported by British Antarctic Survey (BAS) team in 1985 [*Farman et al.*, 1985] (see Figure 1.5). These findings were latter confirmed by satellite data set. Massive decreases in high latitude ozone during spring has become a regular phenomenon, and is widely known as "ozone hole" (also see Figure 1.4). Initially such a decreases were attributed to gas-phase catalytic chemical ozone loss associated with the ClO_x and NO_x. Later it was realized that atomic oxygen (O) required for these reactions can not be available in polar stratosphere due to large solar zenith angle which controls the photochemical decomposition of O_2. In addition, catalytic ozone loss due to halons and CFCs can cause only up to 5-10% of ozone loss in upper stratosphere. But large ozone decreases were observed in lower stratosphere. Later it was realized that PSCs play larger role in ozone loss through heterogenous chemistry [*Solomon et al.*, 1996]. In first step, PSCs absorbs gaseous HCl efficiently followed by heterogeneous reaction,

$$HCl(s) + ClONO_2 \rightarrow Cl_2 + HNO_3 \tag{1.10}$$

where (s) denotes the species on the surface of ice. This reaction occurs when temperatures drop below 200 K. Gaseous Cl_2 released from PSCs in above reaction rapidly photolyses to produce free chlorine atoms, while HNO_3 remains trapped in the ice. Such a trapping of HNO_3 further facilitates catalytic ozone loss by removing NO_x from the system which might otherwise react with ClO to form $ClONO_2$,

$$Cl_2 + h\nu \rightarrow 2Cl \tag{1.11}$$

$$2[Cl + O_3 \rightarrow ClO + O_2] \tag{1.12}$$

Efficiency of ozone loss by above reaction critically depends on cold temperatures and sunlight. Absence of either of them leads to termination of ozone destruction mechanism. Cold temperatures are needed to form PSCs to provide surfaces for heterogenous reactions. The reservoir species such as $ClONO_2$ and H_2O_2 reacts heterogeneously with PSCs on which HCl have been absorbed to form HCl, HOCl or $ClNO_2$. Sunlight is required to photolyse gaseous Cl_2, HCl and $ClONO_2$. Such conditions are available in polar stratosphere during early spring, which causes such large ozone losses and hence the formation of the ozone hole.

Montreal protocol

As noted earlier CFCs are major sources of stratospheric bromine and chlorine. CFCs were developed in the 1930's as a safe, non-toxic, non-flammable replacement of dangerous substances like ammonia that are used as refrigerant and spray can propellants.

Their usage grew enormously over the years. CFCs are diverse organic compounds composed of carbon, fluorine, chlorine, and hydrogen. These halogenated hydrocarbons, notably trichlorofluoromethane (CFC-11, or F-11) and dichlorodifluoromethane (CFC-12, or F-12), have been used extensively for these applications because they can readily be converted from a liquid to a gas and vice versa. During the 1970s, it was discovered that CFCs released into the atmosphere accumulate in the stratosphere, where they had a deleterious effect on the ozone layer.

In the stratosphere, the CFC molecules break down by the action of solar ultraviolet radiation and release their constituent chlorine atoms. These then react with the ozone molecules, resulting in removal of the latter. The lifetime of CFCs in the atmosphere is about 20 to 100 years, and consequently one free chlorine atom from a CFC molecule can do a lot of damage, destroying ozone molecules for a long time. Based on this mechanism, *Molina and Rowland* [1974] noted the potential impacts of the chlorine released by CFCs. Given the crucial function of stratospheric ozone in filtering solar UV radiation (and its role in the overall structure of the atmosphere), the potential of large-scale ozone depletion raised growing concerns about the emissions of CFCs. In the late 1970s, international negotiations were started to limit the use of CFCs, resulting in the 1985 Vienna Convention for the Protection of the Ozone Layer. Indeed, the rise in CFC emissions has resulted in a decrease of global mean ozone concentrations by up to 5% [*WMO*, 2003]. Just after the adoption of the Vienna Convention, *Farman et al.* [1985] discovered the Antarctic ozone hole: a dramatic decrease in ozone columns inside the Antarctic vortex (see Figure 1.5). Following this discovery governments from various countries recognised the need for stronger measures to reduce the production and consumption of a number of CFCs (CFC 11, 12, 113, 114, and 115) and several halons (1211, 1301, 2402). The "Montreal Protocol on Substances that Deplete the Ozone Layer" was adopted on 16 September 1987 at the headquarters of the International Civil Aviation Organisation in Montreal. The protocol came into force on 1st January 1989, when it was initially ratified by 29 countries (for details see *http://ozone.unep.org/Treaties_and_Ratification/*)

1.4 Some aspects of ozone-climate interaction

Long term decrease in stratospheric ozone concentration has been reported in number of studies [*WMO*, 1995, 1999, 2003]. But the coupling between stratospheric ozone and climate (or associated forcing) is quite complex and contains variety of direct and indirect effects and feedback mechanisms. Although ozone abundance is very small (just a few parts per million), it is a strong greenhouse gas and hence plays an important role in determining radiative (and dynamical) structure of the atmosphere. Some of the important mechanisms of ozone-climate interaction are shown in Figure 1.3. Some of these mechanisms contribute significantly to ozone variability while some of them have quite minor influence on ozone. In order to understand future evolution of ozone layer, it is necessary to have a good understanding of their influences. Some of the important

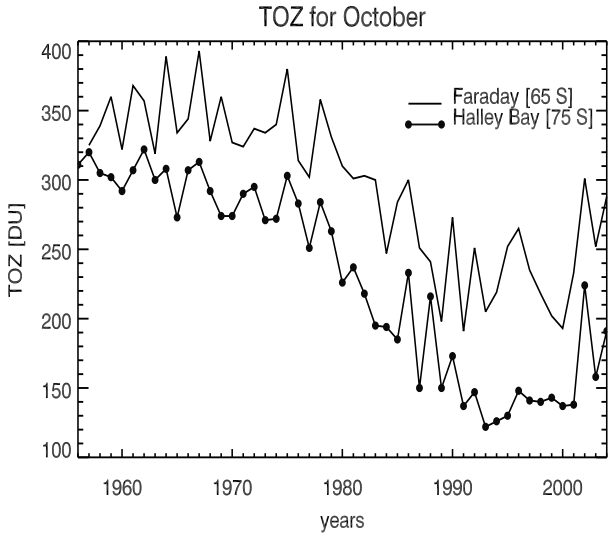

Figure 1.5: Total ozone for October from Faraday [65°S] and Halley Bay [75°S]. Data is obtained from web page *http://www.antarctica.ac.uk/met/jds/ozone*. (Update from *Farman et al.* [1985])

possible mechanisms are discussed below.

Stratospheric temperatures

Changes in stratospheric temperature have a two way effect. The chemical ozone loss in the stratosphere is determined by the amount of chlorine, bromine, nitrogen and hydrogen oxides, and the reactions rates are highly sensitive to the temperatures. A decrease in stratospheric temperatures leads to an increase in heterogenous chemical ozone loss and the decrease in ozone further enhances stratospheric cooling. In addition, changes in temperatures indirectly affect climate by modifying stratospheric (and tropospheric) dynamical processes. As shown by *Ramaswamy et al.* [2001], global and annually averaged stratospheric temperatures have decreased during the past three decades. Radiosonde (and satellite) data indicate statistically significant cooling trend in middle stratosphere after 1980s compared to prior period. It has been suggested that the effects of ozone and CO_2 are responsible for the observed stratospheric cooling [*Ramaswamy et al.*, 2001] and such change may further intensify the strength and duration of the polar vortex and consequently enhance the ozone depletion [*Langematz et al.*, 2003; *Braesicke and Pyle*, 2003, 2004].

Solar variability

The solar radiation changes on short as well as long time scales. Changes in solar UV irradiance influence atmospheric ozone burden through radiative and chemical interaction with climate. The small changes in UV radiation can alter ozone production rate

and hence dynamical structure of the atmosphere through radiative heating. Influence of the 11 year solar cycle on stratospheric temperatures, geopotential height, and wind field have been shown by *Labitzke* [1987] and *Labitzke and Loon* [1988]. There is also observational evidence of increase in ozone in tropics during solar maxima [*Zerefos et al.*, 1997; *Hood et al.*, 1997]. Modelling studies with general circulation models show consistent dynamical response with enhanced solar radiation and associated ozone changes. This response can be amplified through QBO, changes in Hadley cell circulation and movement of Ferrel cell (planetary waves are generated in this region) towards the polar region [*Haigh*, 1999; *Larkin et al.*, 2000].

Changes in greenhouse gases

Significant increases in well-mixed greenhouse gases (GHGs) (CO_2: 31%, N_2O: 16%, CH_4: 150%) is estimated in *IPCC* [2001]. Emissions are still increasing and there is no indication of a future reduction of their atmospheric concentrations. These emissions are generally believed to lead to global warming in the troposphere and cooling in the stratosphere and may accelerate the rate of climate change. Increases in GHGs also have a dual effect. It leads to global warming and global warming increases GHGs emission through natural processes [*Hansen and Sato*, 2004; *Hansen et al.*, 2005; *Zimov et al.*, 2006]. The average global surface temperature is expected to rise by 0.6-2.5° C in the next fifty years, and 1.4- 5.8°C in the next century, with significant regional variation. Evaporation will increase as the climate warms, which will increase average global precipitation. Soil moisture is likely to decline in many regions and intense rainstorms are likely to become more frequent.

Stratospheric water vapor

Observations indicate that stratospheric water vapor (WV) has increased by about 1 % per year since 1981 [*SPARC*, 2000]. It is believed that methane oxidation can contribute to rising levels of WV (or OH concentration) in the stratosphere as well as WV directly emitted by aircrafts in the lower stratosphere. But observed trend is substantially larger than can be attributed to observed changes in stratospheric CH_4. Another possibility is through changes in the stratospheric entry mechanism. It is widely accepted that WV enters the stratosphere through the tropical tropopause [*Rosenlof*, 2003] and trend in H_2O is likely to be caused by changes in the tropical tropopause region. It cannot be simply due to changes in temperatures, since these have actually decreased, and not increased as would be needed for an H_2O increase [*SPARC*, 2000]. Such increasing trends in stratospheric WV can have serious implication in future evolution of ozone layer as it can enhance homogenous as well as heterogenous chemical ozone loss [*Shindell et al.*, 1999b]. Increase in WV can increase amount of odd hydrogen in the stratosphere and can enhance the ozone loss through gas phase chemistry. In addition, the coupling processes between HO_x and NO_x/ClO_x also affect the ozone destruction by other catalytic reaction cycles. The increase in WV can also intensify the denitrification of the Antarctic winter stratosphere caused by an enhanced formation of polar stratospheric clouds

[*Tabzadeh et al.*, 2000]. Thus it further facilitates the catalytic ozone removal by the ClO_x [*Stenke and Grewe*, 2005].

Volcanic eruptions

Strong volcanic eruptions have a significant impact on the earth's climate. Volcanic eruptions inject large amount of fine particles of magma as well as ash and gases into the atmosphere. Volcanic gases are dominated by H_2O ($\sim$80%), and CO_2 ($\sim$10%), and the rest is made up of N_2, SO_2, H_2S, CO, H_2, HCl, and HBr. Volcanic aerosols, formed by sulphur species injected into the stratosphere are the main agents of climate effects [*Robock*, 2000]. These stratospheric aerosols affect the global radiation by absorbing and back-scattering incoming solar radiation; the former leads to stratospheric heating, while the latter to surface cooling. Stratospheric heating results in a perturbation of the atmospheric dynamics by affecting vertical and meridional circulation. The volcanic aerosols may also catalyse a reduction of stratospheric ozone through heterogeneous chemical reactions [*Solomon et al.*, 1996; *Tabzadeh et al.*, 2002]. As ash, water vapor, SO_2, HCl and other gaseous species are injected into the atmosphere, the ash falls out of the atmosphere very rapidly. Ash therefore has little global climate impact beyond local cooling that is often manifested in reduced amplitude of the diurnal cycle of surface temperature variations. Moreover, water vapor and soluble gaseous components like HCl, condense as temperatures drop in the upper troposphere and often rain out within few hours to weeks before they enter the stratosphere. Since most volcanic eruptions are effusive, they have little chance to impact the global atmosphere as their eruption plumes do not reach the tropopause whereas strong eruptions such as El Chichòn (1983) and Mount Pinatubo (1992) injected large amounts of aerosols into the stratosphere. These aerosols then spread globally and remained enhanced for a few years affecting stratospheric temperatures and ozone.

Stratosphere-troposphere coupling

Given that the troposphere contains most of the total air mass of the atmosphere, it is obvious to expect that troposphere is almost entirely independent of stratosphere. Conversely, the stratosphere should have a strong tropospheric influence. Indeed, waves from the troposphere are key driver of stratospheric (and mesospheric) dynamics. As explained earlier, extra-tropical tropospheric waves drive the meridional BD circulation. Equatorial tropospheric waves generate the dominant mode of variability in the equatorial stratosphere, the quasi-biennial oscillation (QBO, see Figure 1.3). In turn, the QBO affects, among other things, the middle atmospheric large-scale circulation and the timing of the breakdown of the wintertime stratospheric polar vortex [*Baldwin et al.*, 2001]. Wave interactions between the troposphere and the stratosphere are also at play in the dominant modes of inter-annual variability at the poles, the Arctic and Antarctic Oscillations. In these cases however, the troposphere is not just a trigger. In fact, stratospheric dynamics are expected to also play an important role in determining tropospheric weather and climate [*Thompson and Wallace*, 1998]. Firstly through

non-local inversion or changes in the potential vorticity (PV) distribution that changes refractive index in lower stratosphere, which guides the upward propagation of planetary waves. Any change in the PV distribution in the lower stratosphere will inevitably give rise to changes in wind and temperature in the troposphere (e.g. stronger down-welling in polar region or tropopause folds at mid-latitude). And the second mechanism is via Rossby wave propagation. The propagation of Rossby waves out of the troposphere might be sensitive through the variation in the refractive properties of the lower stratospheric flow ([*Hartmann et al.*, 2000; *Limpasuvan and Hartmann*, 2000], or there might be downward reflection of Rossby waves from higher in the stratosphere [*Perlwitz and Harnik*, 2004]. Along with the dynamical coupling, chemical properties of these two layers can be influenced by stratosphere-troposphere exchange or STE (for review see *Holton et al.* [1995]). STE significantly influences tropospheric ozone which is considered one of the most critical gaseous pollutants, as it affects the tropospheric oxidation capacity and has adverse effects on human health, on vegetation and on soil microbes and also is a powerful greenhouse gas. The troposphere contains about 10% of the ozone in the atmosphere, 90% being located in the stratosphere. Major part of the tropospheric ozone has stratospheric origin as consequence of the stratospheric intrusions associated with tropopause folding in cyclogenesis processes. Increase in tropospheric ozone is reported at many places that can modify radiative, chemical and dynamical properties of the troposphere. Another important aspect of STE is that it regulates the lifetime of chemically important species such as H_2O or CFCs in the stratosphere which in turn can have significant influences on the future evolution of ozone layer.

Changes in halogen loadings

Discovery of the Antarctic ozone hole in 1985 and the negotiations in the Vienna Convention resulted in the Montreal Protocol (1987) and several subsequent amendments, which prescribed a phase-out of CFCs. The Montreal Protocol has become one of the most successful international environmental treaties, and by now the production and use of CFCs has almost ended. Tropospheric total chlorine concentrations (mostly CFCs) peaked in early 1994 [*Montzka et al.*, 1996, 1999] and will continue to decrease over the coming decades. Stratospheric chlorine loading reached its peak in the late 1990s, and over time, chlorine concentrations are expected to return to pre-1970s levels [*WMO*, 2003].

1.5 Objectives of the thesis

As mentioned earlier, the ozone-climate interaction is very complex. The attribution of current ozone trends to various processes is still difficult and even a more challenging task is to detect changes in ozone trends as a result from recent decreases in stratospheric halogen loading [*Weatherhead and Anderson*, 2006]. Given this positive turn of events (decrease in CFCs), now an obvious question arises if stratospheric ozone starts to recover and the ozone hole diminish, in line with the decreasing chlorine loading? Or will we see a long delay in the recovery, or even enhanced ozone losses

at the poles due to the changes in temperatures and atmospheric dynamics, induced by increases in greenhouse gases (primarily CO_2) and possibly also of water vapor? This question is particularly important for the Arctic, where temperatures in the vortex are close to the threshold for the formation of polar stratospheric clouds (PSCs). Here the uncertainties are not primarily due to the uncertain future anthropogenic emissions. For instance, *Austin et al.* [1992] and *Shindell et al.* [1999b] have suggested that the dynamical response to an increase in greenhouse gases and ozone depletion can create a more stable vortex, which alters planetary wave propagation so that fewer stratospheric warming events occur, creating a colder polar stratosphere. On contrary, other modelling studies [*Rind et al.*, 1990; *Butchart and Scaife*, 2001; *Schnadt et al.*, 2002; *Gillett et al.*, 2003] have suggested that increased planetary wave activity emanating from the troposphere would increase polar down-welling and will heat the polar stratosphere. Such an increase in the strength of the BD circulation might also favour a faster recovery of the ozone layer by enhancing troposphere-stratosphere transport (resulting in a faster removal of CFCs) and by increasing ozone transport from the tropical source regions to the poles. Hence, at this point, there is no consensus on state of ozone layer in a changing climate [*WMO*, 2003].

This thesis is an attempt towards a better understanding and attribution of a dynamical and chemical processes on changes in stratospheric ozone and water vapor using the most updated data sets. The general outline of this thesis is as follows:

- In Chapter 2, different types of data sets used in this study are briefly discussed. One of the major difficulty in attributing a particular process to ozone change is data quality. In order to understand possible error sources in trend estimation due to various data types, advantages and drawbacks of individual ozone data records are briefly discussed.

- Although the influence of planetary wave driving is known for almost four decades, an useful dynamical proxy accounting for this is still missing. Some of the earlier studies suggested various dynamical proxies (such as tropopause height, 50 hPa temperatures, North Arctic Oscillation index), but most of them are insufficient to explain the interannual ozone variability. In this study, a new proxy has been suggested. It was found that accumulated winter heat flux (proxy for tropospheric generated wave activity) represents most of the ozone variability due to dynamical processes. The compact relationship between wave driving and mid-high latitude ozone is discussed in Chapter 3.

- The great advantage of reanalysis data sets providing temperature and wind field is that they are dynamically consistent, but they are not free from bias [*Randel et al.*, 2004a]. Differences and biases among these reanalysis data sets are studied to validate solar response on stratospheric temperatures. In particular, QBO dependent relationship between stratospheric temperatures (and also ozone, geopotential height, wind field) and solar flux cycle using correlation and multivariate regression analysis are presented. Analysis show that solar response on strato-

spheric temperature is seasonal dependent. During solar minima sudden stratospheric warmings (SSWs) occur during early winter month in both hemispheres whereas during solar maxima, mid-winter SSWs are quite common.

- In recent years increase in total ozone in NH mid-high latitudes have been observed. Some of the recent studies speculated that this increase may be a first sign of ozone recovery due to the starting decline in stratospheric chlorine (and bromine) loading. In Chapter 5, an advanced multivariate regression model has been developed and is used to study possible causes of recent increase in northern hemispheric (NH) mid-high latitude ozone. Influence of some of the important processes such as solar cycle, QBO, stratospheric aerosol loading as well as planetary wave driving is carefully assessed.

- Water vapor is another important greenhouse gas in the stratosphere. It has significant influence not only on ozone chemistry but also on radiative properties of the upper atmosphere. An increase in stratospheric water vapor is widely reported by various studies, but satellite data records do not confirm such increasing trends in the stratospheric water vapor [*IPCC*, 2001; *WMO*, 2003]. In Chapter 4, relationship between tropical lower stratospheric water vapor and planetary wave activity is studied. HALOE (1991-2005) and SAGE II (1984-2005) WV data confirm that entry mechanism of stratospheric water vapor is indeed controlled by strength of BD circulation. A strong anti-correlation between lower stratospheric WV and eddy heat flux (dynamical proxy for planetary wave activity) shows that observed increase in stratospheric water vapor in the last decade is probably due to decrease in planetary wave activity which also enhanced polar ozone loss during that period. These results also support that observed sudden decrease in stratospheric water vapor since 2001 is related to an increase in planetary wave activity in both hemispheres.

- During the course of this work significant improvements have been made in quantifying the influence of various climate forcings on the stratospheric ozone and water vapor. Some of the key results are summarised in Chapter 7.

2 Data sets

Long term observations of ozone (and water vapor) and other climate variables such as temperature play an important role in improving our understanding of processes in the atmosphere, ocean and in validation of climate models that are used to predict future changes [*Eyring et al.*, 2005]. More importantly, such data records are essential to determine long term changes and predict future evolution of the atmospheric trace gases such as ozone and water vapor. To detect long term ozone trends of the order of few percent per decade, the necessity of improvements of ozone (and water vapor) measurements have long been recognized [*WMO*, 1995]. This led to great advancement in measurement techniques as well as retrieval techniques in recent years. This chapter provides a brief overview of some of the recent updates of ozone and climate data set. Comparison between these data sets is presented in the relevant chapters of this thesis.

2.1 Ozone data sets

For last few decades, different types of instruments are used for the monitoring of atmospheric ozone. In this section the sources of data used to study long-term trends in atmospheric ozone, including the measurement methods, their characteristics and their error sources, are briefly discussed. This is necessary in order to understand the extent of possible uncertainties on the actual long-term variation. This includes the characteristics of the instruments and those of the data analysis methods used to retrieve the total ozone and ozone profile from the original signals obtained by the instruments.

Ground-based total ozone measurement

Three types of ground based instruments that are generally used for long-term monitoring of total ozone in the atmosphere are Dobson, Brewer, and Filter ozonometers. The longest records of continuous reliable measurements are available from stations equipped with Dobson spectrometers. The Dobson spectrophotometer which is a ground-based instrument was designed by Gordon Dobson in the 1920's. The Dobson spectrophotometer measures ultraviolet light from the sun at 2 to 6 different wavelengths from 305 to 345 nm. By measuring UV light at two different wavelengths, the amount of ozone can be calculated. One of the wavelengths used to measure ozone is absorbed strongly by ozone (305 nm), whereas the other wavelength is less absorbed by ozone (325 nm). Therefore the ratio between the two light intensities is directly proportional to the amount of ozone in the light path from the sun to the observing spectrophotometer. The first regular Dobson measurements started in the 1920s (for review see *Dobson* [1968]). A global network of ozone observing

stations was formed during the International Geophysical Year (IGY) of 1957. Since then, WMO has assumed responsibility for the collection of ozone data from various Dobson stations. In collaboration with the International Ozone Commission, WMO has developed standard procedures and coordination, to ensure uniform high quality ozone measurements. These activities are now part of the Global Atmosphere Watch (GAW) [*Staehelin et al.*, 2003].

The Brewer spectrometer, developed in the early 1980s, can measure total ozone with approximately the same uncertainty as the Dobson spectrometer. All Brewer instruments are calibrated against the Brewer triad at Toronto.

TOMS

The Total Ozone Mapping Spectrometer (TOMS) was launched on various satellite platforms to provide long term ozone measurements. The first instrument also known as Nimbus-7 TOMS (N7 TOMS) was launched on Nimbus-7 in November 1978. Nimbus-7 was a sun synchronous polar orbiting satellite flying at about 955 km altitude with equator crossing time at 1200 noon. N7 TOMS provided global total ozone measurements until May 1993. The N7 TOMS instrument measures backscattered ultraviolet radiance from Earth at wavelength bands centered at 312.5, 317.5, 331.3, 339.9, 360.0 and 380.0 nm. The first four wavelengths are sensitive to ozone; the two longer wavelengths are used for estimating the scene reflectivity necessary for deriving ozone amounts. Total column ozone is inferred from the differential absorption of scattered sunlight in the ultraviolet using the ratio of two wavelengths. For example 312 nm radiation is strongly absorbed by ozone while one at 331 nm is weakly absorbed. Horizontal resolution from N7- TOMS varies from a 50 km x 50 km square at nadir to a 130 km by 300 km at the scan extremes.

The second instrument known as Meteror-3 TOMS (M3 TOMS) was launched in August 1991 but failed in December 1994. Meteror-3 was launched at 1202 km above earth's surface but it suffered from orbit drift (precession period = 212 days). Due to orbital drift, M3 TOMS data differs from the N7 TOMS ozone data which was obtained in a near-noon sun synchronous orbit. The third instrument Earth-Probe TOMS (EP TOMS) was launched in July 1996. Earth Probe was flown in a 500 km polar orbit, rather than the 950 km orbit as for Nimbus-7. Although EP TOMS does not provide daily global coverage of ozone distribution (particularly within 60° of the equator), it gives full coverage at the poles (except during polar nights). In addition, the lower orbit helped to increase spatial resolution due to the smaller "footprint".

Recently total ozone data from TOMS instruments had undergone major revision and new version of ozone data (TOMS V8) has been released. Detailed description and comparison with other satellite instruments ground based instruments is available on *http://toms.gsfc.nasa.gov*. Monitoring the continuing changes in the optical properties

of the front scan mirror of EP TOMS, a latitude dependent error have been reported. Due to this error, it has been suggested that data since 2002 should not be used for trend analysis [*Barthia et al.*, 2004].

SBUV

The first Solar Backscatter Ultraviolet instrument, SBUV on Nimbus 7 (November 1978 -June 1990) was a nadir-viewing instrument to determine total column ozone and ozone vertical profiles by measuring sunlight scattered from the atmosphere in the middle ultraviolet [*Heath et al.*, 1975]. The follow-on SBUV/2 instruments on NOAA-9 (February 1985-February 1998), NOAA-11 (January 1989-May 2003) and NOAA-16 (October 2000-present) were flown on the NOAA series of spacecraft [*Frederick et al.*, 1986; *Hilsenrath et al.*, 1995]. Data from SBUV/2 instrument on NOAA-14 spacecraft suffered from various instrument issues and data is generally excluded from ozone studies.

The SBUV instruments are a nadir viewing double grating monochromators of the Ebert-Fastie type. They measure solar radiation backscattered by the atmosphere in 12 discrete wavelengths through centered at 256, 273, 283, 288, 292, 298, 302, 306, 312, 318, 331, and 340 nm, each with a bandpass of 1.1 nm. The total-ozone algorithm uses the four longest wavelength bands (312.5, 318, 331 and 340 nm). The profiling algorithm uses eight shortest monochromator wavelength channels which are sensitive to ozone profiles from about 20 hPa to about 1.0 hPa. Since the SBUV ozone measurements rely on backscattered solar radiation, data are only taken on the day side of each orbit. There are about 14 orbits per day with 26° orbit spacing at the equator, but NOAA polar orbiting satellites are not exactly sun-synchronous. For NOAA-11 equator crossing times drifted from 1:30 pm (measurements at 30° solar zenith angle at the equator) at the beginning of the data record to 5:00 pm at the end to the data record (measurements at 70° solar zenith angle). As the orbit drifts the terminator moves to lower latitudes and coverage decreases, which can have influence on long term trend estimation. In addition, the cloud cover radiometer operates at 379 nm (i.e., outside the ozone absorption band) with a 3.0 nm bandpass, and is used to determine the reflectivity of the surface. The SBUV/2 also makes periodic measurements of the solar flux and are generally used to determine long term proxy for solar variability. In this study SBUV version 8 total ozone data has been used which is processed using SBUV version 8 algorithm. For details see *ftp://www.orbit.nesdis.noaa.gov/pub/smcd/spb/ozone/dvd_v8 /DVDhtml/V8_Algorithm_Description.html*

GOME

The GOME (Global Ozone Monitoring Experiment) is an instrument aboard the ERS-2 (European Remote Sensing) satellite, launched by the European Space Agency (ESA) on 21 April 1995. Since then it is operational but due to a permanent failure of the ERS-2 tape recorder, data coverage is limited (from June 2003) to the region where ERS-2 is

in direct contact with ground stations. GOME is a scanning nadir-viewing spectrometer which measures earthshine spectra, that is the sunlight reflected and scattered back into space by molecules in the atmosphere and by the surface. The GOME is a double monochromator with four optical channels. The UV channel (channel 1) is divided in two parts Channel 1a (240-307 nm) and channel 1b (307-316 nm). Channel 2 ranges from 300 to 400 nm, channel 3 ranges from 400 to 600 nm, and channel 4 ranges from 600 to 800 nm. The instrument also measures the solar spectrum directly. The ratio between the earthshine and solar signal is a measure of the reflectivity of the earth's atmosphere and surface. GOME measures O_3 and NO_2 as well as important trace gases with comparatively weak atmospheric absorptions amongst which are as BrO, HCHO, SO_2, and OClO [*Burrows et al.*, 1999]. The large spectral range of GOME combined with the high spectral resolution (0.2-0.4nm) permits the application of the DOAS (Differential Optical Absorption Spectroscopy) algorithm to the retrieval of column amounts of many trace gases [*Platt*, 1994]. Recently a new algorithm approach called Weighting Function Differential Optical Absorption Spectroscopy (WFDOAS) has been developed to retrieve total ozone columns from nadir observations of the GOME [*Coldewey-Egbers et al.*, 2005]. Total ozone from WFDOAS algorithm were compared with various ground based data and from the global validation excellent agreement between WFDOAS and ground data with an average agreement is within 1% [*Weber et al.*, 2005]. It was also shown that here is very little seasonal variation in the observed differences, but at polar region and at high solar zenith angles, a positive bias varying between 5 and 8% have been observed. WFDOAS total ozone data shows better agreement with Brewer than Dobson measurements and this is most likely related to neglect of ozone temperature variation affecting mostly the Dobson retrieval [*Weber et al.*, 2005]

TOMS/SBUV merged

Using TOMS V8 (total ozone) and SBUV V8 (total ozone and profile data), a new data set also known as the TOMS/SBUV merged data set has been constructed [*Frith et al.*, 2004]. This is available as monthly-mean zonal and gridded average total ozone with 10° by 5° resolution. An external calibration adjustment has been applied to each satellite data set in an effort to calibrate all the instruments to a common standard. The calibration is done using data from the overlapping period for different instruments. The details about satellite instruments including time period and major issues related to satellite instruments are given in Table 2.1

2.2 Stratospheric water vapor data sets

As noted in Chapter 1, understanding the processes controlling stratospheric WV is important not only for its greenhouse forcing, but also because WV play bigger role in stratospheric chemistry. Due to lack of high quality long term measurements, long term trend detection and characterization of various atmospheric processes on stratospheric WV have been quite difficult. Currently only few good quality stratospheric WV data

Table 2.1: Details about TOMS and SBUV data as used in the merged data set (from *http://code916.gsfc.nasa.gov/Data_services/merged/*)

Instru -ment	**Abbrev -iation**	**Data Start Date**	**Data End Date**	**Data Comments**
Nimbus 7 TOMS	N7 TOMS	November, 1978	April, 1993	
Earth Probe TOMS	EP TOMS	August, 1996	Operational	EP TOMS developed serious degradation problems beginning in 2001. Comparisons to SBUV/2 data suggest a long-term drift beginning in 1999. **No EP TOMS data after July 1999 are used.**
Nimbus 7 SBUV	N7 SBUV	November, 1978	June, 1990	N7 SBUV data after February 1987 are affected by chopper wheel synchronization errors. **No N7 SBUV data after Jan. 1987 are used.**
NOAA 9 SBUV/2	N9 SBUV/2	February, 1985	February, 1998	N9 SBUV/2 data are of poorer quality, and are only used to complete gaps in the time series. Power problems after June 1997 seriously degrade the N9 longitudinal coverage. **No N9 SBUV/2 data prior to 1993 are used. No N9 SBUV/2 after June 1997 are used.**
NOAA 11 SBUV/2	N11 SBUV/2	January, 1989	May,2003	N11 SBUV/2 suffered problems with the instrument grating drive beginning in late 1993, but the data remain usable through February 2001. The N11 satellite was in a near-terminator orbit from January 1995 - July 1997. **No N11 SBUV/2 data used Jan 1995 - Jul 1997** **No N11 SBUV/2 data used after Feb 2001.**
NOAA 16 SBUV/2	N16 SBUV/2	October, 2000	Operational	N16 SBUV/2 periodically experiences electronic interference in measurements that are used in the derivation of total ozone. Total ozone calculated as the sum of the profile total is not sensitive to this error.

sets are available. Among these, the longest near global WV measurements are provided by the Stratospheric Aerosol and Gas Experiment (SAGE II) from 1984 until 2005 and Halogen Occultation Experiment (HALOE) from 1991 until 2005. Both of these instrument use solar occultation technique which leads to limited number of measurements (around 15 sunrise and 15 sunset measurements) and global coverage is obtained in about one and a half months. In addition, Polar Ozone and Aerosol Measurement (POAM III- since 1997) has been providing high latitude water vapor measurements. These data set have been used in this study, to characterize influence of BD circulation on tropical lower stratospheric WV. Some important aspects of these data sets are briefly discussed in this this Section.

SAGE

The Stratospheric Aerosol and Gas Experiment (SAGE) II was launched on board the Earth Radiation Budget Satellite (ERBS) in October 1984. The measurements are done during each sunrise and sunset encountered by the orbiting spacecraft. The instrument uses the solar occultation technique to measure attenuated solar radiation through the Earth's limb in seven channels centered at wavelengths 1020, 940, 600, 525, 453, 448, and 385 nm. Direct solar irradiance is also measured in each channel during each event for use as a reference in determining limb transmittances, which are used for the calibration. The long lifetime of this instrument makes it very useful in quantifying long term trends and as well characterization of variability of measured chemical species. This data set spans the period October 1984 through August 2005. Retrieved data products contains profiles of aerosol extinction at 1020, 525, 453, and 385 nm and number density profiles of ozone, nitrogen dioxide, and molecular density, water vapor mixing ratio, and aerosol surface area and effective radius at a vertical resolution of 0.5 km. It also includes retrieved molecular density from 40-75km on a 0.5 km grid.

A new version of the SAGE II data V6.2 has been released [*Thomason et al.*, 2004]. This version has been extensively validated with various other data set by [*Taha et al.*, 2004]. There is a significant improvement in SAGE II water vapor compared to version 6.1. The dry bias ($\sim$2 ppm) in the vicinity of the hygropause has been significantly reduced. Very low stratospheric WV concentration as well as interference from aerosol and ozone makes stratospheric WV retrieval quite difficult. Although a new version of aerosol model has been used in the water vapor algorithm, there are still some problems with the water vapor data during the years with high stratospheric aerosol loading. As shown by [*Taha et al.*, 2004], aerosol contaminated water vapor profiles with aerosol extinction coefficient at 1020 nm greater than 2 X 10^{-4} km^{-1} are not reliable and are excluded in this study. SAGE II 6.2 data set is obtained from *http://www-sage2.larc.nasa.gov/data/v6_data*.

HALOE

The Halogen Occultation Experiment (HALOE) was launched in the Upper Atmosphere Research satellite (UARS) in September 1991. The instrument uses solar occultation technique to measure vertical profiles of water vapor at 6.61 μm as well as ozone (O_3), hydrogen chloride (HCl), hydrogen fluoride (HF), methane (CH_4), nitric oxide (NO), nitrogen dioxide (NO_2), aerosol extinction, and temperature versus pressure with an instantaneous vertical field of view of 1.6 km at the Earth limb. The altitude range of the measurements extends from about 15 km to 60-130 km, depending on the species. HALOE provides daily 15 sunrise and 15 sunset water vapor profiles. In this study so called HALOE V19 data for the period September 1991 till November 2005 have been used. HALOE water vapor measurements are considered to be very high quality [*SPARC*, 2000] and have been used quite extensively to study tropical tape recorder *Mote et al.* [1996], seasonal cycle in tropical tropopause region [*Randel et al.*, 2001, 2004b], and ascent rate in the tropical stratosphere [*Niwano et al.*, 2003]. HALOE data used in this study are obtained from *http://haloedata.larc.nasa.gov/*

POAM

The Polar Ozone and Aerosol Measurement III (POAM III) instrument was launched on the SPOT-4 spacecraft in March 1998. POAM III has nine channels in visible/near-infrared photometers centered at 353, 439, 442, 603, 761, 779, 922, 935, and 1018 nm. The instrument uses solar occultation technique for making measurements of aerosol extinction, ozone, water vapor, and nitrogen oxide in polar stratosphere. POAM provides 14 profile measurements per day around a circle of latitude in each hemisphere, having successive observations separated by about 25 degrees longitude. The latitudinal variation of the POAM measurement ranges between 54^0-71^0 in northern hemisphere and between 63^0-88^0 in southern hemisphere. All the POAM measurements in NH are made during satellite sunset, while in SH observations are obtained during satellite sunset from April to September and during satellite sunrise from October through March. POAM water vapor measurement are made using the 940 nm water vapor absorption band. The retrieved concentrations are converted to mixing ratio using United Kingdom Meteorological Office (UKMO) T/P profiles. POAM III version 3 algorithm is described in detail by *Lumpe et al.* [2002]. In this study updated POAM III version 4 data set can be obtained from *http://wvms.nrl.navy.mil/POAM/*

2.3 Meteorological data sets

Detection and accurate estimation of stratospheric ozone (and water vapor) trends is possible only if influence of various atmospheric processes is properly removed. For this purpose, it is necessary to have good quality long term observation of various climate variables. Many observations are taken for weather forecasting purposes and global atmospheric analysis are produced in real time operationally. As most of these observation have limited spatial and temporal resolution, most obvious choice is use to

reanalysis data sets. The term ”reanalysis” signifies the reprocessing of all these and other observations with a state-of-the-art system that is held constant in time, thereby improving the continuity of the resulting climate record. In addition, observations may be reanalyzed to take advantage of new and improved analysis tools and the more complete observations assembled in non-real time. In other words, reanalysis corresponds to the production of comprehensive, integrated data sets describing the evolution of components of the climate system by using data assimilation. In this process, background state of the model is obtained from an initialization model that simulates the climate variables that are adjusted to fit the historical observations in a consistent way with appropriate statistical and physical constraints. The general features of reanalysis products are largely influenced by the initialization model. In addition, accuracy and density of the available observations and assimilation methods play an important role in determining the quality of reanalysis data products. This leads to large variation in quality of particular climate variables on both spatial and temporal scale. Such differences can have significant influence on the trend detection. Influence of these discrepancies on the attribution of ozone change must be resolved. This can achieved be comparing various climate variables from different reanalysis data set. Currently there are three well established reanalysis data sets are available from three different climate centers. Important features such as assimilation methods, vertical and horizonal resolution, observational data sources and initialization models of these reanalysis data sets are discussed in this Section.

ERA40

European Center for Medium-Range Forecasts (ECMWF) Re-Analysis (ERA-40) is the latest and most updated reanalysis data set produced at ECMWF (*http://www.ecmwf.int*, *Uppala et al.* [2005]). It is a comprehensive global analysis for the 45 year period covering September 1957 to August 2002. ERA40 uses ECMWF Integrated Forecast System (IFS) approach in which background (first-guess) values are compared with observed values at the observation time rather than the analysis time, and the differences are applied at analysis time. The atmospheric model consists of 60 vertical levels, T159 spherical harmonic representation for the basic dynamical fields, and a reduced Gaussian grid with an approximate uniform spacing of 125 km for surface and other fields. The atmospheric model is also coupled to an ocean-wave model. ERA40 uses three dimensional- variational (3D-Var) data assimilation method whereas ECMWF operational model uses four dimensional variational (4D-Var) data assimilation technique. In 3D-Var assimilation observations are supplied during the synoptic hours and initialization scheme remain same during one time step. Whereas in 4D-Var observations are supplied at the time of observation. ERA40 reanalysis data are also available on 23 pressure levels spanning from 1000 hPa to 1 hPa. The 60-level vertical resolution is same as that currently used operationally at ECMWF (operational analysis data is available at 21 pressure levels). Multiple archives of *in-situ* and satellite observations are assimilated in the model. Among these are the observations from the operational archives of ECMWF, National Center of Environmental Prediction (NCEP),

and the Japan Meteorological Agency. In addition data from other institutions such as National Center for Atmospheric Research (NCAR) and European Organization for the Exploitation of Meteorological Satellites (EUMETSAT), radiance data from Vertical Temperature Profile Radiometer (VTPR) from 1973 to 1978 is directly assimilated in to ERA40.

Due to large variation in availability of observational data records, ERA40 reanalysis data is produced in different streams. Stream 2 (identification number 0018) covers pre-satellite time period between 1957-1972. Major sources of assimilated observational data include upper air wind, temperature and humidity from radiosondes, wind and temperature from dropsondes, wind from pilot balloons, surface pressure, temperature and humidity from land stations and ship reports. Along with above noted observational sources stream 3 (identification number 0020) which covers time period approximately between 1972-1986, includes data from temperature and humidity sensitive radiances from VTPR (1973-1978) and High Resolution Infrared Radiation Sounder (HIRS)/Stratospheric Sounding Unit (SSU)[1979-2002] as well as temperature data from aircraft measurements. With large increase in satellite data in recent years, stream 1 (identification number 0030) includes additional microwave radiances from Micorwave Sounding Unit (MSU) for 1979-2002 and advanced MSU (AMSU-A) for 1998-2002, winds from geostationary satellites, total O_3 from TOMS, SBUV, GOME and O_3 profile from SBUV. It is important to note that ozone is introduced only as a prognostic model variable without interaction with the radiation parametrization. Ozone advection in done using the semi-Lagrangian scheme, with gas-phase chemistry parameterized [*Dethof and Holm*, 2004]

NCEP

The NCEP/NCAR reanalysis provides various meteorological data for the period of 1948-present. The reanalysis model and assimilation method is described in detail in [*Kalnay et al.*, 1996]. The data is produced using T62 (209 km) global spectral model of 28 vertical levels. This assimilation system is similar to NCEP operational model and is kept constant since 1995. It uses 3D-Var assimilation method [*Parrish and Derber*, 1992]. The major sources of assimilated observations are similar to ERA40 for pre-satellite time period. Data from various national meteorological institutes such as China, South Africa, Canada, Brazil, United States are also included. Another important sources of observational data include the Comprehensive Ocean-Atmosphere Data Set (COADS) since 1983 and aircraft data since 1963. Assimilated satellite radiance data are quite similar to ERA40 which include VTPR IR sounders and TOVS (HIRS/SSU/MSU) microwave sounders. It is also important to note that TOVS vertical temperature data between 20°N- 20°S are excluded due to rain contamination and TOVS temperature sounding are used only over land and above 100 hPa. In this study pressure level data available at 17 pressure levels starting from 1000 hPa to 10 hPa are used.

UKMO/METO

Since October 1991, the U. K.Meteorological (Met) office produces daily stratospheric analysis data using a stratosphere-troposphere version of the Met Office data assimilation system. This stratospheric data assimilation system uses an analysis correction scheme [*Swinbank and O'Neill*, 1994]. A particular characteristic of the analysis correction system is that it allows the asynoptic insertion of the data. Observations are gradually inserted in the GCM, over the period beginning 4 hours before each observation time and ending 1 hour after the observation time. The weight given to each observation time is varied so that it is given maximum weight at the time it is valid. This assimilation method is used in a 42- level Unified Model to produce the analysis data set. In addition to standard meteorological parameters from various stations, major sources of assimilation data includes data from various satellite instruments from UARS (Upper Atmosphere Research Satellite).

This assimilation system has undergone various changes over the time period. In November 2000 a new stratospheric data assimilation system was implemented, based on the 3D variational (3DVAR) data assimilation system. The 3DVAR stratospheric system includes the assimilation of radiances (rather than temperature retrievals) from the operational polar orbiting satellites. In October 2003, the assimilation model was changed to use a new semi-Lagrangian dynamical core, usually referred to as "new dynamics". The model is a 50-level configuration of the Unified Model; the tropospheric levels are the same as those used in the 38-level global forecast model, but additional stratospheric levels have been introduced. Assimilation data products are available on 42 levels extending from surface to lower mesosphere (1000 hPa to 0.30 hPa), at equally spaced levels per decade of pressure. The assimilation is carried out at model levels, and then the parameters are interpolated on pressure levels. The analysis consists of temperatures, wind components and geopotential heights on global grid of resolution 2.5° latitude by 3.75° longitude. The analysis data set is produced daily at 12 UTC.

3 Eddy heat flux: A proxy for atmospheric dynamics influencing ozone transport [1]

A decrease in global ozone amount has been widely reported, but the accurate estimation of ozone trends is an area of ongoing research. As noted in Chapter 1, almost 90% ozone resides in the stratosphere and is strongly influenced by several natural (mainly stratospheric) processes that change the ozone amount on short-term, seasonal, interannual, and long-term time scales. To determine long term trends, it is necessary to quantify the influence of these processes on ozone variability. One of the important process is transport of ozone from tropics to higher latitudes. This transport is largely determined by the strength of stratospheric or Brewer-Dobson (BD) circulation. The strength of BD circulation is primarily controlled by breaking of waves by depositing momentum in to the stable stratosphere thereby driving the circulation. Gravity waves and Rossby waves have significant influence on BD circulation. Some aspects of these waves are discussed in Section 3.1. Although importance of this wave activity is known for last four decades, a search of an useful dynamical proxy for long term ozone trend analysis as well for the validation of climate models is still going on. Section 3.3, provides a brief overview of some earlier studies. A brief description of total ozone and meteorological data set used in this study is provided in Section 3.4 and Section 3.5 respectively. A new dynamical proxy has been proposed in Section 3.6. It has been shown that winter-time eddy heat flux (which is proportional to the vertical component of Eliassen-Palm flux) not only controls the high-latitude ozone transport but also regulates polar ozone loss due to heterogenous chemistry. Important findings of this study are discussed in Section 3.7. A latitudinal dependent analysis of this relationship between ozone gain and eddy heat flux is presented in Section 3.8

3.1 Some aspects of atmospheric waves

The atmosphere is a fluid around the earth and is strongly influenced by the rotation of the earth. This gives rise to generation, propagation and dissipation of waves in a rotating fluid, such as gravity, Rossby and Kelvin waves. These waves play important role in transferring momentum in the atmosphere. These waves shows large variation

[1] Sections 3.2-3.7 have been published as M. Weber, S. Dhomse, F. Wittrock, A. Richter, B.-M. Sinnhuber, and J.P. Burrows, Dynamical Control of NH and SH Winter/Spring Total Ozone from GOME Observations in 1995-2002, Geophys. Res. Lett., 30, 1853, doi:10.1029/2002GL016799, 2003 with minor modification

in space and time scales ranging from slow moving planetary scale waves to much faster and smaller gravity waves, each playing important roles in the behaviour of the atmosphere. Among these, gravity waves and Rossby waves are key in transferring momentum in to the upper atmosphere. These waves are generated in the troposphere, propagate upward and break in the upper stratosphere. For e.g. Rossby waves deposit easterly momentum in to the stratosphere causing deceleration of westerly polar vortex (see Fig 1.2). This results in weakening of polar vortex and increase in strength of meridional Brewer-Dobson circulation, thus enhancing ozone transport from tropics to higher latitudes.

Gravity Waves

Gravity waves are generated in the stably stratified atmosphere when the vertically displaced air parcel undergoes buoyancy oscillation. As buoyancy force is responsible for the formation of gravity waves, sometimes theses waves are also known as the buoyancy waves (for recent review on gravity waves see *Fritts and Alexander* [2003]). Unlike the ocean which acts a lower boundary, there is no upper boundary in the atmosphere, this allows gravity waves to propagate vertically as well as horizontally. In vertically propagating waves the phase is function of height. Such a waves are known as the internal waves. Neglecting the Coriolis force, an expression for internal gravity waves in the (x,z) plane can be derived [*Holton*, 1992]. As internal gravity waves are the transverse waves in which parcel oscillations are parallel to the phase lines as indicated in Figure 3.1. A parcel displaced a distance δs along a line tilted at an angle α undergoes a vertical displacement $\delta z = \delta s \cos \alpha$. For such a parcel the vertical buoyancy force per unit mass is $-N^2 \delta z$. Here N is buoyancy frequency also known as the Brunt-Vãsãlã frequency. The component of the buoyancy force parallel to the tilted path along which the parcel oscillates is

$$-N^2(\delta s \cos \alpha) \cos \alpha = (-N \cos \alpha)^2 \delta s.$$

The momentum equation for the parcel oscillation is then

$$\frac{d^2(\delta s)}{dt^2} = (-N \cos \alpha)^2 \delta s \tag{3.1}$$

This equation has the general solution $\delta s = \exp[\pm i(N \cos \alpha)t]$. Thus the parcel executes simple harmonic oscillation at the frequency $\nu = N \cos \alpha$. This frequency depends only on the static stability. Various kinds of gravity wave sources have been identified. The most obvious sources include topography, convection, and wind shear. Other sources that are statistically important include adjustment of unbalanced flows in the vicinity of jet streams and frontal systems, and body forcing accompanying localised wave dissipation. Less significant sources at higher altitudes include auroral heating and eclipse cooling.

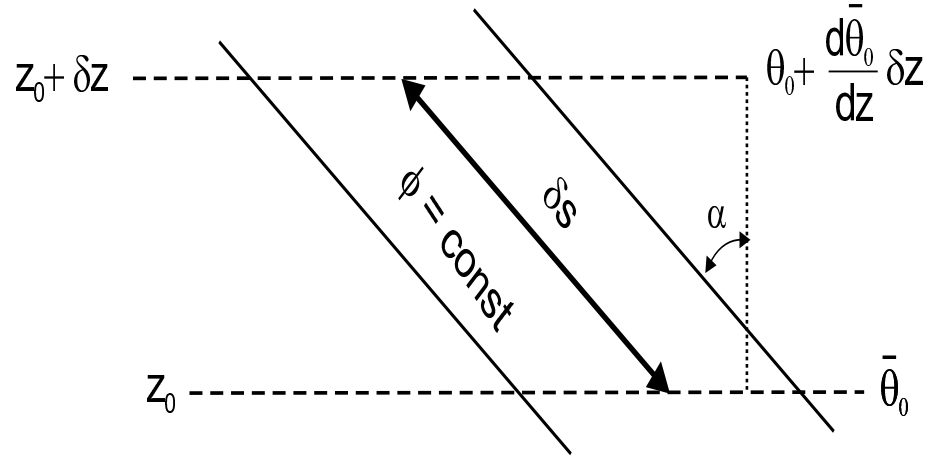

Figure 3.1: Generation of gravity wave through parcel oscillations with phase lines tilted at angle α to the vertical (figure modified from *Holton* [1992]). θ_0 is potential temperature at t=0 and z=z_0. δs is distance at with parcel is displaced at an angle α.

Rossby Waves

The most important type of waves for large scale meteorological processes are the Rossby waves, or planetary waves. A restoring mechanism for Rossby wave is the latitudinal (north-south) gradient of potential vorticity, which is a conserved quantity. Vorticity is simply the circulation of the air or water (any fluid) considered about a point. There are two types of vorticity, planetary vorticity and relative vorticity. The first involves the rotation imparted to the air because of the rotation of the earth, and the second involves the degree of spin imparted to the air as it moves from high to low pressure. Relative vorticity depends on the horizontal velocity components of the air itself. Planetary plus positive relative vorticity added together give the absolute vorticity (η). Potential vorticity is a combination of absolute vorticity and the gradient of potential temperature into a scalar quantity that is conserved under frictionless, adiabatic conditions, because it contains both dynamic (vorticity) and thermodynamic (potential temperature) properties [*Hoskins et al.*, 1985]. Mathematically potential vorticity is expressed as,

$$\mathrm{P} = (\xi + f)(-g\tfrac{\partial\theta}{\partial p})$$

where ξ is relative vorticity, f is Coriolis parameter and θ is potential temperature.

Rossby wave propagation can be explained by considering a closed chain of fluid parcels initially aligned along a latitude circle. The absolute vorticity (η) is given by η=ξ + f. Assuming ξ =0 at time t=0. Now suppose that at time t_1, δy is a meridional displacement of a fluid parcel from the original latitude. Then at t_1,

$$(\xi + f)_{t_1} = f_{t_0}$$

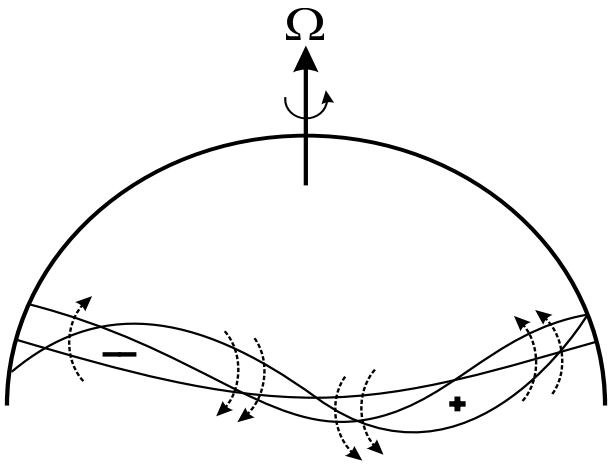

Figure 3.2: Perturbation vorticity field and induced velocity field (dashed arrow) for merdionally displaced chain of fluid parcels. Heavy wavy line shows original perturbation position, light lune westward displacement of the pattern due to advection by the induced velocity (figure modified from *Holton* [1992]).

or

$$f_{t_1} = f_{t_0} - f_{t_1} = -\beta\ \delta y \tag{3.2}$$

where $\beta = df/dy$ is the planetary vorticity gradient at the original latitude.
From equation 3.2 it is evident that if the chain of parcels is subject to sinusoidal meridional displacements under the absolute vorticity conservation, the resulting perturbation vorticity is positive (or cyclonic) for a southward displacement and negative (or anticyclonic) for a northward displacement.

This perturbed vorticity field will introduce a meridional velocity field, which advects the chain of fluid parcels southward west of the vorticity maximum and northward west of the vorticity minimum, as shown in Figure 3.2. Thus, the fluid parcel oscillates back and forth about their equilibrium latitude, and the pattern of vorticity maxima and minima propagates to the west which is known as the Rossby wave. The perturbation needed for generation of Rossby waves is generally caused by flow over topography as well as longitudinally dependent diabatic heating patterns.

Some other important waves

In addition to gravity and Rossby waves, various other types of waves are generated in the atmosphere. Important for stratospheric circulation are the following,

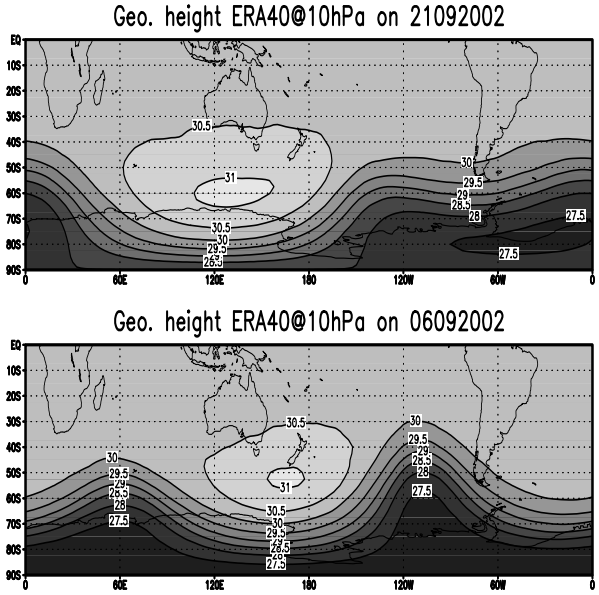

Figure 3.3: Examples for planetary waves in geopotential height fields. Upper panel shows wave pattern 1, in geopotential height (in geopotential meters/ 10000) on 21 September 2002 at 10 hPa whereas lower panel shows wave pattern 2, on 9 September 2002.

Inertio-gravity waves

Gravity waves with a sufficiently long period are influenced by the rotation of the earth [*Fritts and Alexander*, 2003]. In such a case, the restoring force becomes a combination of rotation and buoyancy. These are referred to as inertio-gravity waves. Air or water experiencing buoyancy oscillations will also experience a Coriolis deflection. For instance, zonally propagating waves oscillating in the vertical will feel a Coriolis force that imparts a meridional velocity component. Waves that have both Rossby and inertio-gravity characteristics are referred to as the mixed Rossby-gravity wave. The restoring force is thus the gradient of potential vorticity, static stability, and the Coriolis parameter.

Forced stationary planetary waves

Rossby waves with very long wavelengths (greater than 10,000 kilometers) are referred to as planetary waves. These waves are likely generated by large-scale surface topography like the Rocky Mountains and the Himalaya-Tibet complex (orographically forced) or by land-sea boundaries. These planetary waves do not propagate, but instead are stationary. The fact that they are stationary is related to the topographical forcing occurring at the fixed locations.

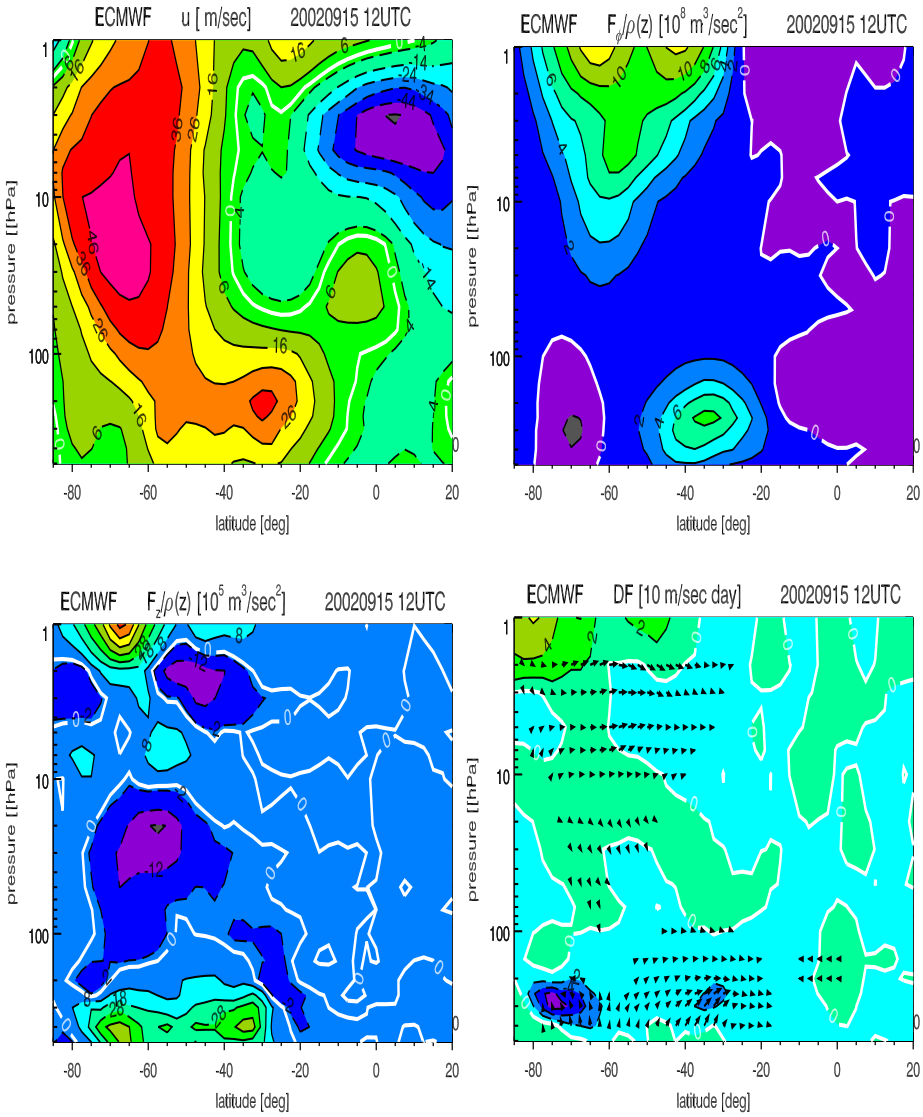

Figure 3.4: Dynamical features of zonal mean state of the atmosphere during mid-winter period with little wave forcing (here shown for 15 September 2002). Zonal mean wind field distribution is shown in upper left panel (in m/s). Upper right panel shows horizontal component of EP flux (m^2/s^2, see Equation 3.7) whereas lower left panel shows vertical component of EP flux (m^2/s^2, see Equation 3.7). Arrows in lower right panel indicates the magnitude and direction of the EP flux and divergence of EP flux (in m/s day - Equation 3.5) is shown with contours. For clarity all the fields (except U wind) are scaled with air density ρ.

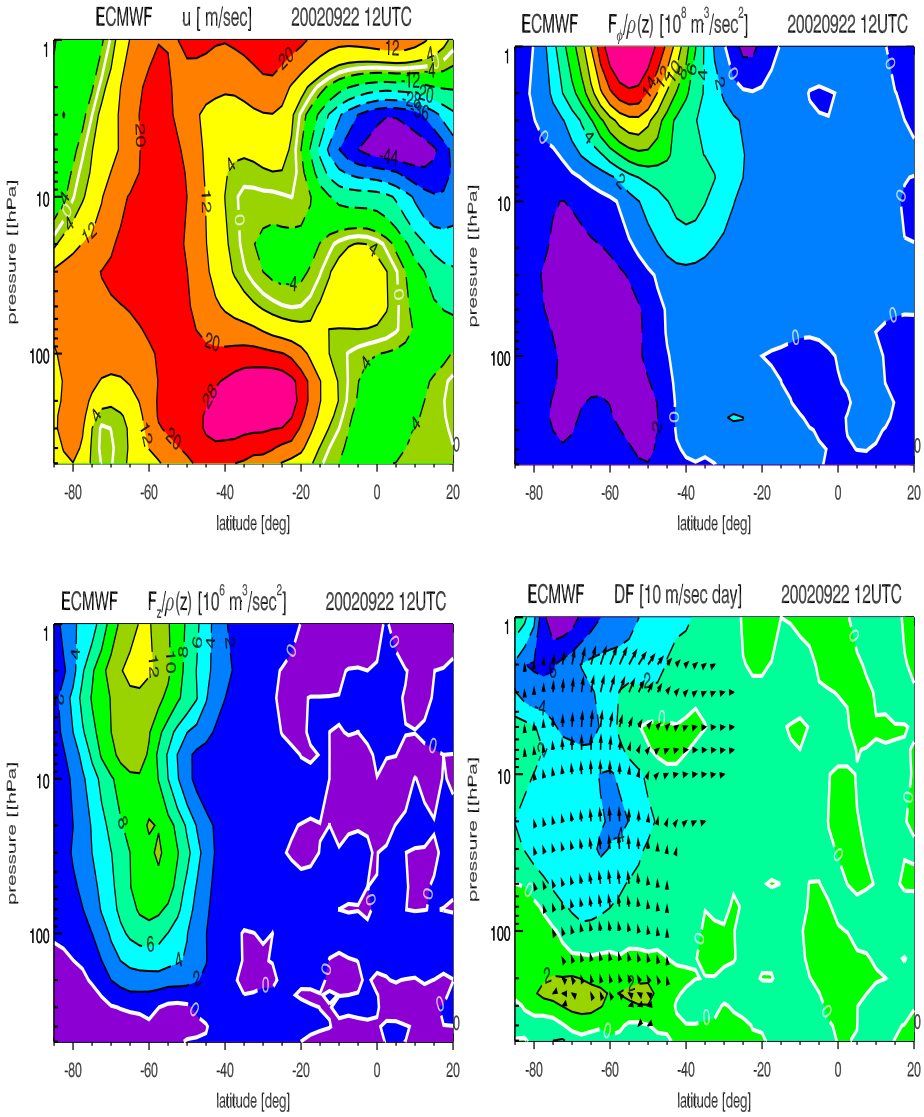

Figure 3.5: Same as Figure 3.4, but for a day with high planetary wave additivity.

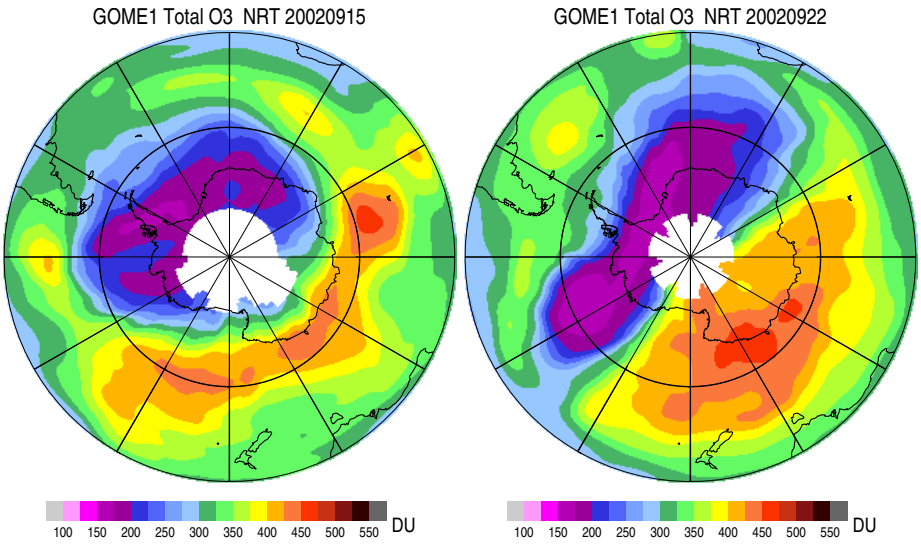

Figure 3.6: Total ozone values measured by GOME for 15 September 2002 and 22 September 2002. Increase in total ozone value at mid-high latitude on 22 September 2002 is clearly visible.

Free travelling planetary waves

Another type of planetary waves are those that propagate with a period of a few days. They are not primarily caused by topographic forcing from below, but instead are free, travelling waves. These are generated by some of natural oscillations present in the atmosphere. The so-called 5-day wave, a westward travelling disturbance in the middle atmosphere with wavelength equal to the distance around a latitude circle, is an example of a free, travelling planetary wave.

Equatorial waves

Various kind of waves are generated in the tropical atmosphere. They include high-frequency eastward and westward moving inertio-gravity waves and low frequency westward moving equatorial Rossby waves. The mixed Rossby-gravity waves propagates eastward at high frequencies like the inertio gravity waves and westward at low frequencies like the Rossby wave. The change in sign of the Coriolis parameter at the equator plays a key role in these waves. In addition, a unique equatorial wave type is the Kelvin wave. It propagates eastward like a pure gravity wave (i.e., a gravity wave whose restoring mechanism is buoyancy only). It has no meridional velocity and its zonal velocity is in geostrophic balance with the latitudinal pressure gradient. Kelvin waves play an important role in the tropical troposphere and stratosphere [*Baldwin et al.*, 2001].

Transformed Eulerian Mean (TEM) formulation

Zonal mean wind distribution is shown in Figure 1.2. Although there are important hemispheric differences, strong westerly wind in mid-latitude stratosphere during winter season at around 60°-75° latitude is clearly visible and its zonally symmetric component is generally referred as mean zonal wind denoted by $\overline{u}$. Some of the above discussed waves induce perturbation (u') in zonally mean flow. The resultant zonal velocity (u) can be written as
$u = \overline{u} + u'$.
Similarly perturbation induced in meridional wind and temperatures can be written as, $v = \overline{v} + v'$ and $T = \overline{T} + T'$.

A clearer picture of wave forcing driving mean meridional stratospheric residual circulation in zonal mean flow, was introduced by *Andrews and McIntyre* [1976], using Transformed Eulerian Mean (TEM) formulation. These equations can be obtained by defining the residual circulation ($\overline{v}^*$,$\overline{w}^*$), as follows

$$\overline{v}^* = \overline{v} - \rho_0 R H^{-1} \partial(\rho_0 \overline{v'T'}/N^2)/\partial z \tag{3.3}$$

$$\overline{w}^* = \overline{w} - R H^{-1} \partial(\rho_0 \overline{v'T'}/N^2)/\partial y \tag{3.4}$$

where,$\overline{v}^*$, $\overline{w}^*$ are meridional and vertical velocities of the residual circulation, ρ_0 is surface density, R is gas constant, H is scale height and N^2 is squared buoyancy frequency. Using above approximations TEM equations for zonal mean zonal momentum and thermodynamic energy equation for quasi-geostrophic in the mid-latitude β plane are written as,

$$\partial\overline{u}/\partial t - f\overline{v}^* = \rho_0^{-1} \nabla \cdot F + \overline{X} \tag{3.5}$$

$$\partial\overline{T}/\partial t + N^2 H R^{-1} \overline{w}^* = \overline{J}/c_p \tag{3.6}$$

where $\overline{X}$, $\overline{J}$ represent zonal mean eddy drag and zonal mean diabatic heating rate. c_p is specific heat of dry air at constant pressure. $\mathbf{F} \equiv \mathbf{j}F_y + \mathbf{k}F_z$, the Eliassen-Palm flux (EP flux), is a vector in the meridional (y,z) plane, which for large scale quasi-geostrophic eddies has the components

$$F_y = -\rho_0 \overline{u'v'}, \qquad F_z = \rho_0 f_0 R \overline{v'T'}/(N^2 H) \tag{3.7}$$

The quantities $\overline{u'v'}$ and $\overline{v'T'}$ are called as eddy momentum flux and eddy heat flux respectively.

Interaction with zonal mean flow

Examples of two kind of planetary waves (wave pattern 1 and wave pattern 2) in geopotential height field at 10 hPa is shown in Figure 3.3. As noted earlier these wave are generated in the mid-latitude troposphere and propagate upward. During

upward propagation they grow in size (because of decrease in density). The upward propagation and wave growth are critically controlled by mean zonal wind. During mid-winter season most of the planetary waves are reflected towards lower latitudes. This is better illustrated in Figure 3.4, indication strong polar vortex (upper left panel) in SH (wind speed up to 50 m/s). Lower magnitude and direction of EP flux vectors (shown with arrows in lower right panel) indicate low wave activity which is mainly reflected towards tropics. Sometimes planetary waves grow rapidly and break in to the stratosphere, which are generally referred as high wave activity period. Figure 3.5, shows an example of such a high wave activity. Comparison of Figure 3.4 and 3.5, shows that polar vortex gets decelerated during high wave activity and planetary waves propagate towards polar region. Divergence of EP flux shows the region where momentum has been deposited.

Breaking of planetary waves influences stratospheric ozone distribution through three processes : ozone transport, horizontal mixing and stratosphere-troposphere exchange (see Figure 1.3. Firstly the momentum carried by planetary waves is deposited in upper atmosphere. It drives the zonal mean meridional circulation in the stratosphere also know as Brewer-Dobson circulation. This circulation has rising branch in the tropics and descending branch in winter-stratosphere. It carries ozone rich air from tropical latitudes to high latitudes. Secondly during wave breaking air parcels undergo large and rapid latitudinal excursions causing them to undergo strong, irreversible, meridional mixing. As a result, most of the chemical species get thoroughly mixed throughout the subtropics and lower middle latitudes. Thirdly, wave braking also causes rapid isentropic transport between upper troposphere and lower stratosphere. Among these, ozone concentration are strongly influenced by ozone transport. Figure 3.6, for the day before high wave activity (15 September 2002) and after high wave activity (22 September 2002). Increase in total ozone values at mid-high latitudes are clearly visible during latter period.

3.2 Abstract

The abnormal high wave activity in austral spring 2002 led to the first observation of a major stratospheric warming in the southern hemisphere resulting in a net winter increase of mid- to high latitude total ozone until September 2002. In previous years chemical ozone depletion inside the Antarctic vortex was sufficiently high to reduce mean total ozone south of 50° in September to values slightly below that of March (fall) as observed by GOME during the period 1995–2001. This unusual event permits us to examine the interannual variability in total ozone and OClO (the latter being an indicator of the level of chlorine activation inside the polar vortex) as measured by GOME combining data from the southern and northern hemisphere. It is shown that the absolute winter eddy heat flux between 43° and 70° latitudes at 100 hPa correlates extremely well (r=0.97) with spring-to-fall ratio of total ozone polewards of 50° and anti-correlates with the winter integrated maximum

OClO column amounts (r=-0.94) using this combined data set. The unusual ozone ratio for austral winter/spring 2002 lies almost midway between typical values for Antarctica and those for recent cold Arctic winter/spring seasons.

3.3 Overview

Interannual variations of winter/spring total ozone have been linked to planetary-scale wave activity as approximated by the extratropical lower stratospheric eddy heat flux [*Fusco and Salby*, 1999; *Randel et al.*, 2002b]. The slow meridional residual circulation also known as the Brewer-Dobson circulation governs the diabatic ascent in the tropics and descent of stratospheric airmasses (and trace gases) in the polar regions [*Haynes et al.*, 1991]. This circulation is driven by planetary-scale waves, typically Rossby and gravity waves, that propagate from the troposphere and break in the stratosphere and higher levels [*Haynes et al.*, 1991; *Rosenlof and Holton*, 1993b]. This process is most efficient during hemispheric winters *Rosenlof* [1995]. The diabatic descent in the polar region is responsible for the steady increase of lower stratospheric ozone over winter particularly in the Arctic region (e.g. [*Chipperfield and Jones*, 1999]). The polar stratospheric temperatures are also controlled by planetary-scale wave forcing. Low midwinter wave activity leads to weaker downward diabatic descent in mid- to high latitudes, stronger cooling of the lower polar stratosphere (closer to the radiative equilibrium temperature), and to a strengthening of the polar vortex [*Newman et al.*, 2001; *Waugh*, 1999]. In addition to changes in transport, chemical depletion due to heterogeneous processes plays an increasing role at lower temperatures (e.g. [*Solomon*, 1999]), such that the winter wave forcing couples both dynamical and chemical change of mid- to high latitude lower stratospheric ozone [*Chipperfield and Jones*, 1999].

Temperatures in the SH polar stratosphere are persistently colder than in the NH resulting in large chemical ozone depletion observed for more than a decade during austral spring (e.g. [*Farman et al.*, 1985]). It is also known that planetary-scale wave activity plays a more minor role in the SH leading to rather minor perturbations of the Antarctic polar vortex. As a consequence the accumulated mid- to high latitude ozone mass is lower during austral spring than in the corresponding NH season. Figure 1 shows the annual cycle of GOME mean total ozone in the 50°–90° latitude band in the southern hemisphere since 1995. This can be compared with the corresponding figure for the NH as shown in Figure 2 of *Eichmann et al.* [2002]. While an increase in total ozone from late summer to spring is clearly detectable in the NH, an ozone reduction is observed in the SH by September. The increase in extratropical ozone in austral winter/spring 2002 is clearly an exception to the general behaviour in previous years and is a consequence of the abnormal midwinter wave activity in 2002 leading to the first observation of a major stratospheric warming in the southern hemisphere [*Sinnhuber et al.*, 2003a]. (referred to as S03 from now on).

As the high interannual variability of winter/spring ozone and temperature in the NH has been subject of many recent investigations (e.g. [*Pawson and Naujokat*, 1999; *Harris et al.*, 2002; *Eichmann et al.*, 2002; *Weber*, 2002]), this year's warming event in the SH motivated a closer look at the connection between planetary-scale wave activity and winter/spring ozone in both hemispheres using meteorological analysis from UKMO [*Swinbank and O'Neill*, 1994] and multi-annual trace gas observations from the Global Ozone Monitoring Experiment GOME from the period 1995–2002 [*Burrows et al.*, 1999]. The links between chlorine activation, winter volume of polar stratospheric clouds, which foster heterogeneous reactions and the build-up of active chlorine from reservoir species, and winter eddy heat flux are investigated using GOME observations of total ozone and OClO column amounts in both hemispheres.

3.4 GOME trace gas data

The GOME spectrometer was launched aboard the European Remote Sensing Satellite (ERS-2) in April 1995. It observes the back-scattered radiation in nadir viewing geometry having an across-track swath width of 960 km yielding global coverage of the sunlit part within three days [*Burrows et al.*, 1999]. From the UV/visible radiance vertical columns of several trace gases, for instance, O_3, NO_2, BrO, and OClO [*Burrows et al.*, 1999; *Richter et al.*, 1998; *Wagner et al.*, 2001] are retrieved using the differential optical absorption technique (DOAS). Total ozone used here are the GOME Data Processor (GDP) Version 2.7 data [*DLR2000*, 2000; *Bramstedt*, 2002]. Zonal mean total ozone values were derived from area-weighted and gridded daily total ozone values as shown in Figure 1.

As OClO is photolysed rapidly, it only achieves significant daytime concentrations under twilight condition near the terminator line. Slant columns have been converted to vertical columns using air mass factors (AMF) computed with a multiple scattering radiative transfer model GOMETRAN [*Rozanov et al.*, 1997] for standard profiles for OClO. The absolute errors of OClO vertical columns under twilight condition are, therefore, conservatively estimated at 50% [*Weber*, 2002]. In order to evaluate the inter-annual variability of chlorine activation for both hemispheres a proxy for the cumulative winter chlorine activation has been defined by summing up the daily maximum OClO vertical column amounts at 90° solar zenith angle between May and September (November and March in NH) and by dividing that number by 365.

3.5 Meteorological analysis

Meteorological quantities are derived from the UKMO assimilation data system [*Swinbank and O'Neill*, 1994]. The eddy heat flux $\overline{v'T'}$, a proxy for the vertical

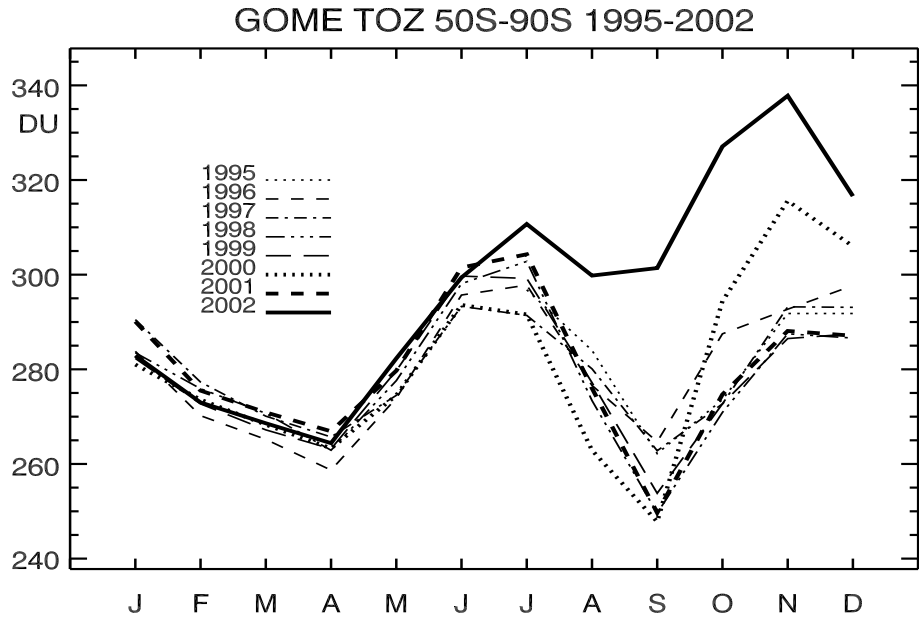

Figure 3.7: Area-weighted GOME total ozone between 50°S and 90°S excluding polar night region

.

component of the Eliassen-Palm flux and the strength of planetary wave activity, is calculated in a similar manner as described by [*Randel et al.*, 2002b]. It was determined at the 100 hPa level and an area-weighted average was calculated from 43° to 70°, the latitude range where it reaches maximum in both hemispheres. Monthly mean heat flux values are calculated from the daily means.

Figure 2 shows the range of the monthly mean and transient heat flux observed during the last decade in the SH. The transient heat flux is here defined as the square root of the sum of the squared differences between daily values and the monthly mean and can be interpreted as the variability within a given month. In winter/spring 2002 the SH transient heat flux was above the usual decadal range (1992–2001) starting in July 2002 and this anomaly was highest in September 2002, almost at twice the maximum value observed within the last ten years. This is in line with the observation that the hemispheric total ozone started to deviate from the typical range observed in previous years (1995–2001) in July 2002 and reached a maximum enhancement of 35–50 DU in September 2002 as shown in Figure 1. The anomalous peak in the (absolute) monthly mean heat flux in September 2002 was followed by an extremely low value in October, which was responsible for the return of the westerly stratospheric circulation at 60°S and 10hPa (not shown here) thus preventing the major warming from becoming an exceptionally early final warming [S03].

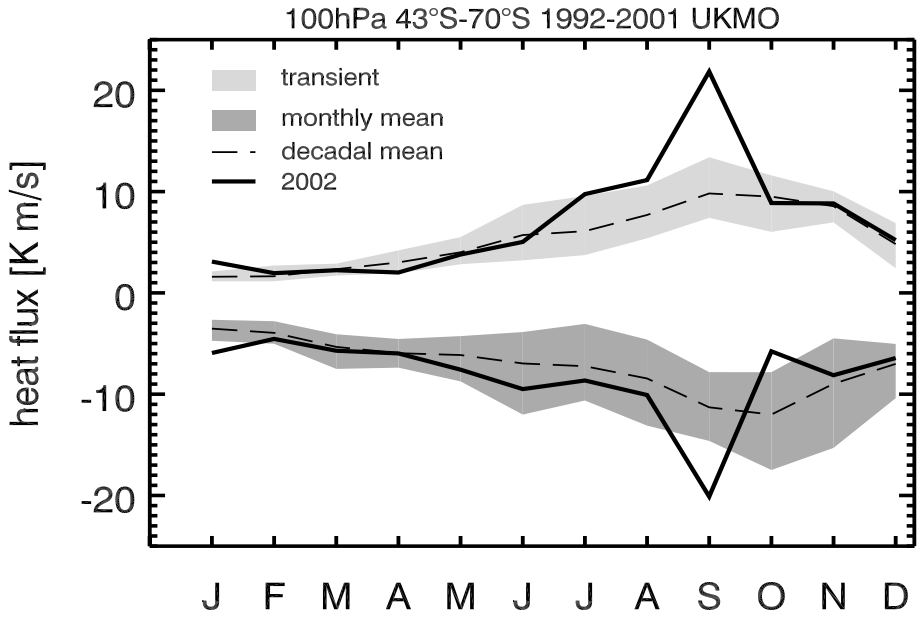

Figure 3.8: UKMO monthly mean and transient heat flux 1992–2002. The shadings indicate the range observed during the last decade with negative values being monthly means and positive values being transient. The dashed lines show the decadal mean while the solid lines show the time series in 2002.

3.6 Dynamical control of spring ozone

Before looking at the connection between winter heat flux and early spring ozone, the relationship between PSC volume, which can be regarded as a proxy for the chemical ozone depletion inside the polar vortex, and winter heat flux is investigated. Figure 3 depicts the correlation between winter heat flux and PSC volume inside the polar vortex for the period 1992–2002. The mean winter eddy heat flux was derived from Gaussian integration of monthly heat fluxes between March and September (between September and March in NH) and by dividing that number by the sum of weights. The average PSC volume, V_{PSC}, was obtained by integrating daily derived volumes of the extratropical region with temperatures below PSC existence threshold temperatures of 195 K between May and October (November and March in NH) and dividing that value by 365 (units km^3).

The clustering of data points can be divided into three regimes, 1) the unperturbed cold Antarctic winter with high PSC volume ($>100\times10^6$ km^2) and low absolute winter heat flux, 2) cold Arctic winters (92/93, 94/95-96/97, 1999/00) with moderate PSC volumes and moderate winter heat fluxes, and 3) warm Arctic winters with low or negligible PSC volumes and high winter heat flux (1993/94,

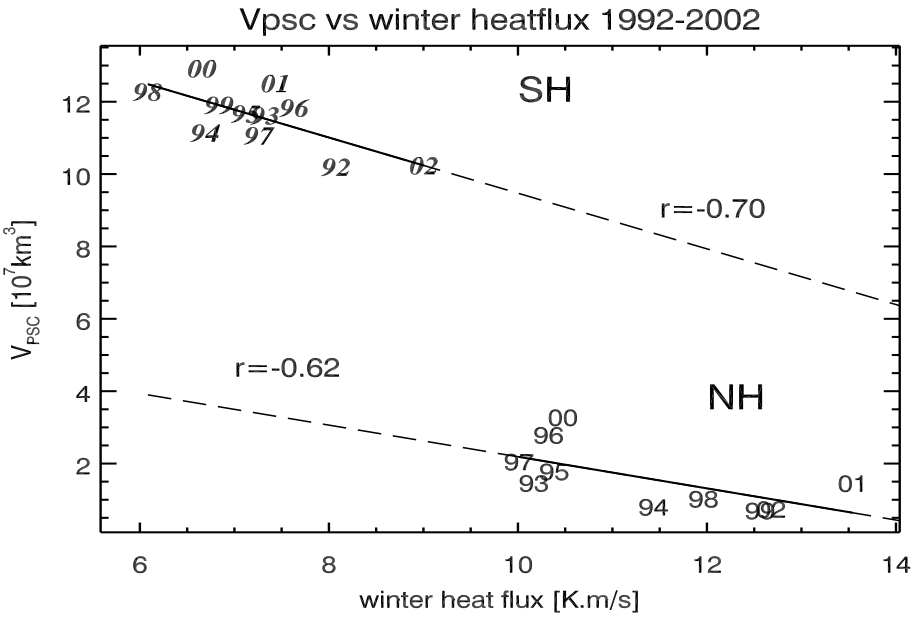

Figure 3.9: Scatter plot of winter integrated PSC volume and winter heat flux at 100 hPa. Years for northern hemispheric winters are given for March (non-italics), e.g. 99 means boreal winter/spring season 1998/99.

97/98, 98/99, and 2000/01, 2001/02). The austral winter/spring season 2002 can be regarded as a new class with elevated winter heat flux and a winter PSC volume, smaller than normal but still considerably higher than one observed during cold Arctic winters. Different fitting curves through the data in Figure 3, two linear curves for each hemisphere (correlation coefficient r of -0.76 and 0.67 in SH and NH, respectively) show that the relationship between heat flux and PSC volume is not as simple as stated earlier. Particular care has to be taken by extrapolating the results from one hemisphere to the other.

In Figure 4 the relation between the winter mean of maximum OClO column amounts observed at 90°SZA in both hemispheres and the winter heat flux is shown. Both quantities show a correlation coefficient of $r = -0.94$. This plot together with Figure 3 proves the strong linkage between chlorine activation (and as a consequence chemical depletion of ozone) in the polar region, stratospheric temperatures (as indicated by PSC volume), and the mid- to high latitude winter wave activity. The linear relationship as shown in Figure 4 is nevertheless in contrast to the non-linear relationship in PSC volume between hemispheres as shown in Figure 3. This may be explained by the fact that assuming complete chlorine activation (like in cold Arctic winters and regularly above Antarctica) the main difference in observed maximum hemispheric OClO columns results most likely from activated air masses extending over a larger altitude range in austral winter/spring [*Wagner et al.*, 2001]

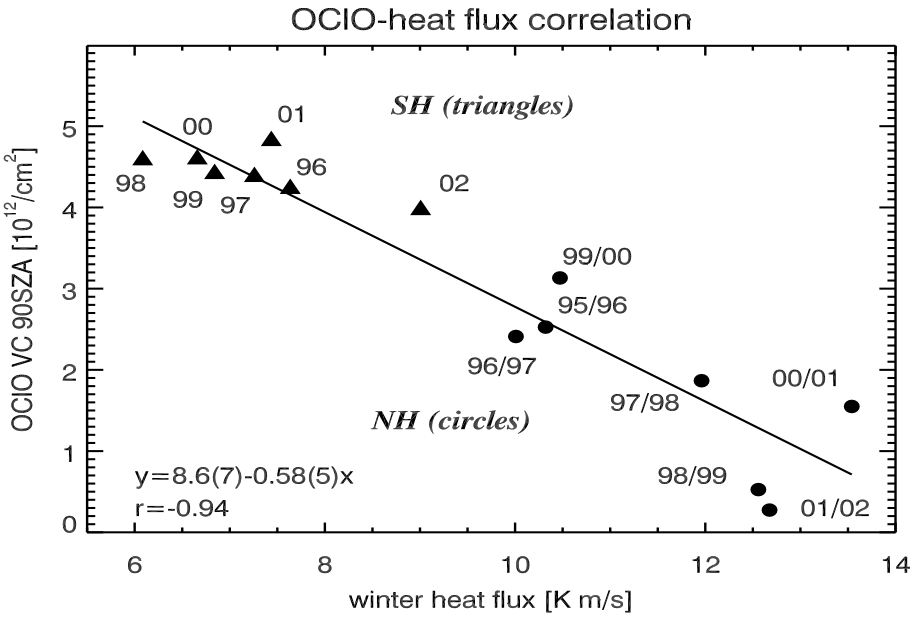

Figure 3.10: Relationship between mean winter OClO vertical column amount and winter heat flux. Note that the SH mean winter heat flux is negative but is plotted with a positive sign.

In Figure 5, the spring-to-fall total ozone ratio poleward of 50° (March over September in NH and September over March in SH) is shown as a function of the average winter heat flux. By combining data from both hemispheres a remarkably compact relationship between both parameters and hemispheres is found. The spring/fall total ozone ratio is generally below one in the SH indicating that the chemical ozone depletion inside the Antarctic vortex more than outweighs the gain resulting from the accumulated diabatic descent during winter (see also Figure 1), except for the 2002 austral spring where the ratio reached 1.15. During cold Arctic winters the GOME spring-to-fall ratio is slightly below 1.4 and well above that value during the so-called warm Arctic winters. The relationship between the winter heat flux and the hemispheric ozone gain shows a correlation of r=0.97 at a 95% confidence level. The same correlation is achieved, if the analysis is based on ozone zonal mean, poleward of 60°. [*Andersen and Knudsen*, 2002] have shown that 75% of the decrease in March total ozone north of 63°N in the mid nineties can be attributed to polar vortex chemical depletion. As shown in Figure 4 of their paper and in this study, two depletion mechanisms are closely coupled. Low winter wave activity reduces the winter supply of ozone through diabatic descent and the low polar stratospheric temperatures associated with it lead to additional chemical depletion due to enhanced PSC formation and chlorine activation in such cold stratospheric winters.

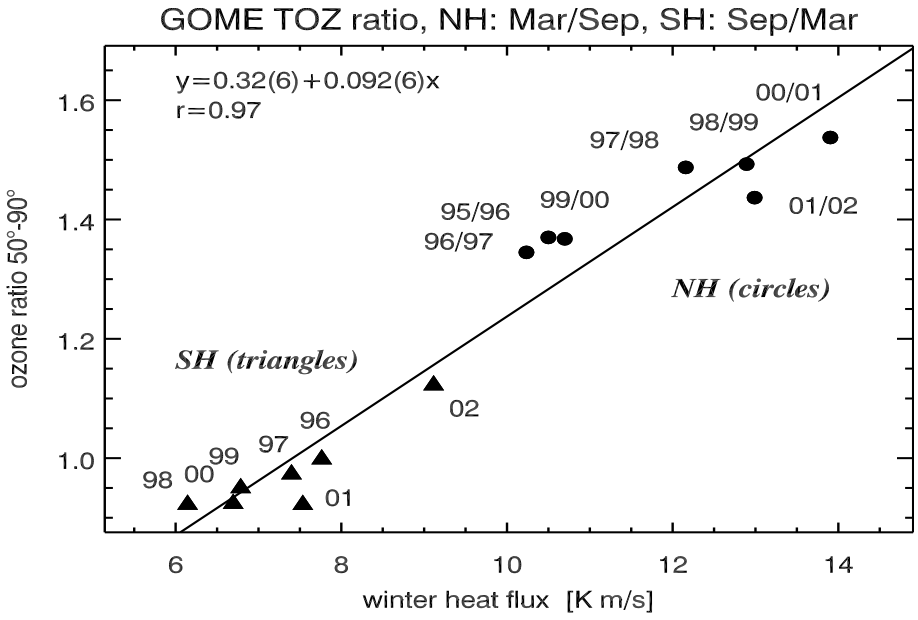

Figure 3.11: Correlation between winter total ozone ratio (SH: Sep/Mar ratio, NH: Mar/Sep ratio) and mean winter heat flux. Note that the SH mean winter heat flux is negative but is plotted with a positive sign.

3.7 Discussion and conclusion

It has been shown that the interannual variability of the mid latitude winter eddy heat flux at 100 mbar correlates extremely well with the variable hemispheric ozone spring/fall ratio when combining data from both hemispheres. This ozone ratio is largely determined by the cumulative effect of the residual circulation driven by the planetary-scale wave activity throughout the winter in conjunction with different levels of chemical depletion. This year's major warming event in the SH clearly proved the robustness of this close relationship. The unusual September 2002 ozone gain lies almost midways between the values for typical cold Arctic winters and all other Antarctic winters observed by GOME. As planetary scale wave activity has an impact on polar stratospheric temperatures [*Newman et al.*, 2001] and PSC formation, the polar vortex ozone depletion becomes closely linked to the planetary-scale wave activity driving the slow meridional circulation. A surprising result was that the abnormal wave activity in austral winter/spring 2002 lead only to a minor reduction in winter OClO in line with the notion of almost no changes in chemical ozone loss compared to earlier Antarctic winters [S03].

Several model studies have demonstrated that the decadal decline in mid- to high latitude ozone in combination with increases in greenhouse gases induce a negative stratospheric temperature trend, which in turn may reduce the strength

of the residual circulation [*Shindell et al.*, 1998, 2001; *Schnadt et al.*, 2002]. This feedback mechanism may potentially delay future ozone recovery despite anticipated decline in stratospheric chlorine levels [*Shindell et al.*, 2001], although there are some indications for a possible intensification of planetary wave activity in the NH [*Schnadt et al.*, 2002]. The observed longterm trends in polar stratospheric temperatures and total ozone in both hemispheres support the notion of a positive feedback mechanism [*Randel et al.*, 1999].

The effect of the planetary-scale activity on ozone and polar stratospheric temperature occur on short time-scales ranging from a month [*Fusco and Salby*, 1999; *Randel et al.*, 2002b; *Newman et al.*, 2001] up to an entire season (this study). This close interaction of meteorology and chemistry on short time scales complicate the identification of the cause-effect relationship on decadal time scales. Identification of longterm changes in the residual circulation beyond the natural variability may, nevertheless, provide an important clue to the connection between climate change and stratospheric ozone. The unusual major stratospheric warming event in the SH may provide a hint that apart from expected changes in halogen loading two competing forcing mechanism may gain importance in influencing future ozone trend: first, stratospheric cooling due to changes in radiative forcing as a consequence of increased greenhouse gases and, secondly, enhanced interannual variability of winter heat flux as a result of a warming trend in the coupled ocean-troposphere system.

3.8 Some additional results

A detailed analysis of the above discussed winter-time eddy heat flux at 100 hPa and ozone gain has been carried out for different total ozone data set such as TOMS V8, SBUV V8, GOME WFDOAS, and ground based station data. Possible influence of eddy heat flux differences between ECMWF (ERA40: 1979-2001 and Operational analysis: 2002-2003) and NCEP on the observed relationship are also studied. Some of the important findings of this analysis are discussed below:

- Figure 3.12 shows the relationship between winter time eddy heat flux and ozone gain relationship using 25 years of SBUV V8 total ozone data [1979-2003]. Eddy heat flux is calculated using meteorological data from ECMWF as explained in Section 3.5. Although overall relationship is quite compact ($r = 0.88$) for last two and half decades of data, most striking feature of this scatterplot is the clustering of data points from both hemispheres. Almost for all the years NH eddy heat flux ranges between 12-17 K m/s, but ozone gain ratios show large variability between 1.2 to 1.5. Such a clustering of data points can seriously undermine the importance or validity of the proposed dynamical proxy. In addition, changes in the ozone gain and eddy heat flux relationship are also shown for three different time period which include initial seven years (1979-1984), last seven years (1996-2003), and 25 years (1979-2003) of data period. Although correlation coefficients are nearly similar for the first and last seven years ($r = 0.91$ and

$r = 0.92$ respectively), changes in the slopes of regression lines (shown in Figure 3.12), have been observed. Regression line for latter years (1996-2003) shows a slightly higher slope compared to the initial years.

Also note that changes in regression lines as well as clustering of data points can also arise due to some other factors, such as quality of meteorological data set, changes in stratospheric aerosol loading due to major volcanic eruptions, and changes in chemical ozone loss mechanism. Firstly, as noted in Chapter 2, almost all reanalysis model have undergone significant changes in the observational data sources on both spatial and temporal scale. As eddy heat flux is a highly derived quantity (second order), changes in reanalysis data set can have a larger role on the observed relationship. Secondly, large ozone losses associated with increase in stratospheric aerosol loading due to major volcanic eruptions such as El Chichón (1982) and Mount Pinatubo (1991) were widely reported [*Solomon et al.*, 1996]. Years with high stratospheric aerosol loading (such as 1984/85, 1992/93,1994/1995) are readily distinguishable in the scatter plots and can significantly distort the ozone-eddy heat flux relationship. Thirdly, change in ozone depleting substances (such as CFCs, Halons) and other reactive species (such as H_2O) can significantly alter efficiency of chemical ozone loss by heterogenous chemistry [*WMO*, 2003]. Changes in stratospheric chlorine and bromine loading are well documented [*Montzka et al.*, 1996, 1999] and hence can play a vital role in altering the relationship between ozone gain and eddy heat flux.

- Nearly similar results were obtained for TOMS/SBUV merged data, but correlation coefficients are quite low (less than 0.5) for zonally averaged station data (not shown here). This implies that the empirical relationship between eddy heat flux and ozone gain is significant only for zonally averaged total ozone from satellite instruments (as explained by theory) but its use is limited for ground-based station data sets with limited geographical coverage.

- For the period of 1996-2003, nearly all the satellite measurements show high correlation between winter heat flux and mid-high latitude winter ozone gain. Using new version of GOME WFDOAS total ozone and eddy heat flux from ECMWF, correlation is slightly higher ($r = 0.98$) than that shown in Figure 3.11. This could be either due to improvements in total ozone retrieval using WFDOAS algorithm specially at higher latitudes [*Lamsal*, 2006] or higher resolution of ECMWF data for eddy heat flux calculation.

- The use of eddy heat flux data from NCEP slightly improves correlation coefficient for 1979-1985 period ($r = 0.94$) than that from ECMWF (see Figure 3.12), but for latter period (1996-2003) correlation coefficients are almost similar. As noted in Chapter 2, both assimilation model and assimilation methods at ECMWF and NCEP have significant differences. In addition, parametrization for gravity waves and wave drag can also play an important role in determining eddy heat flux contribution.

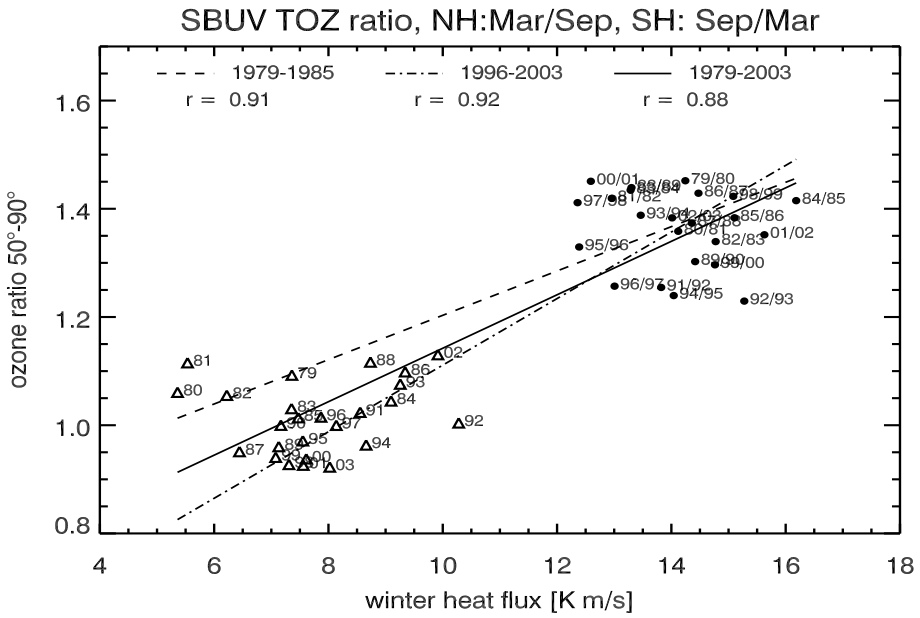

Figure 3.12: Same as Figure 3.11, but for SBUV V8 total ozone [1979-2003] and heat flux from ERA40 [1979-2001] and ECMWF operational analysis [2002-2003]. Regression line and correlation coefficients are shown for three different time period. Linear regression fit for the time period of 1979-2003 is shown by solid line. A fit for first seven years (1979-1985) is shown by dashed line and that for last seven years (1996-2003) is shown by dashed broken line.

- Latitudinal dependence of this relationship is shown in Figure 3.13, Figure 3.14 and Figure 3.15. It shows correlation between winter-time ozone gain (from WF-DOAS GOME total ozone) and eddy heat flux (from ECMWF) for various latitude bands. Although seasonal cycle in total ozone is largest at higher latitudes (e.g. 80°-90°), satellite data are not available during polar night. In March (for NH) and in September (for SH) sufficient number of observations are available for 60°-70° latitude band and winter ozone gain for this latitude band is shown Figure 3.13. As discussed in Chapter 1, BD circulation transports photochemically produced ozone from tropics to higher latitudes. Positive and significant correlation coefficient ($r = 0.95$) for 60°-70° latitude band confirms that increase in eddy heat flux leads to increase in total ozone at higher latitude. The opposite is true for tropical latitudes and is shown in Figure 3.15. For e.g., for 10°-20° latitude band a strong anti-correlation ($r = -0.95$) between wintertime ozone changes and eddy flux has been observed. Higher eddy flux or strong wave activity leads to higher ozone transport at higher latitudes and lowers the ozone concentration at lower latitudes. As noted in earlier sections, SH winter ozone gain in year 2002, lies mid-way between typical Antarctic and cold Arctic winters. This is coherent

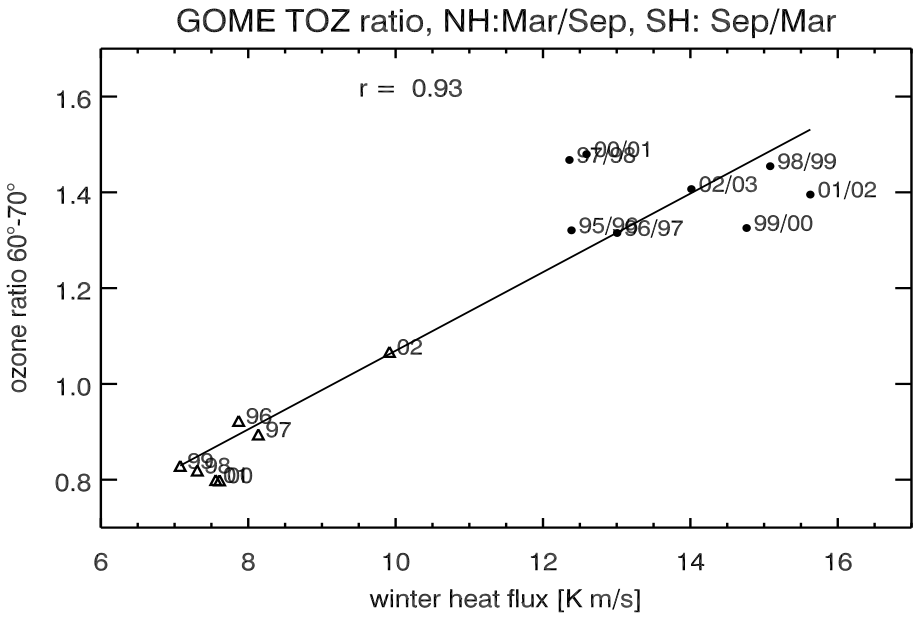

Figure 3.13: Same as Figure 3.11 but for WFDOAS total ozone for 60°-70° latitude band and eddy heat flux from ECMWF

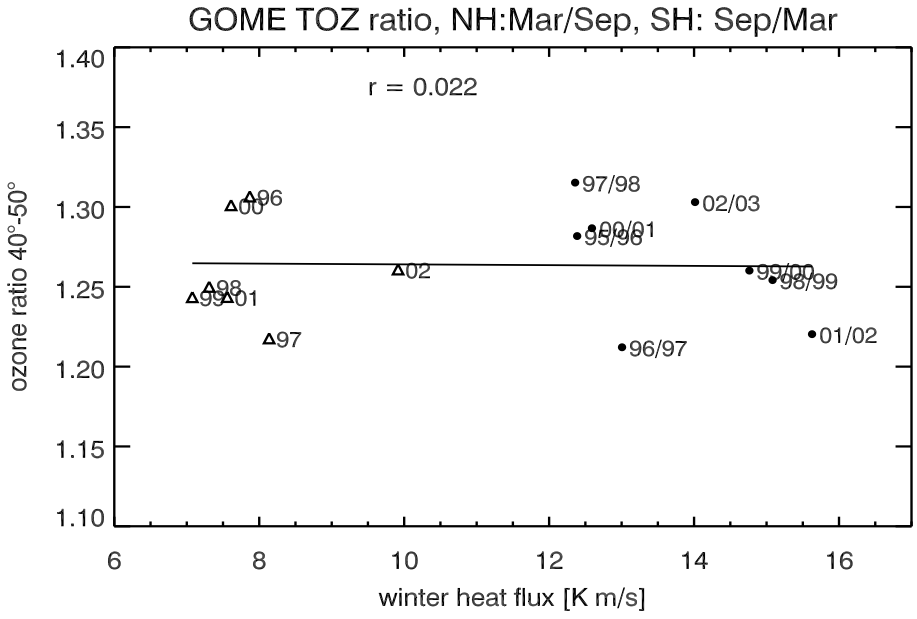

Figure 3.14: Same as Figure 3.11 but for WFDOAS total ozone for 40°-50° latitude band and eddy heat flux from ECMWF

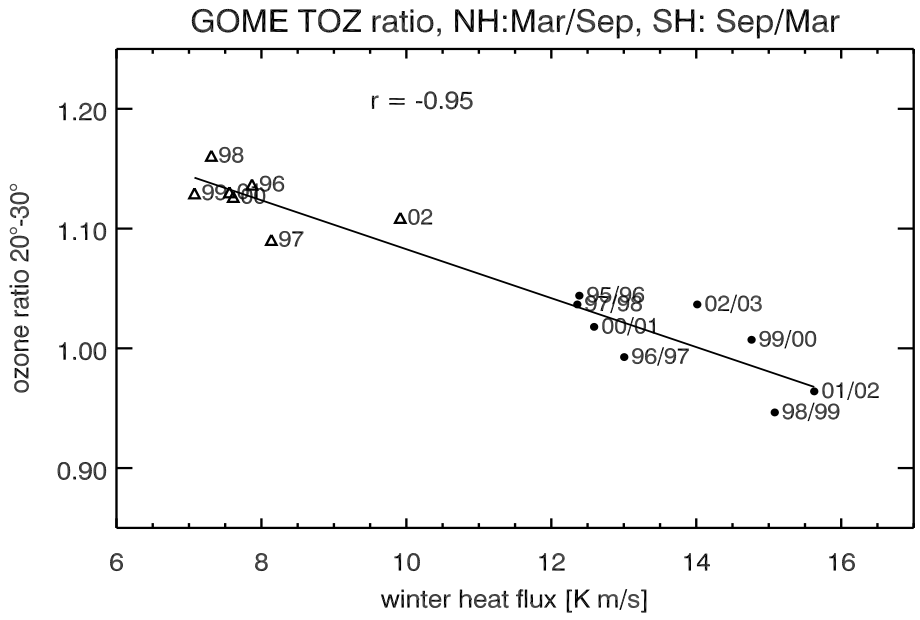

Figure 3.15: Same as Figure 3.11 but for WFDOAS total ozone for 20°-30° latitude band and eddy heat flux from ECMWF

with our current understanding that seasonal cycle in total ozone in tropics and at high latitudes is strongly regulated by planetary wave driving [*Haynes et al.*, 1991; *Rosenlof and Holton*, 1993b]. At mid-latitude, for e.g. 40°-50° latitude band (shown in Figure 3.14) negligible correlation ($r = 0.02$) between ozone gain and eddy heat flux shows that at this latitude band eddy flux has very little impact on ozone. At this latitude band there is a balance between winter ozone gain from tropical latitude through upwelling in tropics and ozone transport at higher latitudes through downwelling branch of BD circulation. These two mechanisms cancel the effect of each other showing no or little influence of planetary wave driving at 40°-50°. Away from these latitudes, effect of wave driving increases with positive correlation at higher latitudes and negative correlation at lower latitudes.

3.9 Concluding remarks

In this chapter a new proxy has been proposed for the attribution of dynamical influence on interannual ozone variability. Mid-latitude winter time heat flux is a useful quantity accounting for both interannual ozone variability due to transport and chemical ozone loss at higher latitudes. Using seven years of GOME total ozone (1996-2002) and eddy heat flux from UKMO data, a compact relationship between winter time ozone gain and planetary wave activity has been demonstrated. Using GOME OClO (which is proxy for springtime chlorine activation) it has been also shown that wave driving not only

controls the high latitude ozone transport but also ozone loss by heterogenous chemistry by controlling the polar stratospheric temperatures. Very strong wave activity in SH in year 2002 led to the first observed major stratospheric warming in the SH. This lead to quite unusual ozone gain for years 2002 in SH which lies almost midway between typical austral winter ozone gain and cold boreal winter ozone gain.

In addition, this analysis was extended for some of the recently updated total ozone satellite data sets such as TOMS, SBUV, WFDOAS GOME. Nearly all the satellite data set shows very good correlation between winter-time ozone gain and eddy heat flux. For longer data records (1979-2003), there is considerable clustering of the data points, which undermines the robustness of the proposed relationship. Although exact causes are not known such a clustering can also arise from some of the other processes such as changes in meteorological data quality, changes in stratospheric aerosol and halogen loading. In addition latitude dependent relationship between wintertime ozone change and eddy heat flux is coherent with our earlier understanding. Increase in mid-latitude eddy heat flux leads to increase in high latitude ozone but decrease in ozone at lower latitudes.

4 Solar cycle variability and the QBO

Solar radiation reaching earth varies with time because of cyclical changes in the sun's activity. Although these variation are quite small in magnitude, it is believed that they translate into climatic variability through various other indirect processes [*Rind*, 2002]. Understanding the nature of these processes is quite important because the solar signal must be distinguished from the anthropogenic signal to understand the human influences on climate change and ozone variability. Using 48 years of data (1958-2005) from ECMWF and NCEP, statistically significant variations in stratospheric temperatures, geopotential heights, and wind field distribution in phase with the solar cycle are shown. Both data set show consistent pattern of Quasi-Biennial Oscillation (QBO) phase dependent atmospheric response to solar variability throughout the low and high latitude stratosphere. In order to firmly establish the existence and nature of the detected sun-climate relationship, a multiple regression analysis is applied to temperature and wind data for the time period of satellite data (1979-2005). Regression analysis shows that the solar response is robust in NH polar stratosphere during winter season whereas in tropics it is observed throughout the year. A weaker solar signal is observed in the SH polar stratosphere using ECMWF temperature data. This is possibly due to the presence of temporal inhomogeneities in ECMWF data having substantial impact on decadal signals, which may strongly affect the observed sun-climate relationship as well as climate trends.

4.1 Overview

Sun is the ultimate driving force of the earth's atmosphere. The amount of solar radiation received at the outer surface of the earth's atmosphere does not change much (normally represented by the solar constant) from an average value of 1366 W/m^2. The variations in total solar output associated with solar cycle are so insignificant (as a percentage of total output) that they remained at or below the threshold of detectability until the satellite era, although a small fraction of ultraviolet wavelengths varies by a few percent. Total solar output is now measured to fluctuate (over the last two 11-year sunspot cycles) by less than 0.1 % or about 1 W/m^2 from minimum to maximum of the 11 year sunspot cycle. Even though these variations are quite negligible, various attempts have been made to detect the possible influence of solar variability on the structure and composition of the earth's atmosphere. Since 1978 satellite data have shown variations over the 27-day solar rotation period of e.g., 6% at 200 nm and 2.5% at 250 nm [*Cebula and DeLand*, 1998]. Variations in stratospheric composition and thermal structure resulting from ultraviolet irradiance changes may have an influence on climate. The first mechanism whereby this might occur is through changes in

radiative forcing [*Haigh*, 1996]. Thus, in addition to a direct increase in downward short-wave irradiance at the tropopause, higher solar activity can cause an increase in downward infrared flux by heating the stratosphere and also radiative forcing due to O_3 changes. However, the response of O_3 to solar variability is not well established.

Some of the two dimensional model simulations [*Haigh*, 1999; *Fleming et al.*, 1995], predicted that the largest fractional changes occur in the middle-upper stratosphere with monotonically decreasing effects towards the tropopause. Using zonally averaged CHEM2D photochemical-dynamical middle atmosphere model, *McCormack* [2003] showed changes in QBO propagation as an effect of the 11-year cycle variation in solar ultraviolet (UV) irradiance. Changes in stratospheric thermal structure may also affect the troposphere through dynamical interactions rather than through radiative forcing. *Kodera* [1995] suggested that changes in stratospheric zonal wind structure, brought about by enhanced solar heating, could interact with vertically propagating planetary waves in the winter hemisphere to produce a particular mode of response. Using a GCM with an upper level at 10 hPa and few stratospheric levels, *Haigh* [1999] showed a pattern of change in zonal mean temperature that was consistent over a range of assumptions concerning the magnitude of the ultraviolet and ozone changes. This pattern consisted of warming in the stratosphere (except in winter high latitudes) and a vertically layered structure in the troposphere due to shifts in the positions of the sub-tropical jets. *Rind and Balachandran* [1995] investigated the impact of large increases in solar ultra-violet on the troposphere with a GCM and confirmed that altered refraction characteristics affect wave propagation in winter high latitudes. *Haigh* [1999],*Shindell et al.* [1999a], and *Larkin et al.* [2000] introduced realistic changes in ultraviolet and ozone into GCMs and found that the inclusion of the ozone has a significant effect on simulated climate through various feedback mechanisms. *Kodera and Kuroda* [2002] found that the stratospheric response originates in the tropical stratopause region, and propagates poleward and downward through the winter. This propagation mechanism involves the interaction of planetary-scale waves with the zonal mean flow so that the net effect is to draw wind anomalies poleward and downward through the stratosphere.

Such modeling studies have important implication on understanding of the response of various forcing on the future climate. But most of these models have their own drawbacks, as most of them rely heavily on parameterizations of some important processes. In particular, most of the GCM have difficulties in reproducing QBO due to its complexity [*Hamilton et al.*, 1999].

Another possibility to study solar influence is to use observational data, but ground based data are extremely inhomogeneous on both spatial and temporal scale. Since beginning of satellite era various instruments have been providing useful global measurements of ozone and temperature. Using UKMO TOVS temperature data, which is compiled using various satellite irradiance data, *Scaife et al.* [2000] detected largest solar response over tropical stratosphere (up to 1 K) between 70 hPa and 1

hPa. Multiple regression analysis of satellite data, as carried out with SBUV data by *McCormack and Hood* [1996] and *Miller et al.* [1996], suggests the largest changes in the upper and lower stratosphere and no, or even slightly negative changes in the middle stratosphere. However, during these studies the data from just one and a half solar cycles were available. These might not have properly accounted for the effects of enhanced volcanic aerosols from El Chichón and Mount Pinatubo during solar maximum condition [*Solomon et al.*, 1996; *Lee and Smith*, 2003].

To study solar-climate interaction evident choice is to use operational analysis or reanalysis data. Although these data sets have their own limitations they are the most reliable simulations of the real atmosphere. Reanalysis data set offer a balanced and dynamically consistent time series of various meteorological parameters to study sun-climate interaction. Using such analysis/reanalysis data set, solar cycle-ozone interaction was presented by *Labitzke et al.* [2002],*Hood and Zhou* [1999], *Crooks and Gray* [2005] indicating a tropical solar cycle signal of about 1 K in the lower stratosphere. Yet, the largest signal is found during winter over the pole [*Labitzke and van Loon*, 1993], where the solar radiation is the least. This might be due to the fact that tropical stratosphere undergoes very small seasonal variation compared to polar stratosphere [*Salby and Callaghan*, 2002a]. Changes of mean zonal wind in the middle atmosphere are usually associated with changes in wave forcing and feedbacks between the two, provides a mechanism for coupling between widely separated atmospheric regions. *Gray et al.* [2003] and *Gray* [2003] found that early winter zonal wind anomalies in the tropical stratopause region are important in modulating the strength of the northern polar vortex. A mechanism, that is similar to that associated with the extra-tropical QBO [*Holton and Tan*, 1980], which states that upward propagation of planetary wave is dependent on the phase of QBO. The key QBO level for maximum extra-tropical correlation in the Holton-Tan oscillation is near 40-50 hPa, whereas in *Gray et al.* [2003] key level is in the upper stratosphere near 1 hPa. Observations provide evidence that the strength of the northern polar vortex is affected by solar-induced circulation changes near the tropical stratopause.

The objective of this chapter is to study solar signal in the two most comprehensive analysis data sets produced by two climate centers, ECMWF and NCEP. Detailed assessment of solar signal is provided using correlation and regression analysis. Section 4.2 gives the details of data used in this study. The modulation of the solar signal by the QBO as well as the Holton-Tan mechanism is discussed in Section 4.3. Correlation between stratospheric temperatures/geopotential heights and solar flux is discussed in Section 4.4. Using multivariate regression analysis for the period of 1979-2005, solar influence on stratospheric dynamics is discussed in Section 4.5, followed by a summary in Section 4.6.

4.2 Data and methodology

Monthly mean temperatures, geopotential height and wind speed from the NCEP reanalysis on 17 pressure levels are used for the period 1958-2005. ERA40 (1958-2001) and ECMWF operational data (2002- 2005) are combined to obtain continuous time series for the period of 1979- 2005 on 21 pressure levels as described in Chapter 2 (hereafter called ECMWF data). From the overlapping period of January 2001- August 2002, offset values have been determined and subtracted from operational data at each grid point and pressure level. They are of the order of -2 K. QBO phases are determined using the mean zonal wind between 10°S-10°N at 44 hPa during early winter (December and January). Use of QBO and temperature/geopotential heights from the same analysis is very useful as it avoids false signal occurring due to changes in the assimilated observations in the reanalysis. As a measure of the solar variability the monthly mean values of the 10.7 cm solar flux are used. The 2800 MHz microwave daily radio flux highly correlates with the daily sunspot number and the two databases are used interchangeably. The 2800 MHz or 10.7 cm responds to the same conditions that produce changes in the visible and X-ray wavelengths. Data is obtained from *ftp://ftp.ngdc.noaa.gov/STP/SOLAR_DATA/SOLAR_RADIO/FLUX/MONTHLY.OBS*.
For correlation analysis statistical significance are calculated after fitting linear regression line. Stratospheric aerosol loading due to volcanic eruptions is same as used in NASA Goddard Institute of Space Studies (*http://www.giss.nasa.gov/data/strataer/*). Time series of temperature anomalies of homogenized radiosonde data for various latitude band is obtained from *http://hadobs.metoffice.com/hadat/hadat2.html*

4.3 QBO

Figure 4.1 shows a time versus pressure plot of the direction and magnitude of the zonal winds averaged between 10°S-10°N from ECMWF and NCEP. Westerly winds are shown by solid lines and easterly winds are shown by dashed lines. The wind phase changes descend about 1 km/month before they reach the tropopause. Just above the descending easterlies are descending westerlies. Although geostrophic wind balance is not valid over the equator, general characteristics of the zonal winds such as QBO phase and downward propagation of wind anomalies are well captured in both data sets. Differences between wind speed from these two data set are shown in bottom panel of Figure 4.1. Both easterly and westerly winds are stronger in ECMWF compared to NCEP. At 10 hPa level maximum differences during westerly and easterly phases are up to 23 m/s. This is possibly due to the fact that 10 hPa is the highest level in NCEP and winds are possibly contaminated at this level by the upper boundary condition. While differences are minimum at lower altitudes, winds are generally stronger in ECMWF. This is better illustrated in Figure 4.2, which shows amplitudes of residual of zonal wind after removing annual and semiannual harmonics at 30 hPa. As expected Figure 4.2 shows that annual and semiannual variation in zonal mean field are almost negligible between 15°S-15°N. The amplitude of residuals (or QBO) is found to be

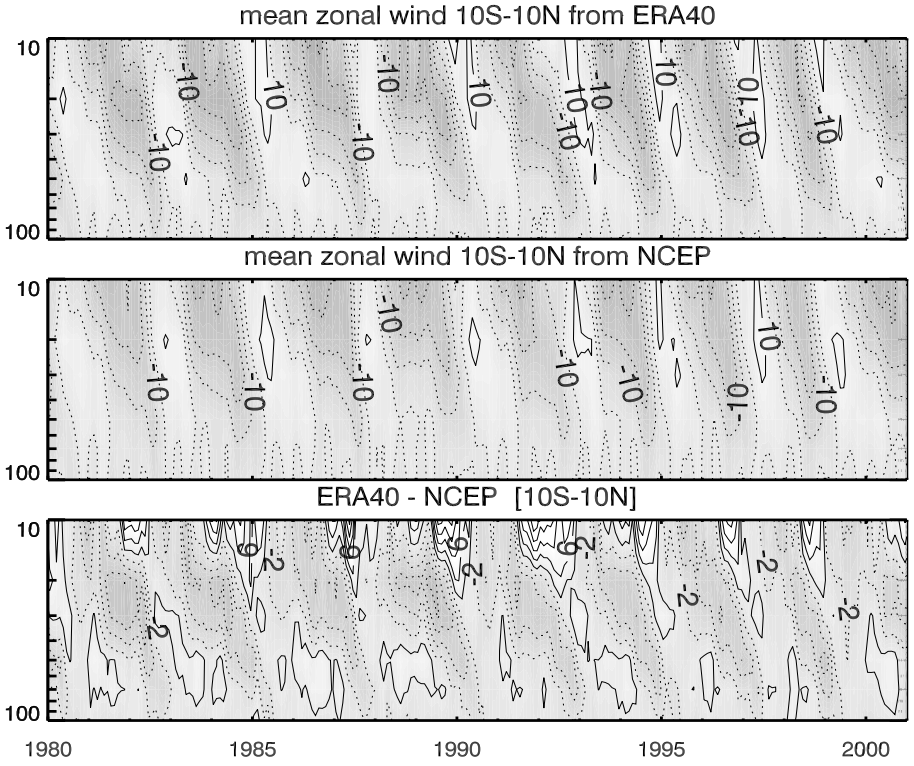

Figure 4.1: Vertical cross section of average zonal wind (10°S-10°N in m/s) from ECMWF (upper panel) and NCEP (middle panel) for 1980-2001. Differences between them are shown in bottom panel. Contour intervals are 10 m/s in upper and middle panels and 2 m/s in bottom panel. Easterly winds are shown by dashed lines whereas westerly wind are shown by solid lines.

symmetric around the equator and is largest around 50 hPa- 30 hPa (not shown here). Due to strong polar vortex in SH, largest seasonal variation are well reflected in the amplitudes of seasonal harmonics and are almost similar in both data sets. While semiannual variability in both data set is more similar in NH, larger differences are observed in SH. At about 65°S, ECMWF data shows nearly zero amplitude of semiannual harmonics, but it is quite large (∼5 m/s) in NCEP data. Another important difference is that during some years phase transition at particular levels is somewhat different in both data sets. Somewhat large differences during phase transition periods in the bottom panel of Figure 4.1 indicate that phase transition is delayed in NCEP by almost 2 months during 1980-1981. This indicates that the speed of downward propagation is probably not well captured in one of the data sets. It is also important to note that the satellite radiance data between 20°S-20°N are not used in NCEP assimilation model whereas ECMWF model is closely tied to radiosonde data [*Randel et al.*, 2004a].

As discussed in Chapter 3, the troposphere influences the stratosphere mainly

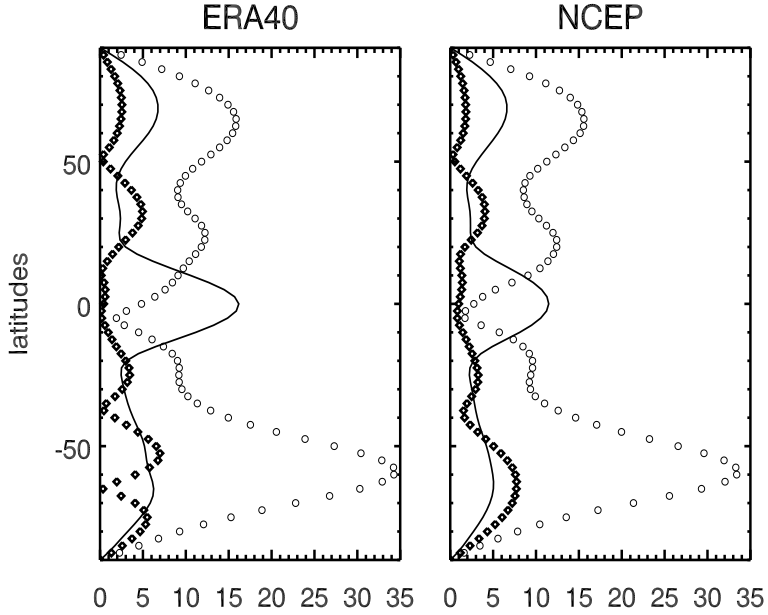

Figure 4.2: Amplitude of average wind speed between 10°S-10° N in m/s at 30 hPa after removing seasonal and semiannual cycle. Amplitude of seasonal and semi-annual harmonics is shown with open circles and squares respectively. Solid line shows the amplitude of residuals (update from *Baldwin et al.* [2001]).

through a variety of atmospheric waves that propagate upward and interact with the stratospheric flow. In the tropics QBO is driven by a combination of gravity, Kelvin, and mixed Rossby-gravity waves [*Baldwin et al.*, 2001]. In the extra-tropics, all the large-scale waves are trapped when the stratospheric flow is easterly, but only longest waves are trapped during winter when the flow is westerly [*Andrews et al.*, 1987]. During northern hemispheric winter planetary-scale Rossby waves propagate upward, refract, and reflect in the stratosphere. It is the circulation of the lowermost stratosphere (particularly in the tropical region) that determines where wave activity propagates. As first noted by *Holton and Tan* [1980], the polar vortex is, on average, weaker when the QBO is easterly.

In order to study the Holton-Tan mechanism, in both analyses, QBO indices are defined slightly differently compared to earlier studies (*Labitzke et al.* [2002] uses Singapur station data). Average zonal winds for 10^0S-10^0N (shown in Figure 4.1) at 44 hPa [*Baldwin et al.*, 2001] are used to define the QBO phase. If average December-January wind speed at 44 hPa is greater than -2 m/s, it is categorized as west phase of QBO while less than -4 m/s is categorized as east phase. There are 23 years classified as west phase of QBO in both analyses and are tabulated in Table 4.1. Classifications of phases are identical in both analyses, the years 1958 and 1995 differ and have been excluded to maintain the consistency of the analysis.

Table 4.1: Years with QBO in east and west phases from ECMWF and NCEP. Phases of QBO are determined from mean zonal wind at 44 hPa for December and January with condition of ≤ -4 m/s (east phase) and ≥ -2 m/s (west phase). Note that year 1958 and 1995 show different phases in ECMWF and NCEP and hence are excluded from the table

QBO	Years
East Phase	1959, 1961, 1963, 1966, 1969, 1971, 1973, 1975, 1977, 1978, 1980, 1982, 1984, 1985, 1987, 1990, 1992, 1997, 1999, 2001, 2002, 2004
West Phase	1960, 1962, 1964, 1965, 1967, 1970, 1972, 1974, 1976, 1979, 1981, 1983, 1986, 1988, 1989, 1991, 1993, 1994, 1996, 1998, 2000, 2003, 2005

Composite analysis of mean JFM temperature differences between east and west phases of QBO is shown in Figure 4.3. As per Holton-Tan mechanism during west phase of QBO, upward propagating planetary waves are generally reflected away from the polar vortex towards low latitudes (see Figure 3.4). This leads to a decrease in BD circulation strength leaving polar vortex colder and stronger. In addition, a decrease in tropical upwelling is responsible for higher temperatures in tropical lower stratosphere and opposite is true during east phase of QBO. As shown in Figure 4.3, this is well presented in both analyses and largest differences occur in the Arctic polar lower stratosphere. In ECMWF temperature differences are larger (about 6 K) compared to NCEP (up to 4 K). This bias in ECMWF data was already noted by *Randel et al.* [2004a]. In tropics, both NCEP and ECMWF shows similar features such as colder temperatures in tropical lower stratosphere and warmer temperatures in middle stratosphere. This is consistent with current understanding that QBO induces a secondary circulation in the mean meridional circulation. Due to this secondary circulation tropical tropopause region is colder during west phase of QBO compared to east phase of QBO [*Baldwin et al.*, 2001]. As ECMWF data extends up to stratopause, some of the other important features are evident. During west phase of QBO, colder temperatures are found ear stratopause region, warmer temperatures in middle stratosphere as well as colder temperatures in tropical lower stratosphere (also known as the three cell structure) are well represented in ECMWF. The three cell structure can be seen in the wind field and geopotential height fields (not shown here). Weaker polar vortex or decrease in westerly wind in mid-high latitude stratosphere is distinguishable in the analysis of the zonal wind field. Warmer temperatures in mid- latitude upper stratosphere is one of the key features during west phase of QBO [*Baldwin et al.*, 2001; *Collimore et al.*, 2003]. This clearly underlines the linkage between QBO phase in the tropical mid-stratosphere (as shown by *Holton and Tan* [1980]) and changes in the dynamical fields in the extra-tropical upper stratosphere ([*Gray et al.*, 2003; *Kodera and Kuroda*, 2002]) work coherently and determine the propagation properties of planetary waves.

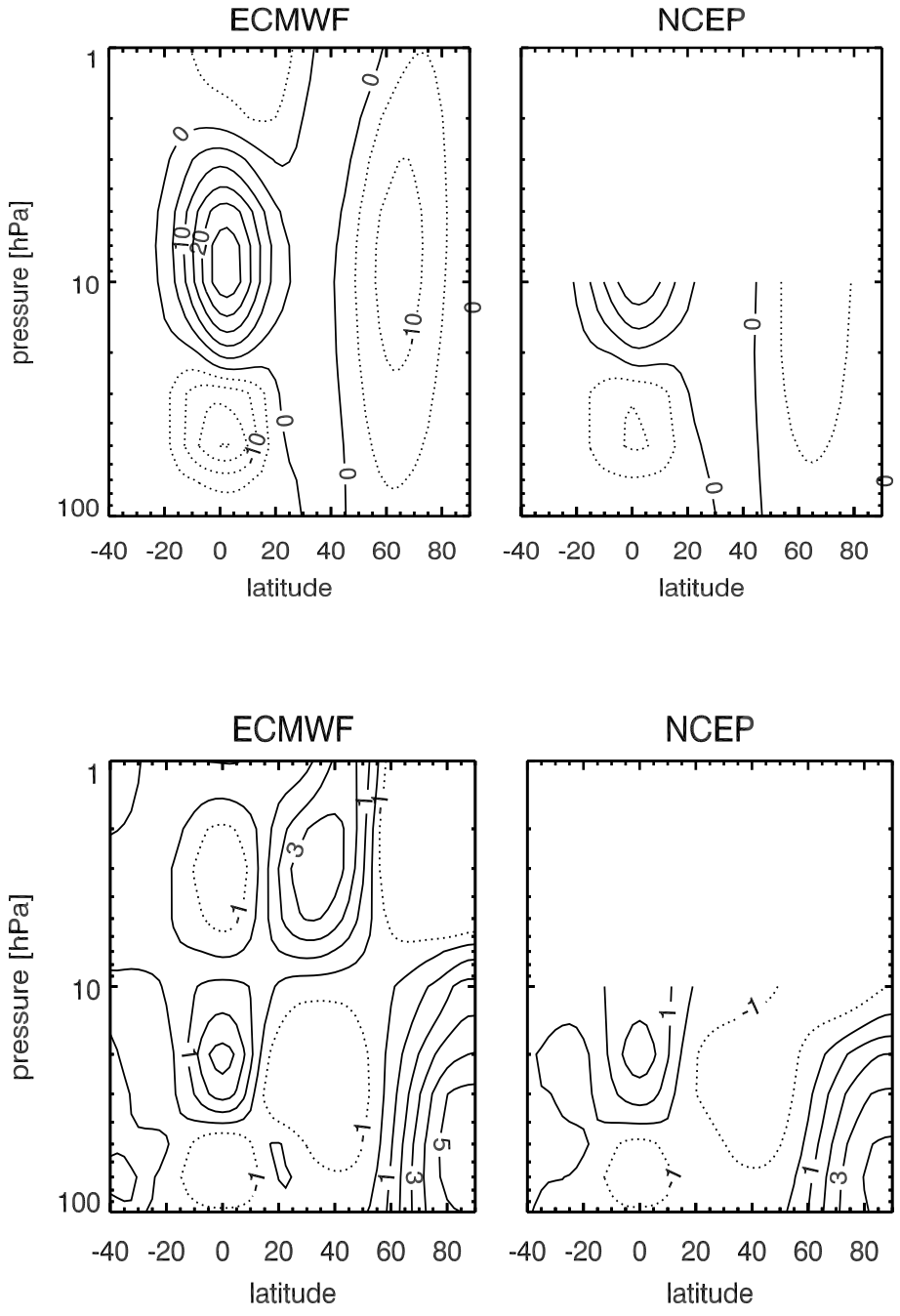

Figure 4.3: Differences of zonal mean wind in m/s (upper panel) and zonal mean temperatures in K (lower panel) during NH winter (JFM) between QBO west phase and east phase (left: ECMWF, right: NCEP).

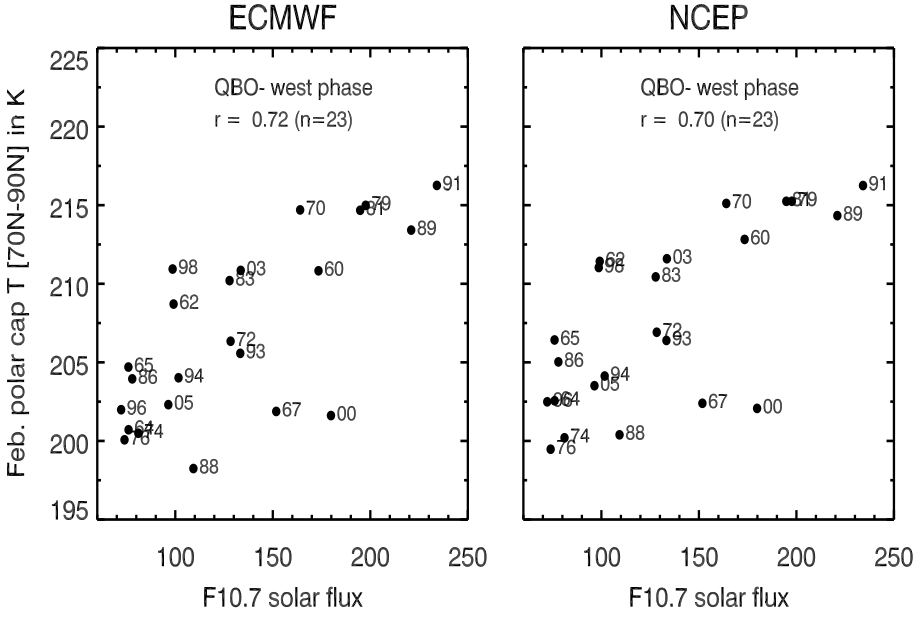

Figure 4.4: Relationship between NH polar cap temperature (70°N-90°N) at 50 hPa in February from ECMWF (left panel) and NCEP (right panel) and solar flux during west phase of QBO.

4.4 Stratospheric temperatures and solar cycle

Labitzke [1987] and *Labitzke and Loon* [1988] showed a remarkable relationship between QBO and stratospheric temperatures at higher latitudes that is well synchronized by the 11-year solar cycle. This response was originally discovered over the northern polar regions in winter and some of the recent studies have shown that this relationship is also valid for SH polar stratosphere [*Labitzke*, 2005].

Figure 4.4 is similar to that from *Labitzke* [2005], except that temperature and QBO data are from ECMWF and NCEP. QBO years with east and west phases are summarized in Table 4.1. As shown in Figure 4.4 polar cap temperatures (70°N-90°N) at 50 hPa in February and solar flux are highly correlated during west phase of QBO in ECMWF (r=0.72) and NCEP (r=0.70). During solar maxima polar cap temperatures are found to be higher and Arctic polar vortex is weaker. This relationship is found to be strongest only during middle to late winter months (highest correlation is found in February). During solar minima, Arctic vortex is more stable leading to lower polar cap temperatures. During easterly phase of QBO, solar flux and polar cap temperatures correlation is quite insignificant in February. Figure 4.6 and Figure 4.7 shows the correlation map of solar cycle and geopotential height during February for both reanalysis data sets. As shown in Figure 4.4, geopotential height changes

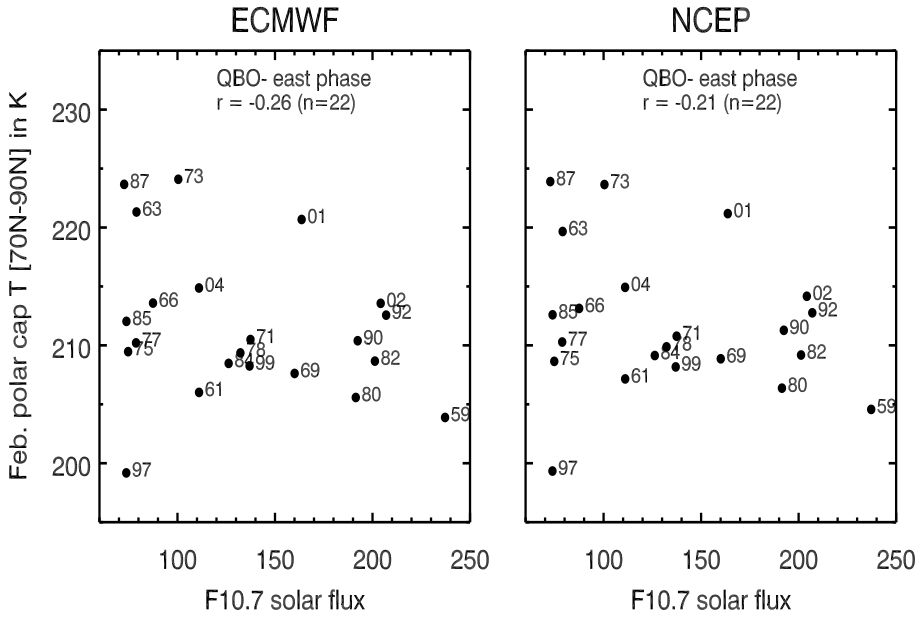

Figure 4.5: Same as Figure 4.4 but for east phase of QBO.

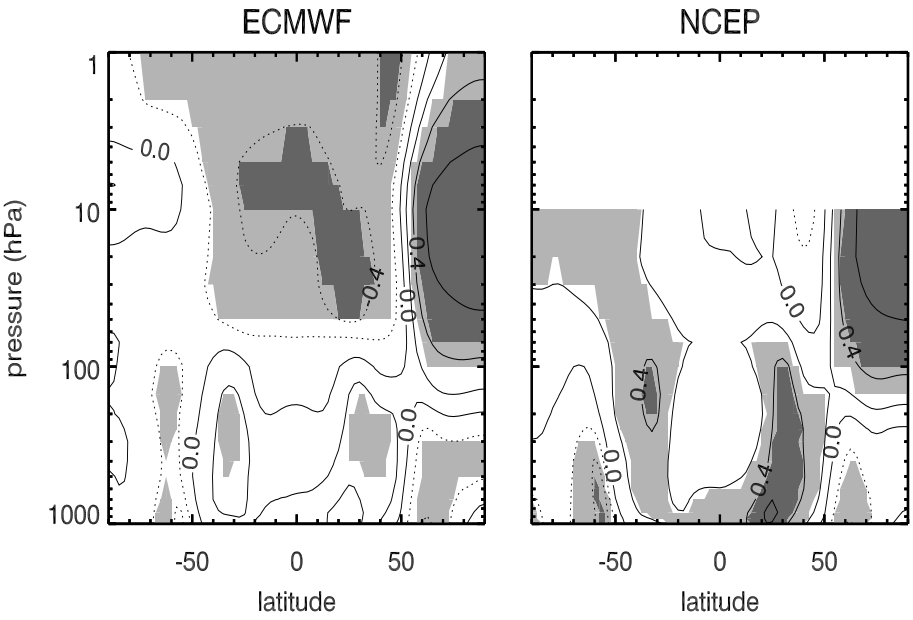

Figure 4.6: Correlation map for zonal mean geopotential height in February and solar flux during west phase of QBO (years as shown in Table 4.1). Shaded regions show 1σ (darker) and 2σ (lighter) significance.

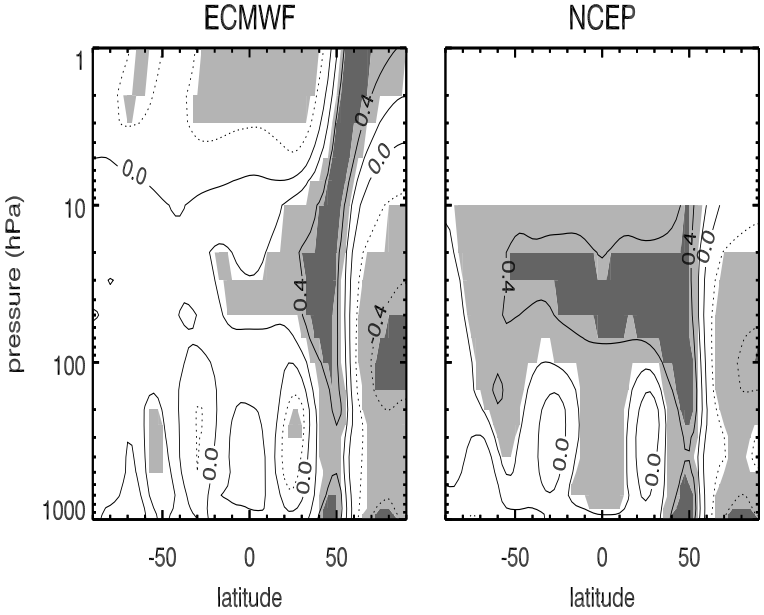

Figure 4.7: Same as Figure 4.6 but during east phase of QBO

are strongly correlated with changes in solar flux during westerly phase of QBO. In polar region, this relationship is statistically significant in both data set and extends up to the stratopause region. Interestingly these two data sets do not agree in the tropical stratosphere as well as in the troposphere. Largest differences are seen in tropical lower stratosphere, where ECMWF data shows significant correlation ($\sim$0.5), confirming possible modulation of geopotential height distribution by solar variability. This correlation is not observed in NCEP data. On the other hand, a mid-latitude tropospheric solar signal is visible in NCEP data, but is insignificant in ECMWF data. During east phase of QBO (Figure 4.7), a significant correlation ($\sim$0.4) is visible in both data set, throughout the stratosphere in the narrow band between 45°N-55°N.

Another important difference seen is the possible influence of solar variability on tropospheric circulation. As shown in Figure 4.6, NCEP data shows significant modulation of the Hadley cell circulation in NH (changes in ITCZ) as well as movement of subtropical jet whereas these features are absent in ECMWF data. These kind of discrepancies between NCEP and ECMWF data can have serious implications in climate models studying possible changes in QBO behavior related to changes in tropical wave driving.

4.5 Regression Analysis

A simple multivariate regression model used in this study has been constructed as follows

$$\begin{aligned} TOZ(n) &= \sum_{m=1}^{12} \alpha_m^{\circ} \cdot \delta_{mn} + \sum_{m=1}^{12} \alpha_m^{lin} \cdot \delta_{mn} \cdot n + \sum_{m=1}^{12} \alpha_m^{sol} \cdot \delta_{mn} \cdot sol(n) \\ &+ \sum_{m=1}^{12} \alpha_m^{qbo30} \cdot \delta_{mn} \cdot \mathrm{qbo30}(n) + \sum_{m=1}^{12} \alpha_m^{qbo50} \cdot \delta_{mn} \cdot \mathrm{qbo50}(n) \\ &+ + \sum_{m=1}^{12} \alpha_m^{aero} \cdot \delta_{mn} \cdot \mathrm{aero}(n) + \varepsilon(n) \end{aligned} \tag{4.1}$$

where $T(n)$ is the monthly mean temperatures for month n, which is a running index from month zero to 323 covering the period 1979 to 2005, α_m° are monthly constants for the annual cycle (m=1,...,12), α_m^{lin} are monthly linear trend coefficients, α_m^{hf} are solar flux variability contribution coefficients, α_m^{qbo30} and α_m^{qbo50}, QBO coefficients at 30 and 50 hPa, respectively, α_m^{aero}, is stratospheric aerosol loading terms due to strong volcanic eruption such as El Chichón and mount Pinatubo. $\varepsilon(n)$ are the residual.
(for details on regression analysis see Chapter 5), respectively. QBO indices at 30 hPa and 50 hPa are zonal mean wind between 10°S-10°N from respective analysis and they account for both both phase and amplitude of the QBO.

Figure 4.8 and Figure 4.9 show the solar signal in zonal mean temperatures for ECMWF and NCEP, respectively. For better clarity the regression coefficients are multiplied by 113 solar flux unit, which is the average change in solar flux from solar minima to solar maxima for the last three decades. The values indicated are average changes in temperature in K from solar minima to solar maxima. Most notable and statistically significant solar cycle response is observed in tropical stratosphere (30^0S-30^0N). As shown in the correlation analysis, regression coefficients also show the three cell structure in tropical stratosphere. Both data set show positive response in tropical lower-middle stratosphere (except for February and October). This is most probably the direct effect of increase in UV radiation [*Larkin et al.*, 2000; *Scaife et al.*, 2000; *Gray et al.*, 2003; *Hood*, 2003; *Crooks and Gray*, 2005]. Though scaling and magnitude of the solar response is different, regression model is in better agreement with most of the earlier studies. Statistically insignificant but slightly negative response in middle stratosphere and positive response in upper stratosphere is in agreement with *Scaife et al.* [2000]; *Hood* [2003], and *Crooks and Gray* [2005]. Detailed examination shows that the positive response in tropical lower stratosphere is in better agreement with *Scaife et al.* [2000] than *Hood* [2003]. Largest solar response (more than 1 K) in the tropical lower stratosphere is observed between June-September. This is due to the fact that planetary wave driving is minimum during these months [*Yulaeva et al.*, 1994] (see also Chapter 6). As a result of weak meridional ozone transport, increase in tropical ozone leads to increase in temperature through radiative heating.

Comparison of Figure 4.8 and Figure 4.9 shows that NCEP data shows slightly larger and homogeneous response in tropical lower stratosphere compared to ECMWF.

In the polar stratosphere, negative solar response during early winter months (December- January in NH and July- August in SH) is clearly visible in both data sets (more significant in NCEP). This confirms the findings of *Gray* [2003] that during solar maxima polar vortex is stronger and colder during early winter months (see also Figure 4.10 and Figure 4.11) and sudden stratospheric warmings (SSWs) occur more frequently during mid-winter months (February and March in NH). A sudden stratospheric warming is an event where a sudden rise in planetary wave activity leads to a deceleration of westerly polar wind speed (in a few days time) that even wind reverse the wind direction. This is accompanied by a sudden rise of stratospheric temperature by several tens of degrees. The opposite is true during solar minima, when polar vortex is weaker and conditions are more favorable for SSWs during early winter months but polar vortex is then stronger during the mid-winter period. As a result, a robust positive response from the solar variability in Arctic stratospheric temperatures is clearly visible in both data sets (up to +8 K at 10 hPa). In ECMWF data, maximum response is observed at about 10 hPa. In SH, both data show similar response during October (+3 K). Related to high frequency of mid-winter SSWs in February (NH) and October (SH) are increase in the strength of Brewer-Dobson circulation leads to strong upwelling in tropical stratosphere. Negative response (or cooling) in tropical stratosphere is caused by the increase in BD circulation (and hence increase in tropical upwelling). The tropical cooling however is not statistically significant.

Another important feature observed in both data sets is the downward propagation of solar response [*Baldwin et al.*, 2003a, b]. Warmer polar stratospheric temperatures in February and October (Figure 4.8 and Figure 4.9) during solar maxima, propagate downward into troposphere in March (NH) and November (SH). Positive response in polar troposphere cannot be a direct response of changes in solar radiation but it is an indirect effect of SSWs during mid-winter through adiabatic compression followed by diabatic descent. It is also important to note that this indirect solar response is statistically significant in NCEP as compared to ECMWF.

Solar response in the zonally averaged wind is coherent with temperature response discussed above (shown in Figure 4.10 and Figure 4.11). Stronger polar vortex (higher wind speed) during solar maxima in December and January is clearly distinguishable in both data sets. Regression analysis shows that in NH largest response occurs in lower-middle stratosphere between 50°-65° latitude band and this response is nearly identical in both data sets. As discussed earlier these results are consistent with *Gray* [2003]. Another key feature of solar response, which is not detected in temperature analysis, is the out of phase response between extra-tropical latitude (30°-40°) and higher latitudes (but correlation analysis clearly shows this feature in both analyses). This symmetrical behavior is consistent, and is possibly associated with changes in the subtropical jet streams [*Haigh*, 1999; *Labitzke et al.*, 2002]. This shows that

some of the key features observed in earlier studies are well reproduced by the regression model. For zonal wind analysis the key difference in ECMWF and NCEP is the negative solar response at polar latitudes (e.g. April in NH and September in SH). This is somewhat overestimated in the ECMWF data and is probably related to the stronger meridional circulation in observed in ECMWF data [*Uppala et al.*, 2005].

4.6 Comparison between NCEP and ECMWF

In the regression analysis largest differences between NCEP and ECMWF are observed in the SH. In order to understand the possible causes of such differences, these two data sets are compared with radiosonde data. Figure 4.12 shows comparisons of monthly mean temperature at 100 hPa between ECMWF and NCEP data with Halley Bay station data (75°S, 26°W) in October. As shown in the figure, a cold bias in ECMWF makes it nearly impossible to use data before 1979. This marks the problems associated with the assimilation method before the satellite era. The cold bias in ECMWF is significant during winter months but no such serious biases are observed in NCEP data. For the period of 1979-2005, there are no significant differences between two data sets.

For tropical latitudes comparison is done using gridded homogenized radiosonde temperature data developed at UKMO (*http://hadobs.metoffice.com/hadat/hadat2.html*). HadAT2 is a new analysis of the global upper air temperature record from 1958 to 2005 based on radiosonde data alone [*Thorne et al.*, 2005]. This analysis makes use of greater number of stations as compared to previous radiosonde analyses (e.g. LKS, *Lanzante et al.* [2003]), combining a number of digital data sources. This makes HadAT2 data suitable to determine possible discrepancies in ECMWF or NCEP data. As mentioned in Chapter 2, assimilation system for NCEP is consistent over the time period of 1958-2005, but it might suffer from changes in the observation sources [*Randel et al.*, 2004a]. This includes quality and density of station data set, radiosondes observations as well as various satellite radiance data sets. The ERA40 analysis was completed in July 2003. The final version of the reanalysis products are created from three main assimilation streams 0020 (December 1957 - April 1972), 0030 (July 1974 - March 1985) and 0018 (January 1989 - August 2002) . For stream 0020, primary data sources are station and radiosonde data, and that for stream 0030 include additional data sources such as some aircraft observations and satellite data radiances. Along with above noted data sources stream 0018 rely heavily upon number of additional satellite and *in-situ* measurements (discussed in Chapter 2). Some extra assimilation streams and shorter rerun assimilations were done due to technical problems or problems with satellite radiance tuning (*http://www.ecmwf.int/research/era*). The set of experiment identifiers and periods from which the final version is being constructed are given in Table 4.2 below.

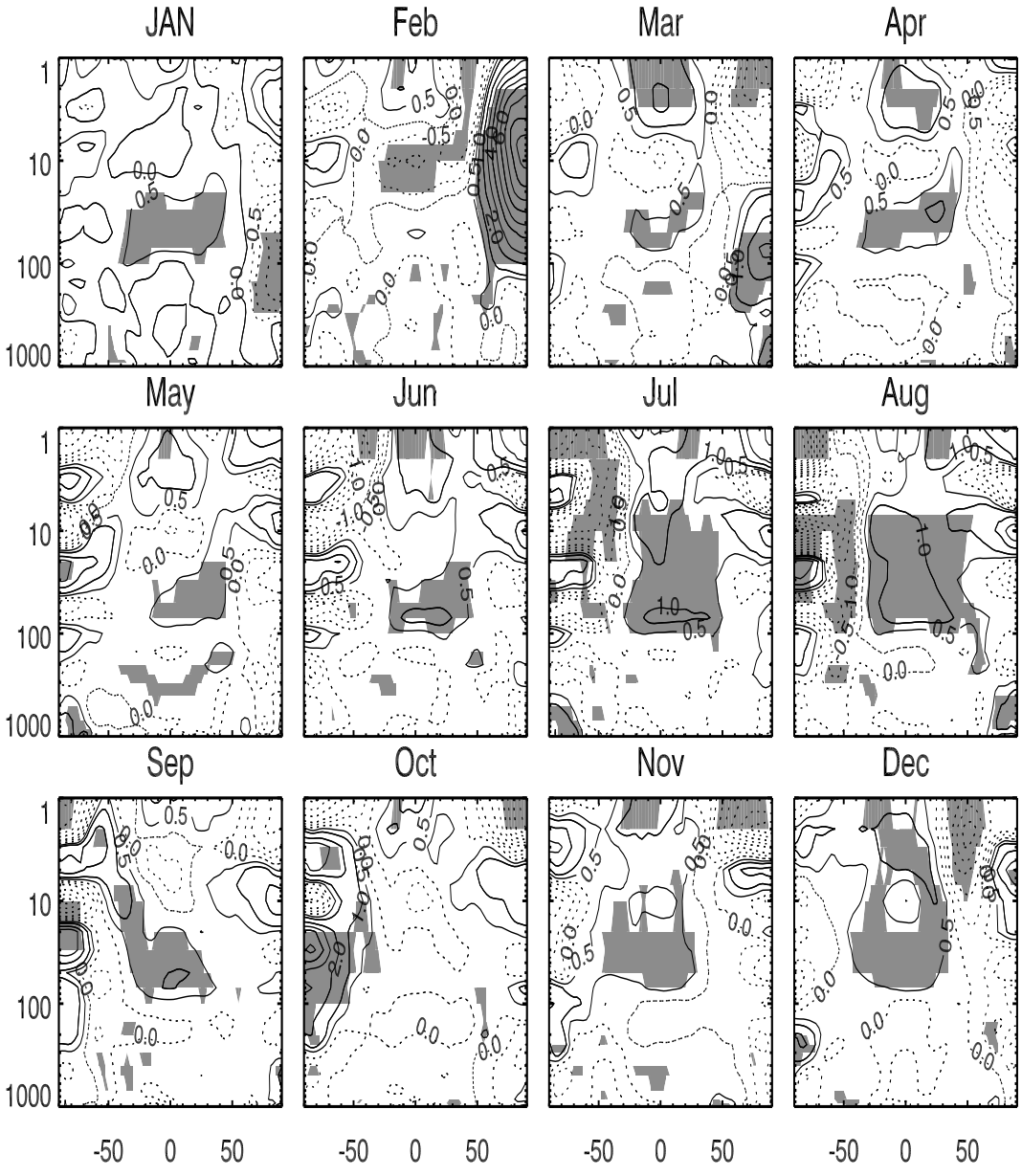

Figure 4.8: Solar cycle response in zonal mean temperature from ECMWF for the period 1979-2005 from regression analysis. Regression coefficients are scaled with mean difference between solar flux during solar maxima and minima using last three solar cycle data (about 113 solar flux units). Shaded regions show 1σ (ligher) and 2σ (darker) significance. Note that contour intervals are 0.5 K for the temperature range between -1 to 1 and beyond this range contour intervals are 1 K.

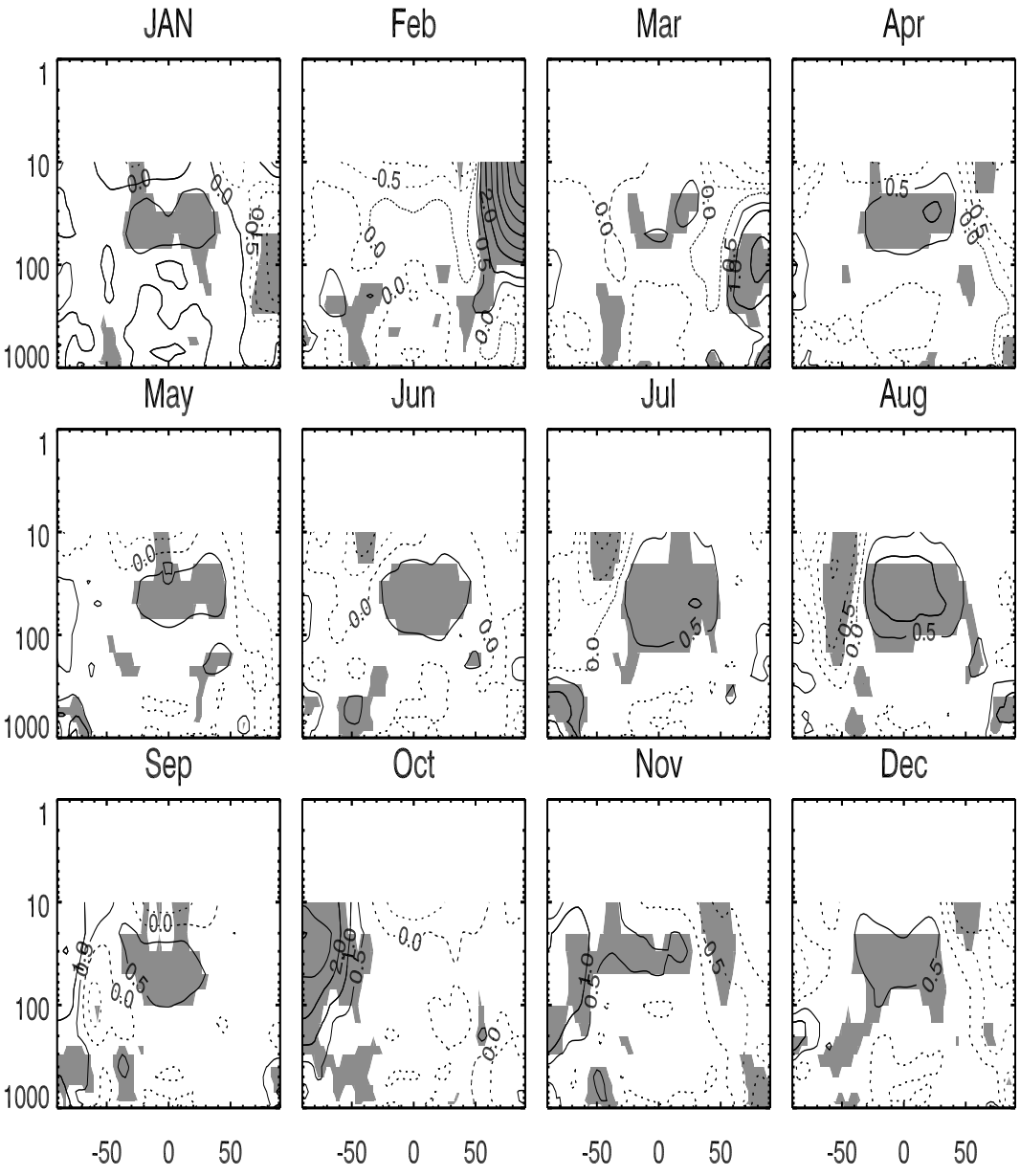

Figure 4.9: Same as Figure 4.8 but for NCEP data.

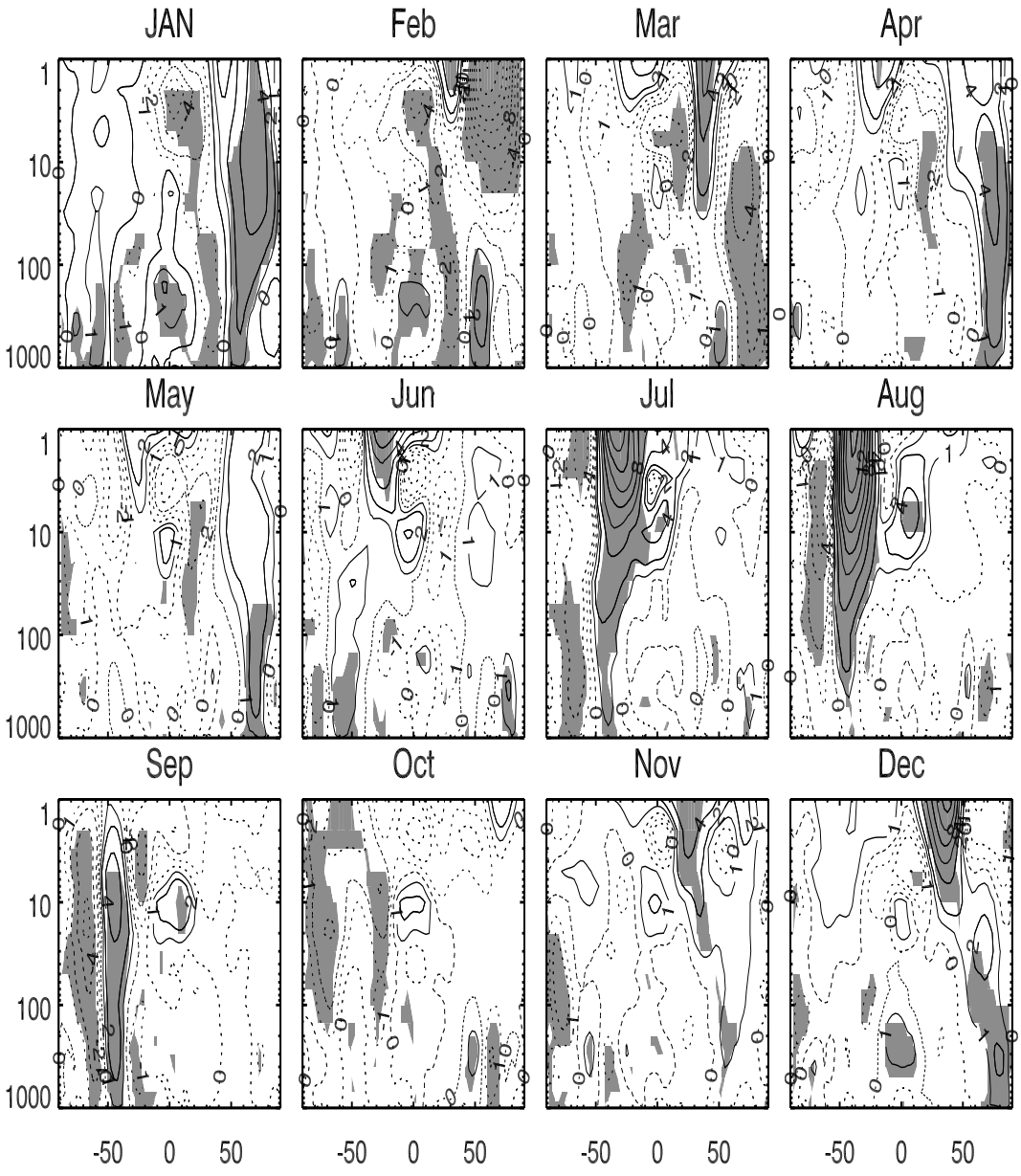

Figure 4.10: Same as 4.8, but for zonal wind from ECMWF (m/s).

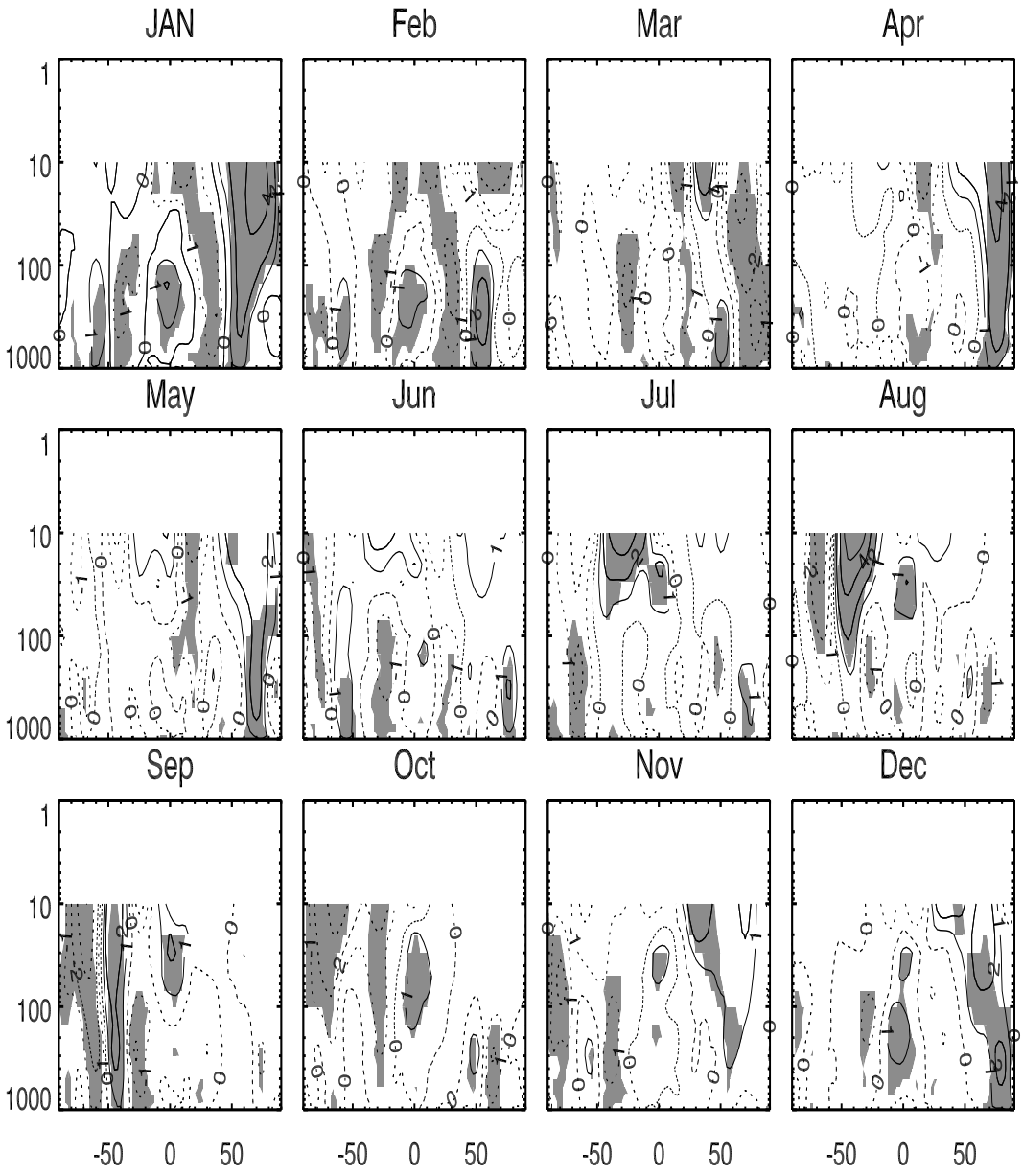

Figure 4.11: Same as Figure 4.10 but for NCEP data.

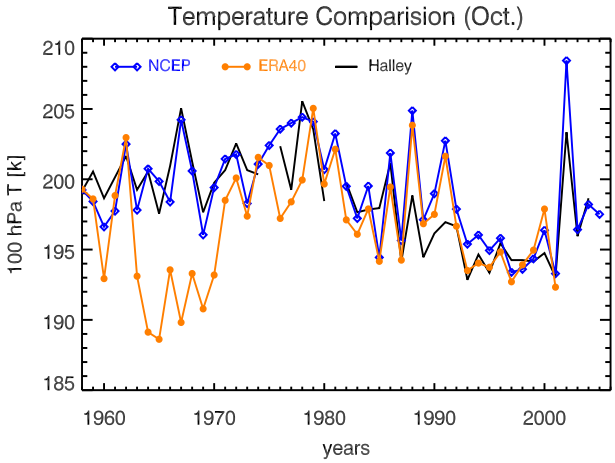

Figure 4.12: Temperature from NCEP and ECMWF compared with Halley station data at 100 hPa. Halley station data are obtained from BAS (British Antarctic Survey) web page http://www.antarctica.ac.uk/met/jds/ozone

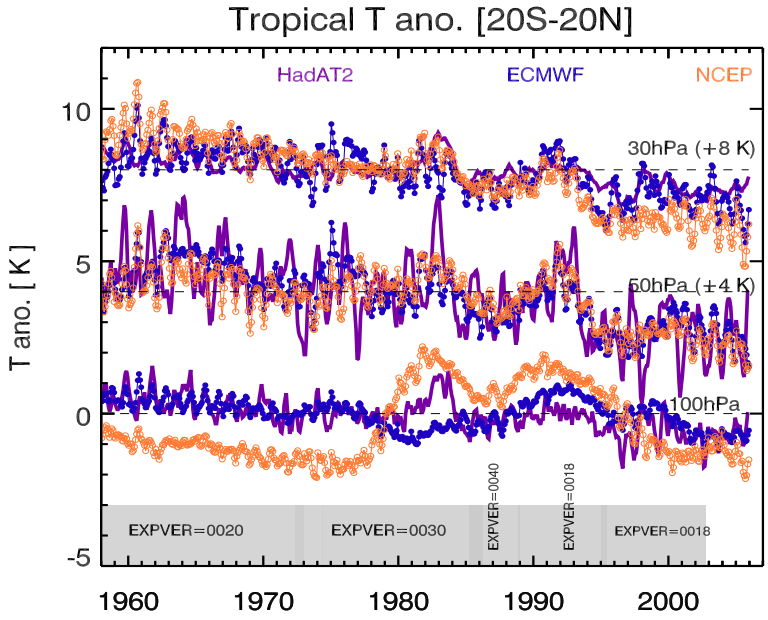

Figure 4.13: Tropical temperature anomalies from HadAT2 (radio sondes), NCEP, and ECMWF data set. Anomalies are calculated with respect to 1965-1995 period. Anomalies from HadAT2 are shown in thick gray line and that for NCEP and ECMWF are shown by squares and filled circles, respectively. Time periods for some of the longest experimental versions for ERA40 are shown in background (see Table 4.2)

Table 4.2: Experimental versions for ERA40

Period	Exp. Version
19570901 - 19571130	EXPVER=0272
19571201 - 19720430	EXPVER=0020
19720501 - 19721231	EXPVER=0334
19730101 - 19740430	EXPVER=0030
19740501 - 19740630	EXPVER=0335
19740701 - 19850331	EXPVER=0030
19850401 - 19860331	EXPVER=0050
19860401 - 19881031	EXPVER=0040
19881101 - 19881231	EXPVER=0338
19890101 - 19941231	EXPVER=0018
19950101 - 19950430	EXPVER=0274
19950501 - 20020831	EXPVER=0018

Figure 4.13 shows comparison of temperature anomalies from ECMWF, NCEP, and HadAT2 for the 20°S-20°N latitude band at 100 hPa, 50 hPa, and 30 hPa. Temperature differences are quite small at 50 hPa and 30 hPa (maximum are up to 1 K in 1958-59 and in 1972). The good agreement between anomalies from reanalysis data set and HadAT2 independently confirms the observed solar signal in tropical stratospheric temperatures which is greater than the uncertainty estimated by the regression model. Largest differences are observed at 100 hPa which is near the tropical tropopause region. Problems associated the radiosondes to measure at very low temperatures are partially responsible for the large uncertainty in this part of the atmosphere [*SPARC*, 2000]. Significant jumps in NCEP data after 1979 (beginning of satellite era) might have contributed to the difficulties in detecting the exact magnitude of solar influence in tropical lower stratosphere. As ECMWF assimilation system is more closely tied with radiosonde data, better agreement can be seen between HadAT2 and ECMWF data.

4.7 Summary and conclusions

An assessment of solar cycle influence on stratospheric temperatures and winds using two different meteorological analyses have been done. It is postulated that solar signal on climate system is either amplified through QBO or changes in solar radiation modifies the QBO. Such strong coupling between these two forcing makes it necessary to study the QBO characteristics in detail. Analysis of zonal wind data from ECMWF and NCEP, show that QBO is well represented in both data sets. Stronger QBO amplitude in ECMWF and timing of phase transition during some of the years can have some implication in diagnostic studies. In addition, separating QBO phases using identical criterion (23 years -west phase, 22 years- east phase) show that the Holton-Tan mechanism, which describes modulation of upward propagating planetary wave activity by QBO, is well represented in both data sets. Due to higher vertical resolution of

ECMWF data, the three cell structure in tropical lower stratosphere as well as changes in the extra-tropical stratopause region are observed. This confirms that QBO phase in tropical lower stratosphere as well as changes near the extra-tropical stratopause act simultaneously to modulate the course of upward propagation planetary waves and hence influence the global stratospheric circulation.

A strong relationship between solar flux and polar stratospheric temperatures [*Labitzke*, 1987] during west phase of QBO (23 years data) is well reproduced in both data sets. Correlation analysis of solar flux and temperatures shows significant differences in the tropical stratosphere. Positive correlation observed in ECMWF data is absent in NCEP data. In SH, correlation between solar flux and temperature is quite low and is somewhat higher in NCEP than ECMWF. Solar-climate interaction has been studied using a multivariate regression analysis for the period of 1979-2005. In NH largest solar response is observed at high latitudes during February and in SH during September. Warmer polar stratospheric temperatures and weaker polar vortex during these months indicate that during solar maxima conditions are more favorable for mid-winter SSWs. These results are in agreement with *Gray et al.* [2003], where they show that during solar minima SSWs occur in early winter months whereas during solar maxima mid-winter SSWs are more common. Solar response at higher latitude is somewhat stronger in ECMWF than that NCEP, possibly due to stronger BD circulation in ECMWF [*Uppala et al.*, 2005].

Regression analysis for longer time period (1958-2005) shows somewhat weaker but similar solar response in NH, but large differences are observed in SH. Comparison with station data and HadAT2 data confirms significant biases in ECMWF in SH before 1979 indicating that ECMWF data in SH before satellite era should not be used to study solar-climate interaction.

5 Total ozone trends using satellite data [1]

One of the main objective of this work is to detect the earliest signs of ozone recovery due to successful implementation of the Montreal protocol and its amendments to ban ozone depleting substances. This chapter provides a detailed assessment of ozone trends using recently updated total ozone data set from various satellite instruments. A multivariate regression model has been applied to zonally averaged total ozone data between 60°S-70°N for 1979-2005. Influence on some of the individual processes such as stratospheric aerosol loading, solar flux variability, QBO, ENSO have been discussed. Possible causes of increase in mid-high latitude total ozone in both hemispheres since mid-nineties have been analysed. The regression analysis shows that such an increase in mid-high latitude total ozone is mostly due to increase in planetary wave driving (strengthening of BD circulation) and solar variability. Changes in ozone trends due to decrease in ozone depleting substances are not yet distinguishable from long term linear ozone trends.

5.1 Abstract

Global total ozone measurements from various satellite instruments such as SBUV, TOMS, and GOME show an increase in zonal mean total ozone at northern hemispheric (NH) mid to high latitudes since the mid-nineties. This increase could be expected from the peaking and start of decline in the effective stratospheric halogen loading, but the rather rapid increase observed in NH zonal mean total ozone suggests that another physical mechanism such as winter planetary wave activity has increased which has led to higher stratospheric Arctic temperatures. This has enhanced ozone transport into higher latitudes in recent years as part of the residual circulation and at the same time reduced the frequency of cold Arctic winters with enhanced polar ozone loss. Results from various multi-variate linear regression analyses using SBUV V8 total ozone with explanatory variables such as a linear trend or, alternatively, EESC (equivalent effective stratospheric chlorine) and on the other hand planetary wave driving (eddy heat flux) or, alternatively, polar ozone loss (PSC volume) in addition to proxies for stratospheric aerosol loading, QBO, and solar cycle, all considered to be main drivers for ozone variability, are presented. It is shown that the main contribution to the recent increase in NH total ozone is from the combined

[1] Section 5.2-5.9 have been been published as S. Dhomse, M. Weber, J. Burrows, I. Wohltmann, and M. Rex, On the possible cause of recent increases in NH total ozone from a statistical analysis of satellite data from 1979 to 2003, Atmos. Chem. Phys., 6, 1165-1180, 2006, with minor modification

effect of rising tropospheric driven planetary wave activity associated with reduced polar ozone loss at high latitudes as well as increasing solar activity. This conclusion can be drawn regardless of the use of linear trend or EESC terms in our statistical model. It is also clear that more years of data will be needed to further improve our estimates of the relative contributions of the individual processes to decadal ozone variability. The question remains if the observed increase in planetary wave driving is part of the natural decadal atmospheric variability or will persist. If the latter is the case, it would trigger to faster recovery of atmospheric ozone layer.

5.2 Overview

Long-term ozone observations at mid to high latitudes spanning several decades display both steady decline and high inter-annual and intra-annual variability. Figure 5.1 shows the monthly total ozone anomaly time series in the 50°N-60°N latitude band for different satellite data sets from 1979 to 2003: SBUV V8, merged TOMS/SBUV V8, and GOME WFDOAS V1 (1995-2003). Also shown in the figure are the annual mean total ozone for all data sets. It is evident that an increase in total ozone is observed in all data sets since about the mid-nineties following a steady decline during the eighties and early nineties [*WMO*, 1999]. The effect of the Mount Pinatubo eruption in 1991 resulted in extremely low spring values for few years until 1994. The mid-nineties were also characterised by occurrences of several cold Arctic stratospheric winters with enhanced polar ozone losses [*Pawson and Naujokat*, 1999; *WMO*, 2003]. After this period a steady rise in NH total ozone is observed. As an effect of higher total ozone in the late nineties, the long-term linear downward trend in ozone was reduced as compared to earlier studies [*WMO*, 2003]. This chapter tries to address the issue which physical and/or chemical processes may have contributed to the recent increase.

The main contributions to decadal ozone variability are changes in solar flux, ozone depleting substances, and ozone transport. In order to study long-term changes in ozone, it is necessary to separate the influence of various dynamical and chemical processes as well as processes that act on short- and long-term time scales such as the quasi-biennial oscillation (QBO), El Niño/Southern Oscillation (ENSO or SOI) [*SPARC*, 1998; *WMO*, 2003], volcanic eruptions, heterogeneous chemical losses on the surface of polar stratospheric clouds (PSC), gas phase chemical losses, and tropospheric driven planetary wave activity which controls ozone transport into high latitudes as part of the wave driven residual circulation [*Fusco and Salby*, 1999].

In the following the relevant processes that are known to contribute to ozone variability are briefly summarised.

Residual circulation and planetary wave driving

The zonally averaged transport circulation in the wintertime stratosphere consists of a single mean meridional cell in each hemisphere with a rising branch in the tropics, poleward flow at mid-latitudes, and downward mass transport at higher latitudes. This circulation is driven by momentum deposited into the stratosphere by wave breaking [*Andrews et al.*, 1987]. Planetary waves propagate from the troposphere to the stratosphere, break at critical levels, and decelerate the mean zonal wind. Coriolis force and pressure gradient are not in equilibrium anymore and poleward motion sets in. The mass transport from the equator to the pole leads to adiabatic heating at high latitudes and drives stratospheric temperatures away from radiative equilibrium [*Newman et al.*, 2001]. Adiabatic cooling sets in and leads to subsidence of air masses. This residual circulation tightly controls the wintertime ozone buildup at high latitudes [*Fusco and Salby*, 1999; *Randel et al.*, 2002b]. It influences ozone in several ways: a stronger residual circulation means that more ozone is transported from its source region at the equator to higher latitudes, that meridional mixing is stronger, more ozone is transported downwards at high latitudes, where it is photochemically more stable, stratospheric temperatures rise, and less ozone is chemically depleted via heterogeneous reactions [*Weber et al.*, 2003]. The ability of waves to propagate vertically is dependent on the zonal mean flow and, therefore, wave activity is strongest in the winter of the respective hemisphere. The impact of the strength of the residual circulation of a given winter on the inter-annual ozone variability remains detectable until next autumn [*Fioletov and Shepherd*, 2003].

The magnitude of momentum transport from the troposphere into the stratosphere by planetary waves is presented by the divergence of Eliassen-Palm (EP) flux. The eddy heat flux $\overline{v'T'}$, which is directly proportional to the vertical component of Eliassen-Palm (EP) flux vector and approximately proportional to the EP flux divergence, is found to be a very attractive proxy for ozone transport (for details see Chapter 3). It determines the magnitude of the wave activity [*Fusco and Salby*, 1999; *Newman et al.*, 2001; *Weber et al.*, 2003]. Other dynamical proxies such as Arctic Oscillation (AO) or North Atlantic Oscillation (NAO) index, polar jet strength index, polar stratospheric cloud (PSC) volume, 50 hPa temperature are to some degree correlated with each other and can be linked to planetary wave activity [*Randel and Cobb*, 1994; *Baldwin and Dunkerton*, 1999; *Chipperfield and Jones*, 1999; *Fusco and Salby*, 1999; *Randel et al.*, 2002b; *Salby and Callaghan*, 2002a; *Plumb and Semeniuk*, 2003; *Steinbrecht et al.*, 2003].

QBO

The quasi-biennial oscillation of the equatorial zonal winds and temperatures has an obvious influence on the inter-annual variability of the tropical and subtropical ozone column [*Baldwin et al.*, 2001](also see Chapter 4). It mainly induces a secondary adiabatic circulation which transports more or less ozone from the altitudes of pho-

tochemical production to the altitudes where ozone can be considered a conserved tracer [*Reed*, 1964]. Typical amplitudes are 5–10 DU that are a considerable part of the inter-annual variability in the tropics. But the QBO has also been connected to ozone changes in mid-latitudes and even polar latitudes [*Bowman*, 1989; *Lait et al.*, 1989; *Chandra and Stolarski*, 1991]. The tropical signal is confined equatorward of about 15° and has no seasonal dependence, while at higher latitudes the QBO response to ozone has largest amplitudes in winter and spring [*Tung and Yang*, 1994; *Randel and Cobb*, 1994; *Baldwin et al.*, 2001]. Possible reasons for the QBO influence in mid-latitudes could be the modulation of the wave propagation in mid-latitudes, transport of equatorial anomalies to higher latitudes or changes in meridional mixing. The modulation of wave propagation is called the Holton-Tan effect [*Holton and Tan*, 1980]. The influence on total ozone depends on both phase and strength of the QBO [*WMO*, 2003; *Steinbrecht et al.*, 2003].

Stratospheric halogen loading

The impact of anthropogenically produced CFCs on ozone depletion has been widely studied since the early 1970s [*Molina and Rowland*, 1974; *Stolarski and Cicerone*, 1974; *WMO*, 2003]. International measures to curb these emissions led to the introduction of the Montreal protocol (1987) and subsequent amendments to reduce emissions of chlorine and bromine containing species. The various halogen compounds have different potentials to deplete stratospheric ozone depending on their physical and chemical properties. EESC (equivalent effective stratospheric chlorine) is a quantity which is the sum of chlorine containing species multiplied by the number of Cl atoms contained in the compound and weighted by their fractional stratospheric release rate. It also accounts for the effect of bromine species [*WMO*, 2003]. Like the stratospheric hydrogen chloride [*Anderson et al.*, 2000], that is a measure of the total amount of chlorine in the upper stratosphere, the EESC has peaked in 1997 and started a slow decline afterward as displayed in Figure 5.2.

Heterogeneous chemistry

Large ozone depletion has been regularly observed at high latitudes in late winter and early spring. It is caused by heterogenous chemistry on polar stratospheric clouds (PSCs) that activate large amounts of chlorine that catalytically destroy ozone inside the winter polar vortex [*Solomon*, 1999]. This phenomenon is regularly observed in the southern hemisphere and is commonly known as the ozone hole [*Farman et al.*, 1985]. In contrast, large inter-annual variability in polar ozone loss is observed in the northern hemisphere. A high correlation between PSC volume integrated over the winter and the amount of polar vortex chemical ozone loss in the Arctic has been found [*Rex et al.*, 2004]. Long-term trends in polar ozone have also an impact on mid-latitude trends due to airmass mixing after the polar vortex break-up [*Knudsen and Grooss*, 2000; *Fioletov and Shepherd*, 2005].

Solar variability

Significant influences of solar variability on different meteorological quantities have been identified [*Rind*, 2002]. The solar activity-ozone relationship has been taken into consideration in all international ozone trend assessments [*WMO*, 1999, 2003]. As discussed in Chapter 4, the main support for this relationship are variations in the solar ultraviolet spectral irradiance that modify ozone production rates in the upper stratosphere [*Brasseur*, 1993]. The secondary effect may include sudden increases in solar energetic particle precipitation causing short-term decreases in high altitude ozone concentration related to downward transport of NO_y from the mesosphere down to the upper stratosphere [*Jackman et al.*, 2000; *Sinnhuber et al.*, 2003b]. There is evidence that indirect effects from solar activity influence lowermost stratospheric ozone via dynamical coupling [*Labitzke and van Loon*, 1993; *Kodera and Kuroda*, 2002]. Analysis of various ground based and satellite records extending over 2-6 decades indicate the existence of decadal scale variation of total ozone that correlates with the solar cycle [*Jackman et al.*, 1996; *Miller et al.*, 1996; *Hood et al.*, 1997; *Zerefos et al.*, 1997; *Ziemke et al.*, 1997; *McCormack et al.*, 1997].

Stratospheric aerosols

Large enhancements in stratospheric aerosols were observed after major volcanic eruptions like El Chichón in 1982 [*Hofmann and Solomon*, 1989] and Mt. Pinatubo in 1991 [*Parrish et al.*, 1998]. Very low ozone values were observed following the Pinatubo event [*Randel et al.*, 1995; *Solomon et al.*, 1996; *Tabzadeh et al.*, 2002] in the NH. A similar ozone deficit, however, was not observed in the southern hemisphere. *Solomon et al.* [1996] showed that major volcanic eruptions affect atmospheric dynamics and radiative forcing through scattering and absorption of solar radiation. They also showed that the occurrence of two major volcanic eruptions nine years apart during declining phases of solar cycles may lead to some confusion in separating volcanic and solar influence on ozone.

El-Niño/Southern Oscillation

ENSO is more or less a zonal phenomenon and normally leads to lower stratospheric temperature and total ozone anomalies that are opposite to the temperature anomalies in the troposphere [*Gettelman et al.*, 2001; *Steinbrecht et al.*, 2003]. The changes in ozone anomalies during strong El Niño and La Niña events may introduce additional variance and modify the ozone field [*Shiotani*, 1992; *Zerefos et al.*, 1997; *Logan et al.*, 2003].

This Chapter presents a statistical analysis of twenty five years of total ozone data using various explanatory variables that represent physical and chemical processes that are known to modify the global ozone distribution as just briefly described above. Such analyses have been regularly applied to determine long-term trends in ozone [*WMO*, 1999, 2003]. The major difference to other studies is that additional

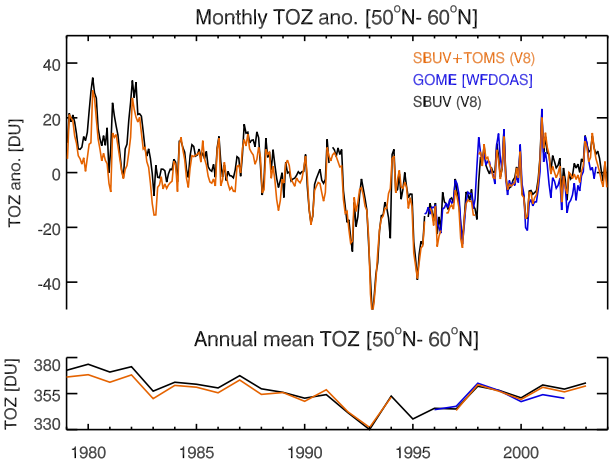

Figure 5.1: Monthly mean zonal mean total ozone anomaly for 50°N-60°N from different satellite data sets between 1979 and 2003 (Top). Annual mean total ozone is displayed in the bottom panel. All satellite data show the increase in northern hemispheric total ozone at higher latitudes since 1995. Data from TOMS/SBUV V8 merged data set (orange), SBUV 8 (black), and GOME WFDOAS (blue) are shown.

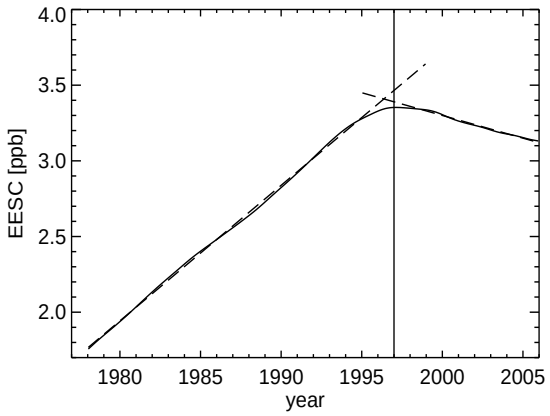

Figure 5.2: Equivalent effective stratospheric chlorine loading (EESC) in ppb [*WMO*, 2003]. The straight lines show linear fits to the inclining phase up to December 1995 (slope of 0.9 ppb/decade) and to the slow decline after January 1999 (slope of -0.3 ppb/decade), respectively (dashed lines). A 9 DU/decade total ozone decrease during the first phase would correspond to a 3 DU/decade increase after 1999 if the ozone change is solely due and anti-correlated with EESC.

proxies such as PSC volume and eddy heat flux terms representing ozone chemistry and transport are added to better elucidate on the contribution of individual processes. This allows us to discuss the possible causes of the recently observed increase in middle to high latitude ozone and to quantify the contribution of the various processes to the inter-annual variability observed in the total ozone record.

In Section 5.3 the total ozone data sets from SBUV, SBUV/TOMS merged (both 1979-2003), and GOME (1995-2003) are briefly described, followed by a presentation of proxies for planetary wave driving (Section 5.4) and PSC volume (Section 5.5) that are used as explanatory variables standing for dynamical and chemical ozone processes. Other commonly used proxies, among them solar flux and QBO, are briefly described in Section 5.6. After briefly summarising in Section 5.7 the regression model as applied to the SBUV total ozone data, the results are discussed in detail in Section 5.8 with major conclusions drawn in Section 5.9.

5.3 Satellite ozone data

Total column ozone data used in this study are SBUV V8 data from Nimbus 7 (01/1979–12/1989), NOAA11 (01/1990–12/1993, 07/1997–12/2000), NOAA09 (01/1994–06/1997) and NOAA16 (01/2001–12/2003) [*Barthia et al.*, 2004]. The SBUV/TOMS V8 merged data set were obtained from Goddard Space Flight Center web site http://code916.gsfc.nasa.gov/Data_services/merged/mod_data.public.html [*Frith et al.*, 2004]. GOME total ozone data from 1995 to 2003 have been processed using the Weighting Function DOAS approach [*Coldewey-Egbers et al.*, 2005; *Weber et al.*, 2005]. All data sets agree well among each other. From Figure 5.1 it appears that the SBUV/TOMS merged data set as well as GOME show lower values than SBUV after about year 2000 and it is also lower during the earlier record. The positive bias in the SBUV data record with respect to TOMS was also found in the comparison with ground data [*Labow et al.*, 2004]. A big advantage of the SBUV data set is that the various data sets from Nimbus to NOAA16 show small differences during periods of overlapping missions and, thus, are well suited for long-term trend studies [*Barthia et al.*, 2004; *Labow et al.*, 2004]. The comparison between data sets highlights the critical issue of maintaining long-term time series using multiple satellite data sets.

5.4 Proxy for planetary wave driving

Eddy heat flux at 100 hPa averaged over mid-latitudes have been used as as a proxy for ozone transport due to variation in planetary wave driving. Monthly mean eddy heat fluxes at 100 hPa are calculated using ECMWF 40 year reanalysis data (ERA-40) [*Uppala et al.*, 2005] for the period of 1979-2001 and from operational data for the period 2002-2003 and have been area weighted and averaged between

45° -75° for the respective hemispheres.

Meridional ozone transport and mixing related to planetary wave driving is mainly confined to winter and spring. In late spring and summer total ozone changes are mainly controlled by NO_x and photo-chemistry [*Brühl et al.*, 1998]. The photochemical lifetime does not vary from year to year [*Randel et al.*, 2002b], but initial conditions vary, e.g. winter anomalies due to variation in the buildup of ozone are still observed in late summer ozone anomalies [*Fioletov and Shepherd*, 2003] as shown in Figure 5.3. To account for this combined dynamical effect of wintertime ozone buildup and persistent ozone anomalies in spring and summer, the cumulative eddy heat flux proxy for a given month of ozone observation is calculated by integrating the monthly eddy heat flux from last fall (October for NH and February for SH) to that month. For example, the October cumulative eddy heat flux for NH is simply the monthly mean eddy heat flux from October, while for April, it is averaged from preceding October until April, and for September from preceding October until September. The cumulative eddy heat flux for a given month can be described as follows,

$$h^*(m) = \frac{\int_{m'=m_0}^{m} h(m')\,dm'}{\int_{m'=m_0}^{m} dm'} \tag{5.1}$$

with m_0 being the starting month (here October). Summer eddy heat fluxes are fairly small so that the main contribution to the cumulative eddy heat flux, which is used as a proxy for planetary wave driving and as an explanatory variable in the regression, comes from the winter and early spring months.

Using GOME total ozone data and UKMO eddy heat flux data from the period 1996–2003, *Weber et al.* [2003] proved that a compact relationship between winter integrated eddy heat flux and the winter time ozone build up exists. Figure 5.4 shows the ozone build-up for the 50°N-60°N latitude band during the last 25 years of SBUV data. Winter time ozone gain is calculated by subtracting the October total ozone value from the next year's April total ozone and it is correlated with the cumulative eddy heat flux from ERA-40. For the period 1979-2003, correlation exceeds 0.56 in NH. As an effect from the Pinatubo eruption, ozone deviates from the regression line in winter 1992/93. For all late winter months (January to April) the correlations are quite significant for middle to high latitudes. Correlations are positive at high latitudes and are negative in the tropics.

In tropics (<30°N) this cumulative effect from the planetary wave driving is short-lived due to the photochemical production of ozone. The approximate photochemical relaxation time is somewhere between one and three months at 25 km altitude in the tropics (see Figure 2 in *McLinden et al.* [2000]). An average of the two previous months is taken for the cumulative heat flux, e.g. for April, the mean between March and April is computed. From August to November (during SH winter/spring) the equivalent southern hemispheric two month eddy heat flux proxy, here averaged from

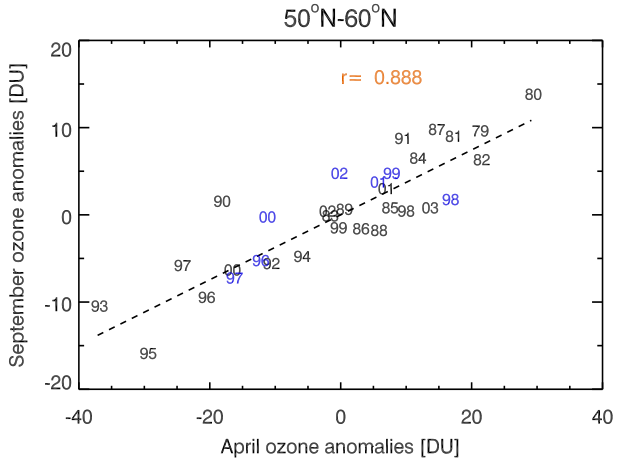

Figure 5.3: Correlation of SBUV V8 total ozone anomaly in April with September anomalies between 50°N and 60°N. High (low) ozone anomalies in spring lead to (low) high ozone anomalies in late summer. This relationship is valid for all summer months [*Fioletov and Shepherd*, 2003]. Data in blue are anomalies obtained from GOME data.

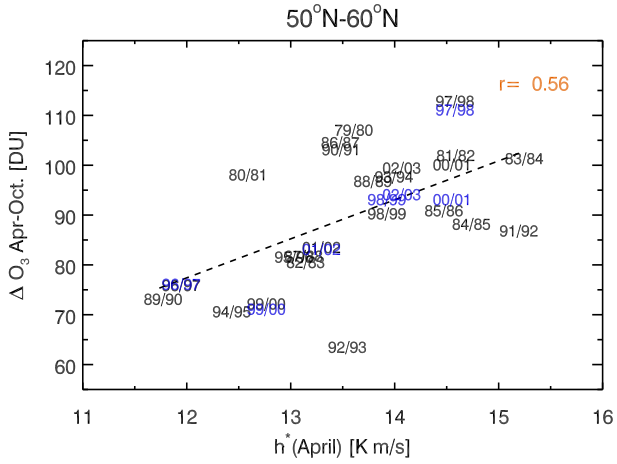

Figure 5.4: Relationship between winter/spring ozone build up (April-October difference) at 50°N-60°N as a function of the accumulated eddy heat flux h^* (April) as given by Eq. 5.1. Monthly mean zonal mean ozone are from SBUV V8. The effect of Pinatubo eruption can be clearly seen in 1992/93. Blue years indicate GOME values.

45°S to 75°S, is included in the statistical model. The NH two month mean eddy heat flux is used from December until May in the tropics.

5.5 PSC volume proxy

The PSC volume is a suitable proxy for heterogenous chemical (i.e. polar) ozone loss [*Solomon*, 1999; *Rex et al.*, 2004]. It has been calculated from NCEP reanalysis data set by counting all grid points north of 60°N below the formation temperature of NAT (nitric acid trihydrate) and weighting them with their volume. NAT formation temperatures have been calculated according to *Hanson and Mauersberger* [1988] as a function of nitric acid mixing ratio, water vapor mixing ratio, and pressure. A constant water vapor profile of 5 ppm and a nitric acid profile [*Kleinböhl et al.*, 2003] of 5, 6, 7, 8, 10, 10, 7, and 5 ppb for atmospheric pressures of 200, 150, 100, 70, 50, 30, 20, and 10 hPa, respectively, have been assumed. Monthly PSC volumes used in this study are integrated from the preceding October to the respective month of ozone observation. The proxy is set to zero for October and November since PSC volumes are negligibly small during these months. Stratospheric circulation is mainly zonal during winter and air is continuously processed over the winter months inside the polar vortex such that the ozone loss accumulates over winter and spring. In addition, the level of chlorine activation on PSC surfaces responsible for heterogenous chemical ozone loss depends also on the available inorganic chlorine and the PSC volume must be multiplied by the EESC. The modified polar ozone loss proxy is then defined as follows

$$V^*_{psc}(m) = \frac{\int_{m'=m_0}^{m} EESC(m') \cdot V_{psc}(m')\, dm'}{\int_{m'=m_0}^{m} dm'}. \tag{5.2}$$

with m_o being October. In the statistical regression either the PSC volume or eddy heat flux terms have been included.

5.6 Other proxy data

The southern oscillation index (SOI) is obtained from the Climate Prediction Center (CPC, www.cpc.ncep.noaa.gov/data/indices/). Both QBO indices at 30 hPa and 10 hPa, respectively, are from The Free University Berlin (FUB) analysis (B. Naujokat, personal communication). Most of earlier regression models use QBO harmonics to account for time lags. Two QBO indices at 30 hPa and 10 hPa are used, which are sufficient to adjust for both strength and phase of QBO. It also avoids the necessity to search for an optimum time lag for the fitting [*Randel et al.*, 1995; *Ziemke et al.*, 1997]. The monthly stratospheric aerosol loading as a response to volcanic eruptions are from NASA Goddard Institute of Space Studies (www.giss.nasa.gov-/data/strataer/), and are monthly mean aerosol optical depths at 550 nm (update from *Sato et al.* [1993]). EESC concentration were obtained from the European Environment Agency web site www.eea.eu.int. For solar flux data we used the MgII index

(ftp://ftp.ngdc.noaa.gov/STP/SOLAR_DATA/SOLAR_UV/NOAAMgII_dat.htm), which is a better proxy for UV solar flux variability than either F10.7 cm flux or sunspot number data [*Viereck et al.*, 2001, 2004]. The MgII index has been smoothed with a boxcar with five months full width in order to remove short term solar variability.

5.7 Regression model for trend studies

The regression model used in this study is quite similar to other regression models used in the past to study ozone trends [*SPARC*, 1998; *Shindell et al.*, 1999a; *WMO*, 1999; *Randel et al.*, 1999; *Ziemke et al.*, 1997; *Staehelin et al.*, 2001]. It has been constructed as follows

$$\begin{aligned} TOZ(n) &= \sum_{m=1}^{12} \alpha_m^{\circ} \cdot \delta_{mn} + \sum_{m=1}^{12} \alpha_m^{lin} \cdot \delta_{mn} \cdot n + \sum_{m=1}^{12} \alpha_m^{hf} \cdot \delta_{mn} \cdot h^*(n) \\ &+ \sum_{m=1}^{12} \alpha_m^{qbo30} \cdot \delta_{mn} \cdot \mathrm{qbo30}(n) + \sum_{m=1}^{12} \alpha_m^{qbo10} \cdot \delta_{mn} \cdot \mathrm{qbo10}(n) \\ &+ \alpha^{sol} \cdot \mathrm{sol(n)} + \alpha^{SOI} \cdot \mathrm{SOI}(n) \\ &+ \alpha^{aeroc} \cdot \mathrm{aeroc}(n) + \sum_{m=1}^{12} \alpha_m^{aerop} \cdot \delta_{mn} \cdot \mathrm{aerop}(n) + \varepsilon(n) \end{aligned} \tag{5.3}$$

where $TOZ(n)$ is the monthly mean total ozone of month n, which is a running index from month zero to 299 covering the period 1979 to 2003, α_m° are monthly constants for the annual cycle (m=1,...,12), α_m^{lin} are monthly linear trend coefficients, α_m^{hf} are eddy heat flux contribution coefficients, α_m^{psc}, the heterogenous chemical loss coefficients, α^{sol}, coefficient for solar flux variability, α_m^{qbo30} and α_m^{qbo10}, QBO coefficients at 30 and 10 hPa, respectively, α^{SOI}, the El Niño/ Southern Oscillation coefficient, and α^{aeroc} and α_m^{aerop}, two stratospheric aerosol loading terms due to El Chichón and Pinatubo eruption, respectively. δ_{mn} is one when index n corresponds to one of the months of a given year and otherwise zero. $\varepsilon(n)$ represents the unexplained variance of the statistical model or, in short, the residual.

There are twelve monthly constants in our regression model and they account for the seasonal variation of ozone. The monthly linear trend terms or, alternatively, the EESC terms account for the contribution from gas phase chemical ozone loss [*Zerefos et al.*, 1997]. There are twelve eddy heat flux, PSC volume, QBO, and Pinatubo aerosol fitting parameters used in the regression model to separate the effects into individual months. The El Chichón stratospheric aerosol contribution turned out to be comparatively small so that a separation by individual months was not needed.

The linear trend term is traditionally associated with the gas phase chemical ozone loss as expected from the steady increase in stratospheric chlorine loading. As already discussed the EESC has started to decline after peaking in 1997, so that a change from linear trend should be expected. Both EESC and linear terms are used to elucidate on the significance of the EESC in the total ozone time series. Linear trend terms have been replaced by corresponding EESC terms in some regression runs as follows:

$$\sum_{m=1}^{12} \alpha_m^{lin} \cdot \delta_{mn} \cdot n \quad \longrightarrow \quad \sum_{m=1}^{12} \alpha_m^{EESC} \cdot \delta_{mn} \cdot EESC(n). \tag{5.4}$$

In some fits the eddy heat flux term has been replaced by the accumulated PSC volume proxies as follows:

$$\sum_{m=1}^{12} \alpha_m^{hf} \cdot \delta_{mn} \cdot h^*(n) \quad \longrightarrow \quad \sum_{m=1}^{12} \alpha_m^{psc} \cdot \delta_{mn} \cdot V^*(n) \tag{5.5}$$

It was found that a simultaneous fit of eddy heat flux and PSC volume did not improve the fit significantly, in particular after applying the auto-regression corrections as described below. This is not unexpected since planetary wave driving, polar stratospheric temperatures [*Newman et al.*, 2001], and chlorine activation [*Weber et al.*, 2003] are linked. Implication of the exchange of these terms on the statistical fitting are investigated in the following section.

After applying the regression, the residuals $\varepsilon(n)$ show non-negligible auto-correlation and this violates the assumption in the least-squares fitting with random (Gaussian distributed) noise in the data. It is a common practice to apply a Cochrane-Orcutt transformation to the regression equation using an estimate of the auto-correlation with time lag of one month [*Cochrane and Orcutt*, 1949; *Tiao et al.*, 1990; *Weatherhead et al.*, 1998; *Plets and Vynckier*, 2000; *Bodeker et al.*, 1998; *Reinsel et al.*, 2002]. After fitting the transformed model, the remaining residuals should be normally distributed, otherwise this procedure has to be repeated as just described. Even though most of the fitting coefficients do not change much after the transformation, the parameter error nevertheless increases and this is important with regard to the judgement of statistical significance of individual processes. The occurrence of auto-correlation in the residuals may be due to either measurement errors, for instance time drift in observational data, due to uncertainties in the explanatory variables particularly with regard to the cumulative proxy data, or due to some missing processes which are not accounted for in our model. Most likely it is a combination of all three. In this study it sufficed to apply one Cochrane-Orcutt transformation to Eq. 5.3 to obtain an improved estimate of αs.

5.8 Results

Monthly mean zonal mean total ozone anomalies for the 50°N-60°N latitude band from TOMS/SBUV V8 merged, WFDOAS GOME, and SBUV V8 data sets are

shown in Figure 5.1. The regression model with linear trend terms has been only applied to SBUV V8 data and the reconstruction of monthly total ozone anomalies (after subtraction of the monthly constants) are shown in Figure 5.5 for both 30°N-40°N and 50°N-60°N bands. The ozone reconstruction with EESC terms replacing the linear trend terms is shown for the same latitude bands in Figure 5.6. Both regression models with either linear or EESC terms show about the same significance in the overall fitting. The issue of linear versus EESC trend in the ozone reconstruction is discussed further down below. In general, the correlation between modeled and observed total ozone anomalies is in the range of 0.8 to 0.9.

General features like the observed downward trend until the mid-nineties, significant ozone losses following Mount Pinatubo eruption, and increase in ozone after the mid-nineties are well captured in both ozone reconstructions. The contributions from individual explanatory variables have been added in Figs. 5.5 and 5.6 (top of each time series). Linear (EESC) and eddy heat flux terms are only plotted for April and September for better clarity.

The influence of the QBO on spring total ozone can be clearly seen in the 30°N-40°N latitude band (up to 20 DU from easterly phase to westerly phase and vice versa) while at high latitudes it is somewhat smaller (about 10 DU). In the tropics (below 10°N) the QBO influence is observed in all months, while its effect is limited to winter spring at higher latitudes (see Chapter 4). Linear terms (or EESC term) and eddy heat flux contributions increase with latitude. Aerosol loading terms associated with the Pinatubo eruption explain about a maximum decrease of 50-60 DU in the 50°N-60°N latitude band and about 15-20 DU at 30°N-40°N during winter/spring 1991/92. Solar flux cycle explains up to 15 DU ozone variability from solar maximum to solar minimum. At higher latitudes the eddy heat flux explains up to 20 DU increase in ozone during dynamically active Arctic winters (e.g. mid-eighties and end of nineties).

Typical residuals from the regression analysis of Eq. 5.3 with linear trend terms at 30°N-40°N and 50°N-60°N are shown in Figure 5.7, respectively. In these figures both residuals with (red) and without auto-regressive adjustment (black) are shown. Also indicated are the various satellite platforms of the SBUV instruments. There appear to be no jumps in residuals after changes of instrument platforms confirming the consistency of the data set as stated earlier. For all latitude bands residuals do not show any significant auto-correlation after one Cochrane-Orcutt transformation.

Analyses have been performed for seven 10° wide latitude bands from equator to 70°N. Figure 5.8 shows the observed and modelled ozone anomalies for spring (April) and late summer (September) months for all latitude bands from 10°N-20°N to 60°N-70°N in the NH. Ozone reconstructions displayed here are based upon regression with linear trend terms. Also shown are GOME observations that particularly after 2002 show somewhat lower values than SBUV. In general the

linear decrease up to the mid-nineties and increase in the total ozone since then are clearly captured by the model for both months. As discussed earlier the September changes are closely coupled to changes in the previous winter [*Fioletov and Shepherd*, 2003, 2005]. It can be also noted that the modeled ozone anomaly agrees better with observations in the nineties and later than the earlier period. A likely explanation is the fact that both observational data as well as meteorological analyses from which most of the proxies have been derived have improved in quality in recent years [*Uppala et al.*, 2005].

The ozone variability due to the different proxy terms in Eq. 5.3 is shown in Figure 5.9 for all NH latitudes in April and September, respectively. The 2σ variability has been calculated from the variance of the proxy time series multiplied by the corresponding fitting coefficient [*Steinbrecht et al.*, 2003]. The vertical bars for each explanatory variable account for the uncertainty in the fitting coefficients (alphas in Eq. 5.3). The 2σ variabilities of the SBUV and modelled ozone time series are also shown (black and orange bars without vertical bars). In late spring, where usually the highest inter-annual variability is observed (up to ± 40 DU), the model tends to underestimate the observed variability by about 5 DU at high latitudes during spring as shown in Figure 5.9. This difference corresponds to a maximum of 15 DU unexplained 2σ variance (as verified by the 2σ value of the observed residual time series). In late summer the overall variability is reduced and the contribution from various processes are generally not statistically significant.

Highest contribution to ozone variability at low latitudes are from QBO and solar variability (up to ± 5 DU each). QBO influences are observed at all latitudes during spring while it is limited to lowest latitudes below 10°N during summmer/fall in agreement with *Baldwin et al.* [2001] and *Steinbrecht et al.* [2003]. The solar cycle signature is observed at all latitudes and seasons. Separating solar term fitting into individual months (12 fitting constants) slightly reduces the solar signal variability in summer/fall by about 2 DU (not shown here). Various earlier studies [*Solomon et al.*, 1996; *Hood et al.*, 1997; *Randel et al.*, 2002b] suggested that it is difficult to separate the effect of solar cycle and volcanic eruption on the long-term ozone change. Both major volcanic eruptions, El Chichón in 1982 and Pinatubo in 1991, occurred during solar maximum conditions, in an easterly phase of QBO, and during a strong El-Niño event. Our analysis shows that the solar maximum of the present solar cycle has experienced no major volcanic eruption. That may improve the separability of stratospheric aerosol and solar influences. The rise of solar cycle 23 until early 2000s has positively contributed to the recent increase in total ozone in the absence of another major volcanic eruption. Nevertheless a few more years of data particularly during declining phase of the current solar cycle will be important to further strengthen our point made here [*Steinbrecht et al.*, 2004].

Eddy heat flux contribution is observed to be maximum during winter months (up to ± 30 DU) at higher latitudes. This contribution is only significant beyond 50°N

from January until May, but has non-negligible contribution at low latitudes (see Figure 5.9). Apart from the eddy heat flux the largest variability is produced by the Pinatubo signal that reduced total ozone at high latitudes by about 60–70 DU during winter/spring 1991/92. In agreement with earlier trend assessments the volcanic aerosol contribution to stratospheric ozone is maximum during winter/spring and minimum during summer/fall [*Bodeker et al.*, 2001, for instance]. The effect from the El Chichón eruption is only very modest and decreases did not exceed 10 DU for all latitudes after 1983.

As shown in Figures 5.5 and 5.6, ozone reconstructions using either linear trend or EESC terms (stratospheric chlorine loading trends) work about equally well. However, the choice of either terms may alter the impact from other processes. In Figure 5.10 the contributions from solar, eddy heat flux, and Pinatubo aerosols are shown for both ozone reconstructions in the 50°N-60°N latitude band. Using linear trend terms, the solar and Pinatubo influence on ozone increases by about 4 DU (from solar minimum to maximum) and 10 DU (additional decline in April 1993), respectively. Modification of the eddy heat flux term is rather minor with respect to the choice of linear or EESC terms. A significant change is, however, observed in the linear part of the EESC trend until December 1995 that amounts to about -16 DU/decade in April (see Figure 5.10). This is larger than the overall trend of the linear proxy of -8 DU/decade for the entire period until 2003.

Figure 5.11 shows the long-term ozone decrease from the linear trend assumed for the entire period up to 2003 for all latitudes and months based upon the full regression model as described by Eq. 5.3. The trends are statistically significant at the 2σ level only in winter and early spring above 35°N with a maximum of -10 DU/decade in February at mid-latitudes. By replacing the linear trend terms in Eq. 5.3 with the EESC terms in the full regression model (see Eq. 5.4) leads to larger downward trends during the growth phase of the stratospheric chlorine loading until 1995 with maximum values of -15 to -18 DU/decade in February and March at high latitudes as shown in Figure 5.12. This translates into a -17 to -20 DU/ppb EESC change. The slope of the EESC curve in the declining phase after 1999 corresponds to about one third of the initial increasing rate (see Figure 5.2), so that a recovery of up to 5 to 6 DU/decade at high latitudes in winter/spring can be associated with the turnaround of the chlorine loading.

In a second step, the eddy heat flux terms were replaced by the PSC volume proxy (Eqs. 5.3, 5.4, and 5.5) and this has a significant effect on the EESC contribution by reducing the linear trend up to 1995 by nearly half at higher latitudes during winter/spring with a maximum declining trend of 10 DU/decade. It practically removes the statistical significance of the EESC contribution (at 2σ level) as shown in Figure 5.13. Similar to Fig. 5.10, the effect on other terms from the exchange of PSC volume and eddy heat flux is shown in Fig. 5.14. In general only small changes in solar and aerosol components in the 50°N-60°N

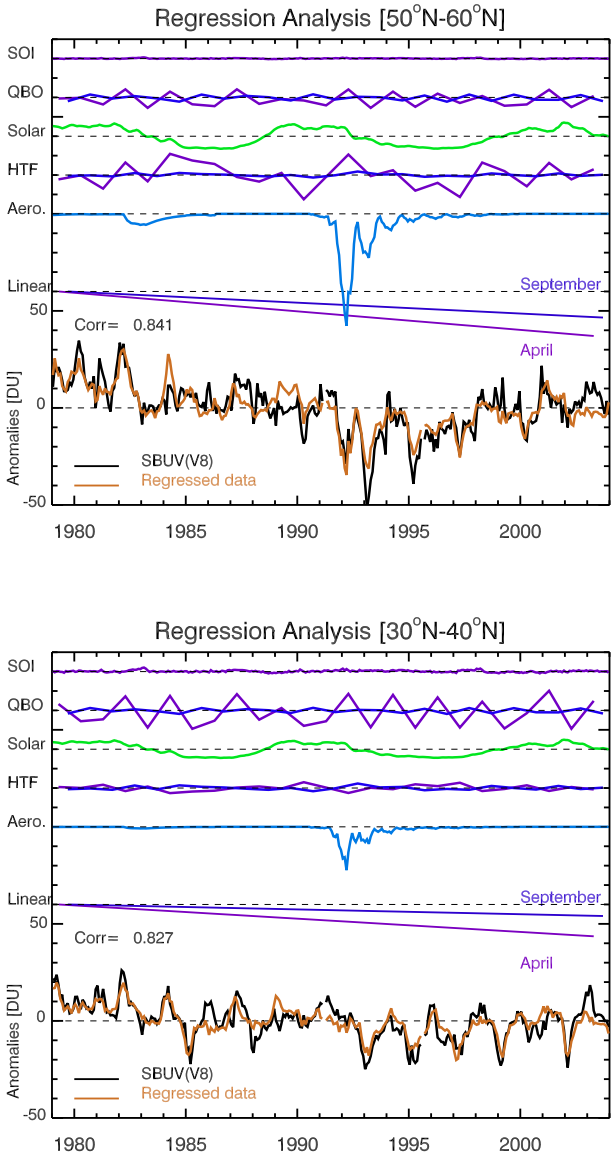

Figure 5.5: Regression plots for the monthly mean total ozone anomaly from SBUV V8 data set for the 30°N-40°N (bottom) and 50°N-60°N (top) latitude bands. In the bottom of each plot the fit (orange) along with the observational data (black) are shown. The ozone anomalies for both observations and model were calculated by subtracting the respective long-term mean for each month of the year from the monthly total ozone time series. In the top of each plot the contributions from individual explanatory variables are shown. Contributions from linear trend term, eddy heat flux, and QBO are only shown for April (violet) and September (gray), while others are shown for all months.

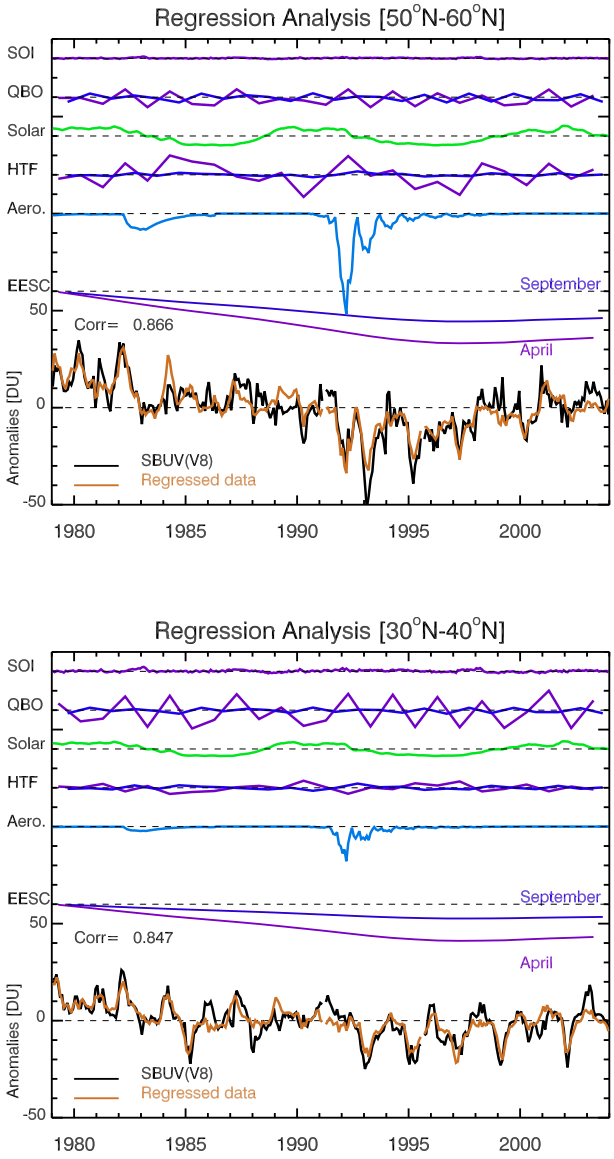

Figure 5.6: Same as Figure 5.5, but model fits with EESC terms replacing linear trend terms as indicated by Eq. 4.

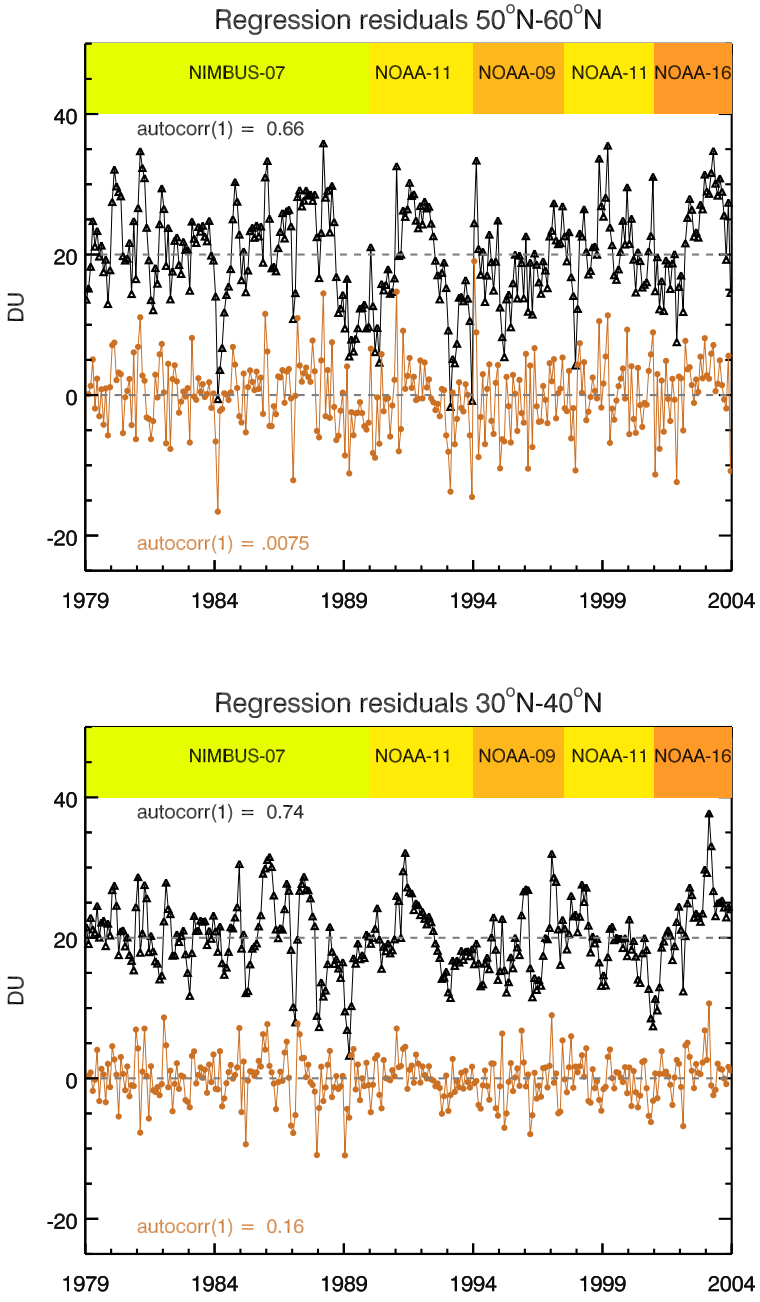

Figure 5.7: Regression residuals in the 30°N-40°N (bottom) and 50°N-60°N (top) latitude bands. Black line marks the residuals from a regression without auto-regression correction (shifted by +20 DU for better clarity). The orange line marks the residual of the transformed model, e.g. residuals of the time series $TOZ(n) - \hat{\rho} \cdot TOZ(n-1)$, where $\hat{\rho}$ is the auto-correlation coefficient with time lag of one month before the transformation. Also indicated are the various satellite platforms for the SBUV instruments from which the SBUV ozone time series was constructed.

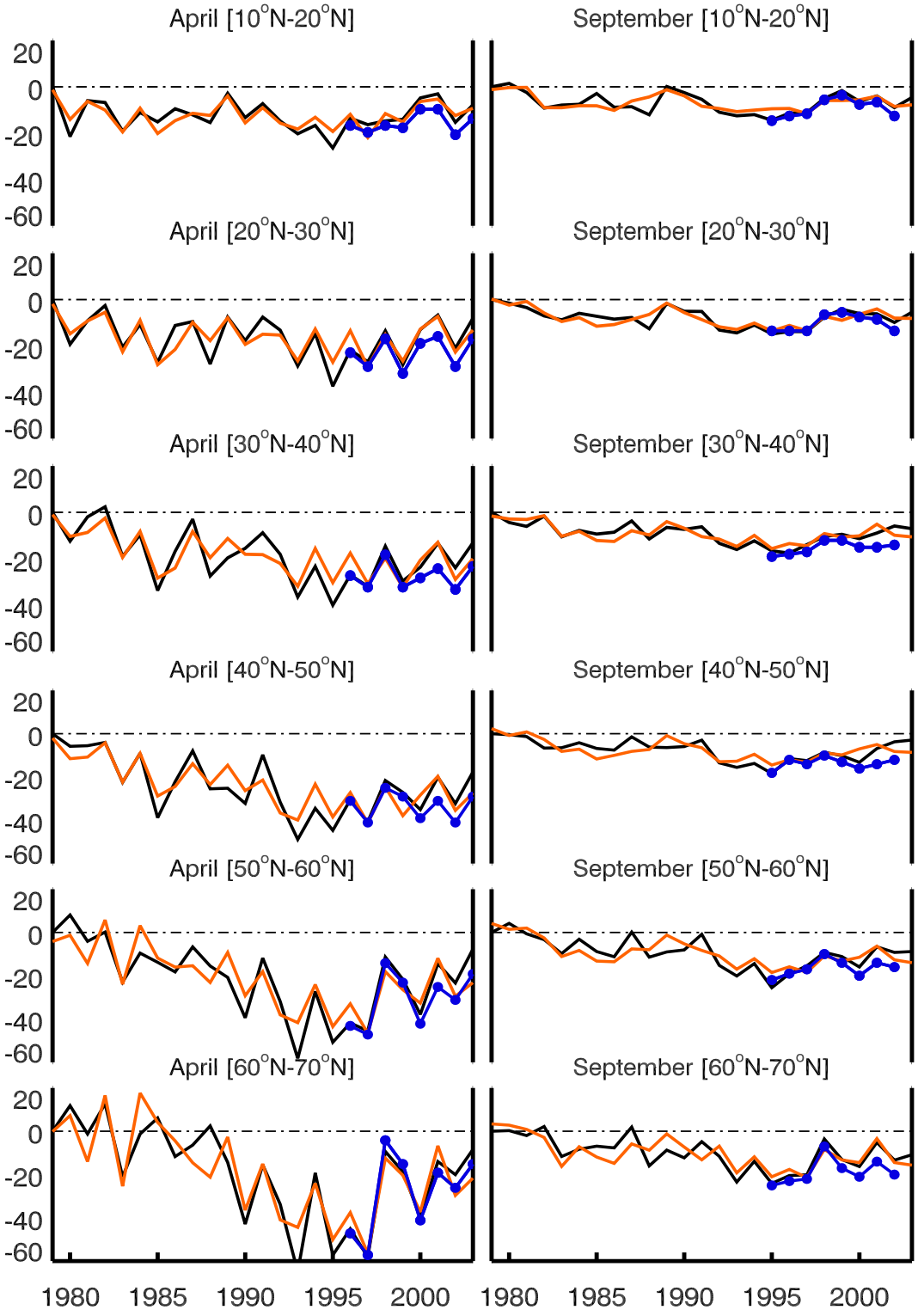

Figure 5.8: Observed SBUV V8 (black) and modelled (orange) total ozone anomalies for all NH latitude bands in April (left) and September (right) based upon multi-variate regression (Eq. 5.3) with linear trend and eddy heat flux terms. Similar results are achieved when linear terms are replaced by EESC terms (Eq. 5.4). Observations from GOME (1995-2003) are shown in gray.

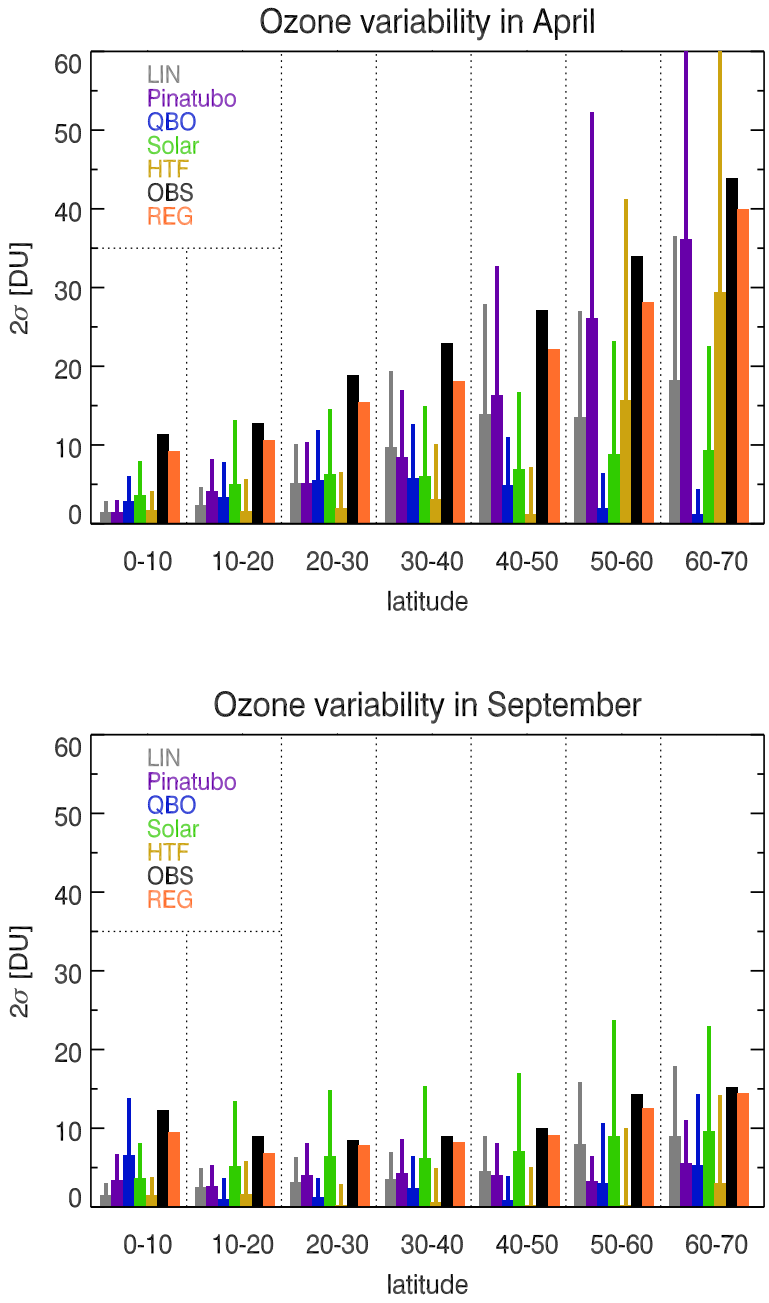

Figure 5.9: Two-σ ozone variability of individual processes in April (top) and September (bottom) from Eq. 5.3. Vertical bars indicate error contribution from the uncertainty of fitting coefficients in the regression equation. Black and orange bars are observations and model results, respectively.

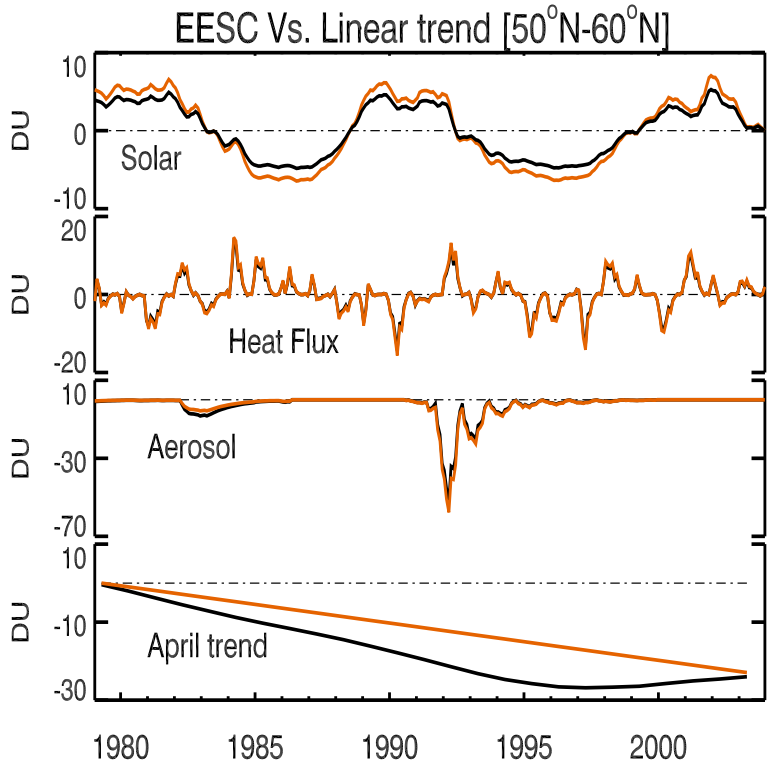

Figure 5.10: Contribution from selected explanatory variables when either linear terms (orange) or EESC terms (black) are used in the full regression model of Eq. 5.3. Overall statistical significance (R^2 value) does not change significantly, but contribution from aerosol term and solar flux term slightly differ.

band are found when PSC volume replaces eddy heat flux terms. In Arctic winter 1999/2000 a drop of about 30 DU can be associated to the polar ozone loss that exceeds the effect from eddy heat flux by a factor of about two. The PSC volume contribution is only significant during winter/spring at latitudes higher than about 50°N similar to the eddy heat flux. The mid-latitudes are influenced by polar ozone loss most likely via airmass mixing after the polar vortex break-up in early spring as discussed before [*Knudsen and Grooss*, 2000; *Fioletov and Shepherd*, 2005]. Comparing the eddy heat flux and PSC volume contribution in Fig. 5.14, it is evident that during the nineties minima in eddy heat flux match minima in accumulated PSC volume, however, in the mid-eighties this is not the case for a couple of winters.

The contribution of the EESC turnaround to the recent NH ozone increase is fairly minor (up to 5-6 DU/decade in the regression with eddy heat flux or about 3 DU/decade with PSC volume during the last five years) compared to other processes such as planetary wave driving (or PSC volume) as well as solar flux variability that

explain roughly a 30 DU increase in the 50°N-60°N band during winter months as shown in Fig. 5.10. When replacing eddy heat flux terms with PSC volume representing polar chemical ozone loss (Fig. 5.13), the EESC contribution standing for background gas phase chemistry has an insignificant impact (at the 2σ level) on the total ozone trend. In other words, the variability in polar (here Arctic) ozone loss suffices to explain major parts of the observed turnaround in NH mid-latitude and polar ozone after decreases until early 1990s that experienced a series of cold Arctic stratospheric winters [*Pawson and Naujokat*, 1999]. It is important to note that the polar ozone loss is dynamically driven by temperature changes related to the wave driving as discussed before. This also means that the polar ozone loss proxy accounts in addition for dynamically driven ozone variability related to ozone transport and synoptic meteorology [*Hood and Soukharev*, 2005; *Wohltmann et al.*, 2005].

In the linear trend model from Eq. (5.3), so-called change of trend terms (beginning in January 1996) have been included as proposed by *Reinsel et al.* [2005]. In our study the change of trend terms were statistically insignificant at 1σ (not shown here), most likely due to the too short period after 1995.

The observed increase in eddy heat flux in recent winters strengthened ozone transport from lower to higher latitudes and increased Arctic stratospheric temperatures [*Fusco and Salby*, 1999; *Newman et al.*, 2001; *Weber et al.*, 2003]. This is in line with observations of smaller PSC volumes in recent years [*Manney et al.*, 2005] albeit reducing the polar ozone loss contribution. A positive trend in the eddy heat flux is observed in all recent reanalysis data sets as shown in Figure 5.15. Even though there are significant differences in assimilation schemes for ERA-40, NCEP and UKMO, all three analyses confirm the recent increase. This indicates that there are changes in the strength of the Brewer-Dobson circulation and associated with it changes in polar and tropical lower stratospheric temperatures. Increases in lower stratospheric temperatures over the NH polar region and decrease over tropical regions during winter months (DJF) are the expected responses from the circulation changes as shown in Figure 5.16 [*Yulaeva et al.*, 1994; *Newman et al.*, 2001].

5.9 Conclusions

In this study total ozone data from SBUV and other satellite data is used to investigate the cause of recent increases in NH total ozone. Several new proxies such as the cumulative eddy heat flux, cumulative PSC volume, and EESC have been added in a multivariate linear regression model as explanatory variables standing for chemical and dynamical processes that are known to contribute to inter-annual ozone variability. The effects of various dynamical and chemical processes have been systematically included and analysed. Important conclusions are:

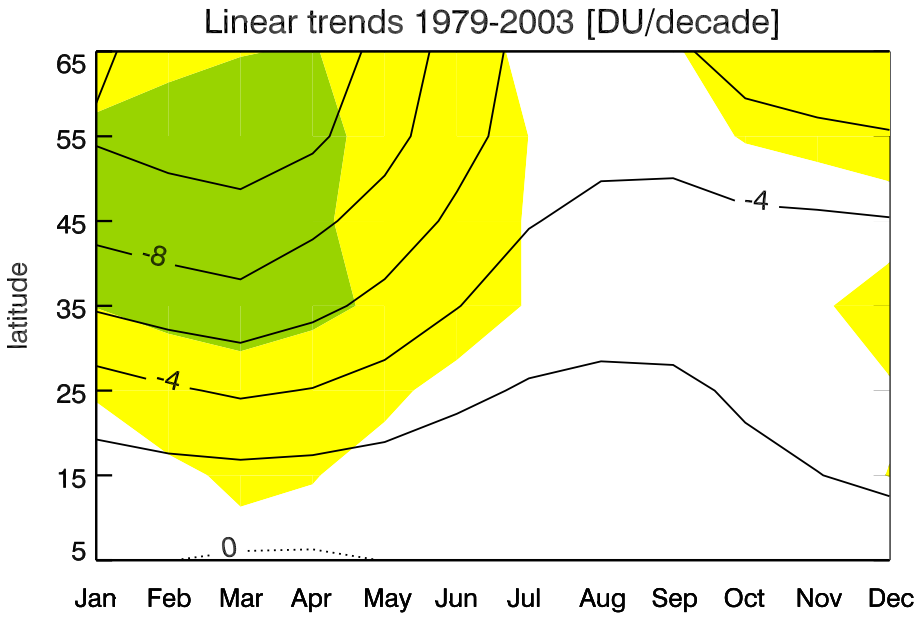

Figure 5.11: Linear trends in DU/year for individual months using SBUV V8 total ozone for various NH latitude bands during the period 1979-2003 based upon the full regression model as described by Eq. 5.3. Linear trends significant at 2σ level are observed at higher latitudes during winter/spring months (dark shadings). Lighter shadings correspond to significance exceeding 1σ.

1. One of the key findings is that recent increases in the NH total ozone are mainly related to increases in eddy heat flux (or reduced polar ozone loss after a series of cold Arctic winters in the mid-nineties [*Pawson and Naujokat*, 1999]) and, to a lesser extent, increased solar activity. The series of cold Arctic winters with extended PSC volumes at the peak of the stratospheric chlorine loading in combination with the strong Pinatubo volcanic event contributed to the pronounced minimum in total ozone anomalies during the mid-nineties at middle to high northern latitudes. This made the recent increase in total ozone appear to be rather rapid. At high northern latitudes (above 50°N) the contribution to the recent increase is about +10 DU from solar cycle (all seasons) and a maximum of +50 DU and +20 DU from stratospheric aerosols and planetary wave driving, respectively, during winter/spring. Replacing the eddy heat flux terms by the PSC volume proxies, the contribution is +30 DU due to reduced polar ozone loss. The linear downward trend for the entire period until end of 2003 has dropped to a maximum of -10 DU/decade during winter/spring that is about half of the downward trend of -16 DU/decade until end of 1995 as derived from fitting EESC terms in the regression model.

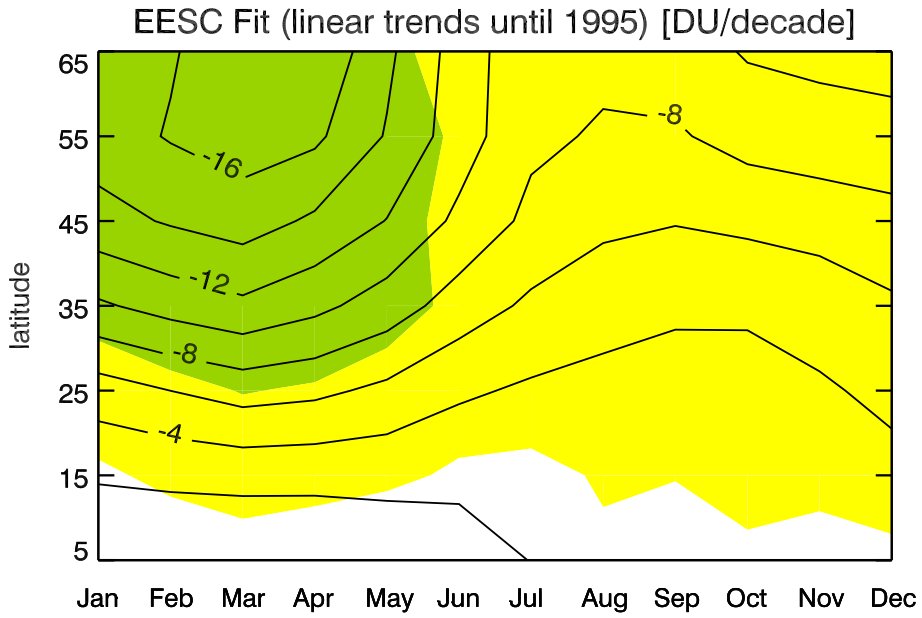

Figure 5.12: Linear trends until end of 1995 in DU/year for individual months using SBUV V8 total ozone for various NH latitude bands from a fit using the same regression model as in Figure 11, but EESC terms replacing the linear trend terms (see Eq. 5.4). For statistical significance see caption for Figure 5.11. A decrease of 12 DU/decade until 1995 is equivalent to a 4 DU/decade increase after the turnaround in EESC.

2. Most of earlier studies have pointed out the difficulties in finding out the exact influence of stratospheric aerosol loading and solar variability on ozone. The recent solar cycle 23 experienced no major volcanic eruption and, therefore, solar term and aerosol loading signatures are better separable in the regression.

3. When the linear trend term is replaced by the EESC term, overall statistical significance of the regression model does not change. Both the linear trend and the EESC terms are commonly associated with gas phase chemistry involving halogens. The relative contribution of the eddy heat flux (or polar ozone loss) and the solar term are slightly reduced and a modest decrease in aerosol contribution is found with the EESC model. The turnaround in the EESC after peaking in 1997 only contributed in a minor way to the recent increases in NH total ozone with a maximum of 5-6 DU/decade during winter/spring at high latitudes.

4. The recent increase in middle to high latitude NH ozone since the mid-nineties led in a recent study to the conclusion that this may be a result of the recent decline in EESC [*Reinsel et al.*, 2005]. They analysed total ozone data from SBUV data as used here and identified a positive and significant change in

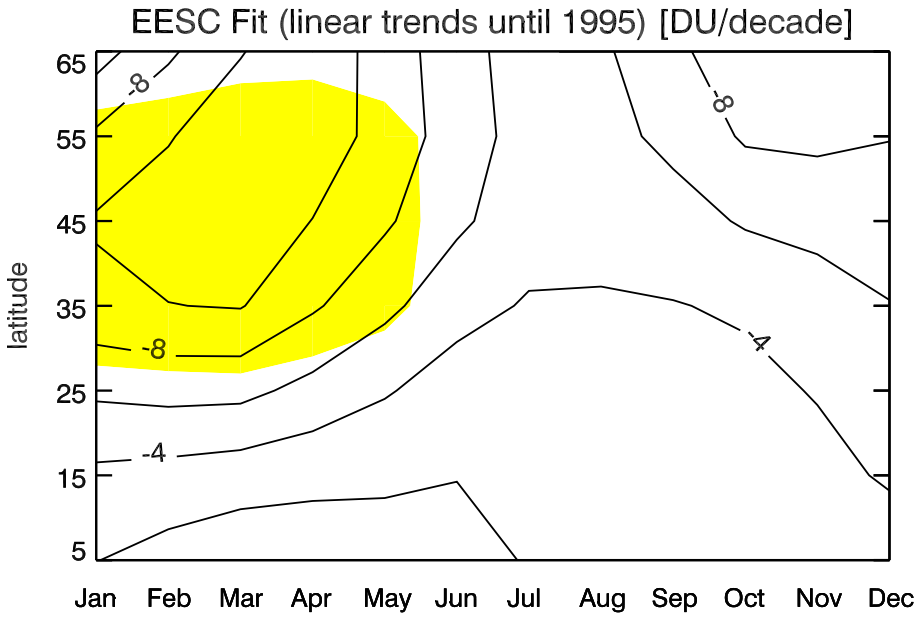

Figure 5.13: Same as Figure 5.12 except that in the full regression model eddy heat flux terms were now replaced by PSC volume proxies (Eq. 5.5). For statistical significance see caption for Figure 5.11.

NH trends after 1996 with and without contribution from dynamical variables included in their statistical model. We find that dynamical factors and, associated with them, variations in chemical processes such as polar ozone loss are believed to have contributed to the recent ozone increase in NH in combination with rising solar activity during solar cycle 23. Similar conclusions have been reported from a model study that identified dynamical processes as the main cause for the recent ozone increase in the NH [*Hadjinicolaou et al.*, 2005].

5. Changes in the strength of the residual circulation are observed in recent years. Using ERA-40, NCEP, and UKMO reanalysis data sets, it has been found that there has been an increase in the eddy heat flux at 100 hPa in recent years (Fig. 5.15). This is reflected in the lower stratospheric temperature over the NH polar cap region which has been increasing in recent years and is accompanied by a cooling of the tropical lower stratosphere (except for year 2000) as shown in Fig. 5.16. It is consistent with our understanding of temperature response to wave driving [*Yulaeva et al.*, 1994; *Newman et al.*, 2001]. Most climate model results indicated that in a future changing climate global warming will lead to stratospheric cooling that will have a negative impact on the expected ozone recovery [*Shindell et al.*, 1999b]. However, some climate model runs indicate that NH planetary wave driving may increase as a result of climate change [*Butchart and Scaife*, 2001; *Schnadt et al.*, 2002]. It remains to be

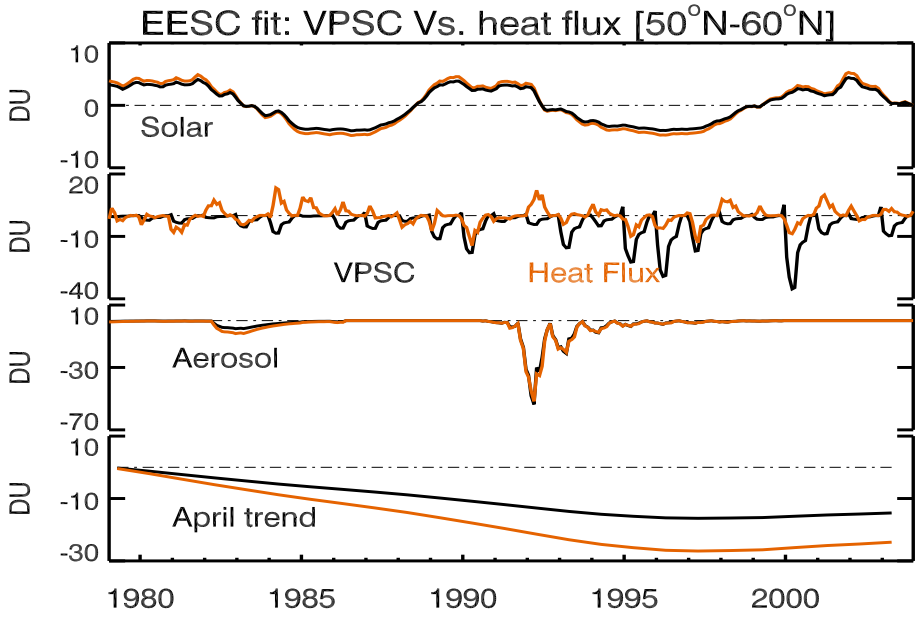

Figure 5.14: Contribution from selected explanatory variables when either eddy heat flux (orange) or PSC volume proxy terms (black) are used in the full regression model (Eq. 5.3) with EESC contribution (Eq. 5.4))for the background gas phase chemistry. Little change is observed in the solar and Pinatubo aerosol component of total ozone, but EESC contribution is reduced at higher latitudes during winter and spring.

seen if the recent increase in planetary wave driving (and less polar ozone loss) that was responsible for the recent NH total ozone increase is just part of a natural decadal variability or will persist. If the latter is the case, we may then expect an accelerated ozone recovery due to possible climate change.

5.10 Some additional results

Above discussed analysis have been extended to year 2005. for both hemispheres. Because of large data gaps in total ozone data at high latitudes during polar nights, the analysis have been restricted up to 60°S-70°N. Eddy heat flux proxy for SH is calculated similar to the that of NH (see Eq. 5.1), but with starting month October.

Figure 5.17 shows the regression analysis for 40°S-30°S (bottom) and 60°S-50°S (top) latitude bands. Ozone anomalies (in black) at the bottom of each shows that SH total ozone undergoes very little seasonal variation compared to NH (Figure 5.5). In general, correlation between ozone anomalies and regressed series (shown in orange) ranges between 0.79 to 0.85 in SH, which is slightly lower than tropical and NH mid-high latitudes. Contribution from individual physical process is also shown in

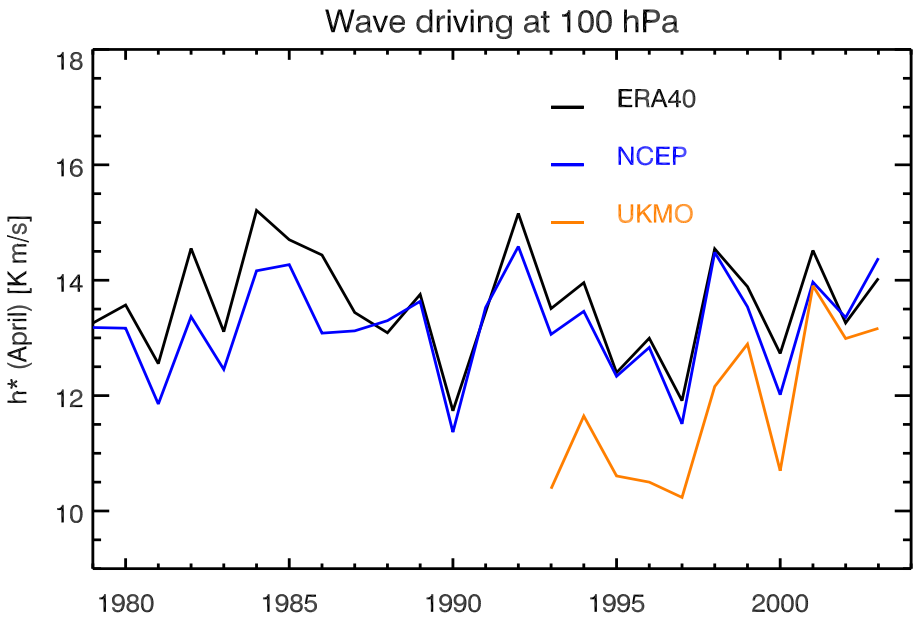

Figure 5.15: Average winter eddy heat flux at 100 hPa (from October to April) between 45°N and 75°N from various meteorological analysis: ERA-40 reanalysis [*Simmons and Gibson*, 2000], NCEP reanalysis [*Kalnay et al.*, 1996], and UKMO (METO) data sets [*Swinbank and O'Neill*, 1994]. Differences between analyses are due to different model resolution and different parameterization schemes. All analyses show an increase in winter eddy heat flux since mid-nineties.

each plot. As expected September downward ozone trends are much higher (∼12 DU) for 60°S-50°S latitude band compared to 40°S-30°S (∼4 DU) due to the more stable polar vortex in SH. Interestingly there is very little influence of enhanced stratospheric aerosol loading due to large volcanic eruption on SH total ozone, although differences in aerosol optical depth are relatively small between SH and NH. Moreover slight increase in total ozone during El Chichòn eruption in 1984, indicate that increase in aerosol during that period led to a slight warming of the polar vortex. Effect of Mount Pinatubo eruption which caused up to 60 DU ozone loss in NH high latitudes is also quite minor in SH (up to 10 DU).

Some additional interhemispheric differences are observed in QBO and solar cycle contribution, both of them show stronger influence on SH ozone variability compared to NH. This is probably due to the fact that planetary wave activity is quite low in SH. This leads to very stable polar vortex with little intra-annual variability and probably helps for a better separation of influence of individual processes from a time series.

Long term linear trends are shown in Figure 5.18, (like Figure 5.11) for both

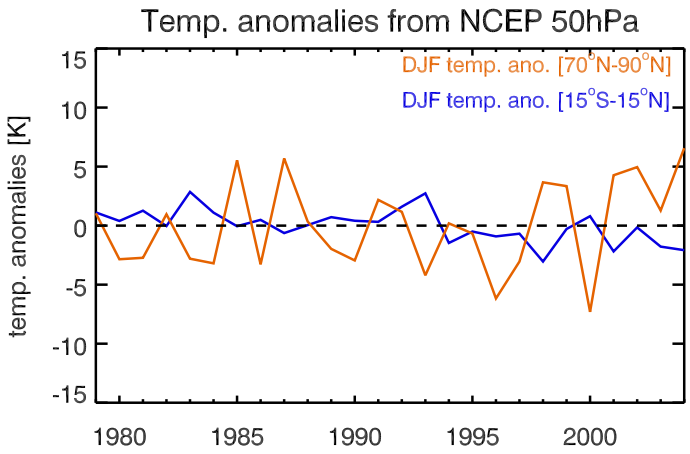

Figure 5.16: December to February (DJF) temperature anomalies from NCEP reanalysis dataset over the Arctic (70°N-90°N) and the tropics (15°S-15°N) at 50 hPa. Decrease in lower stratospheric temperatures over tropics and increase in polar stratospheric temperature since 1997 (except for 2000) is clearly observed. Same features are observed in ERA-40 and UKMO(METO) data sets. MSU channel 4 dataset, which samples the atmosphere between 16-20 km, shows a similar signature.

hemispheres and for the extended time period 1979-2005 using SBUV/TOMS merged ozone data. Overall long term linear trends in NH are similar to SBUV V8 for period 1979-2003 and there are no significant changes in NH trends for the extended period (1979-2005). This supports the stability of the regression model as used in earlier part of this chapter. In general, ozone trends are higher in SH mid-high latitudes (up to 12 DU/decade). This is coherent with our understanding that less wave activity in SH hemisphere causes very cold and stable polar vortex which leads to massive heterogeneous chemical ozone loss during spring season. These low ozone concentrations remain evident in the summer season [*Fioletov and Shepherd*, 2003].

Figure 5.19 shows the ozone trends when linear term is replaced by EESC term. As noted earlier these trends corresponds to linear trends till 1995. For NH, the trends are nearly similar to that shown in Figure 5.12, which shows almost 4 DU/decade ozone increase since EESC turnaround. But in SH, changes are much larger. For 50°S-60°S latitude band ozone trends are changed from 8 DU/decade to 16 DU/decade. This shows that ozone trends are changed by almost 8 DU/decade since the EESC turnaround. Such a changes in EESC concentration are probable most import factor in determining increase in ozone concentration in SH in last decade.

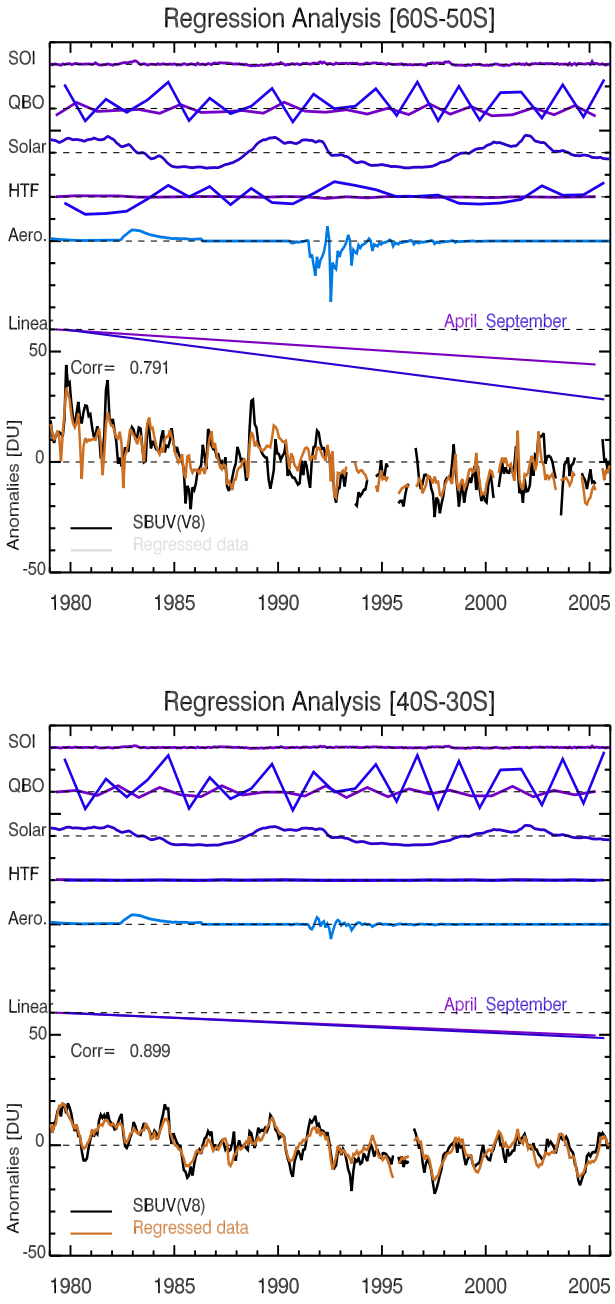

Figure 5.17: Same as Figure 5.5, but using TOMS/SBUV merged total ozone between 40°S-30°S (bottom) and 60°S-50°S (upper) for 1979-2005. In the bottom of each plot the fit (orange) along with the observational data (black) are shown. The ozone anomalies for both observations and model were calculated by subtracting the respective long-term mean for each month of the year from the monthly total ozone time series. In the top of each plot the contributions from individual explanatory variables are shown.

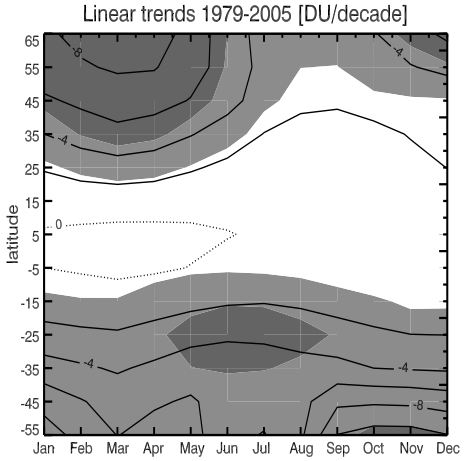

Figure 5.18: Same as Figure 5.11, but using TOMS/SBUV merged total ozone between 60°S-70°N for the time period 1979-2005. Note that in SH, magnitude of linear trends is similar to NH with very little seasonal variation in long term trends.

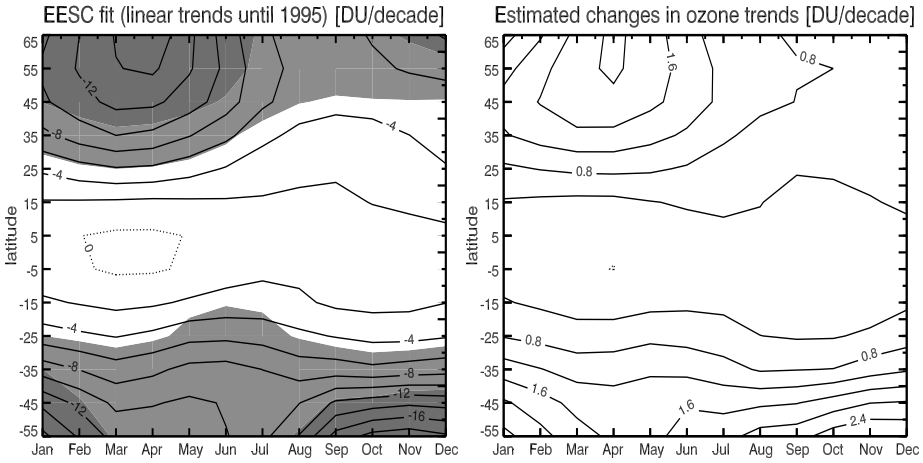

Figure 5.19: Same as Figure 5.12 (left panel), but using TOMS/SBUV merged total ozone between 60°S-70°N for the time period 1979-2005. Figure in right panel shows the estimated changes in ozone trends due to changes in EESC concentration. These estimates are done in a following way. Long term linear trends for 1979-2005 period (model with linear trend term) are subtracted from trends for 179-2005 period (model with EESC trend term). As shown in Figure 5.2, changes in EESC concentration slope for 1997-2005 period are almost one-third than that of 1979-1997 period. So, the differences between long term trends (one with linear terms and one with EESC term) are divided by three and are shown in right panel of the figure.

5.11 Concluding remarks

Long term trends are determined using multivariate regression using total ozone data from various satellite instrument for 1979-2005. In general magnitude of observed ozone trends is higher in SH compared to NH. In addition, influence of QBO and solar variability is slightly higher in SH, probably due to the fact that less ozone variability help for better separation of the influence of individual processes. Significant changes in ozone trends were observed after replacing linear term (linear trends up to 2005) with EESC term (linear trends up to 1995). In NH high latitude changes in ozone trends are $\sim$4 DU/decade and in SH high latitudes they are up to $\sim$8 DU/decade.

6 Tropical Lower Stratospheric WV and Brewer-Dobson Circulation [1]

6.1 Abstract

Using water vapor data from HALOE and SAGE II, an anti-correlation between planetary wave driving (here expressed by the mid-latitude eddy heat flux at 50 hPa added from both hemispheres) and tropical lower stratospheric (TLS) water vapor has been obtained. This appears to be a manifestation of the inter-annual variability of the Brewer-Dobson (BD) circulation strength (which is proportional to the mid-latitude eddy heat flux) and the amount of water vapor entering into the tropical stratosphere. Some years such as 1991 and 1997 show, however, a clear departure from this linear relationship which suggests that the water vapor changes in TLS can not be attributed solely to changes in extratropical wave activity. After 2000 a sudden decrease in lower stratospheric water vapor has been reported in earlier studies based upon satellite data from HALOE, SAGE II and POAM III indicating that the lower stratosphere has become drier since then. This is consistent with a sudden rise in the combined mid-latitude eddy heat flux with nearly equal contribution from both hemispheres as shown here and with the increase in tropical upwelling and a decrease in cold point temperatures as found by *Randel et al.* [2006]. The low water vapor and enhanced strength of the BD circulation has persisted until the end of the satellite data records. From a multi-variate regression analysis applied to 27 years of NCEP and HadAT2 temperatures (up to 2005) including contributions from solar cycle, stratospheric aerosols and QBO, the BD circulation changes after 2000 are estimated to contribute up to 0.7 K cooling to the overall TLS temperature change during the period 2001-2005 when compared to the period 1996-2000. NCEP cold point temperature show an average decrease of nearly 0.4 K from changes in BD circulation, which is consistent with observed mean TLS water vapor changes of about -0.2 ppm after 2000.

6.2 Introduction

Stratospheric water vapor plays an important role in determining radiative and chemical properties of the middle atmosphere. As a primary source of odd hydrogen

[1] Contents of this chapter are the part of the revised version of the manuscript S. Dhomse and M. Weber and J. Burrows, The relationship between Brewer-Dobson circulation and tropical lower stratospheric water vapor, *Atmos. Chem. Phys. Disc., 6, 9563-9581, 2006*

in the stratosphere, it controls ozone loss through gas phase chemistry. In addition, the coupling processes between HO_x and NO_x/ClO_x affect ozone destruction by other catalytic reaction cycles and heterogeneous chemistry on polar stratospheric clouds responsible for polar ozone loss. An increase in stratospheric WV can have serious implications on the future evolution of the ozone layer [*Shindell et al.*, 1999b; *Tabzadeh et al.*, 2000; *Stenke and Grewe*, 2005] and, therefore, delay ozone recovery [*Shindell*, 2001]. The longest *in situ* time series of stratospheric water vapor measurements are available from balloon measurements in Boulder, Colorado (40°N, 105°W). The water vapor volume mixing ratios (VMRs) in the lower stratosphere above Boulder have been increasing by about 1% per year since 1981 [*Oltmans et al.*, 2000]. Trends in stratospheric water vapor above 18 km are, however, lower in the satellite data records [*SPARC*, 2000; *Randel et al.*, 2004b].

Initially it was believed that methane oxidation as well as WV directly emitted by aircrafts might have contributed to rising levels of water vapor in the stratosphere. The observed changes in stratospheric methane at most contribute only about one third to the water vapor trend [*SPARC*, 2000]. Another important source of stratospheric water vapor variability are changes in the tropical tropopause temperatures which determines the water vapor VMRs of the air entering in to the stratosphere [*Brewer*, 1949; *Rosenlof*, 2003]. But tropical tropopause temperatures are not increased as would be needed for a stratospheric H_2O increase [*SPARC*, 2000; *Randel et al.*, 2004b].

The stratospheric water vapor trends are influenced by changes in the Brewer-Dobson (BD) circulation that impacts both constituent transport and, with regard to water vapor more important, stratospheric temperatures. The BD circulation transports most of the chemical species from the source region (tropics) to the mid- to high latitude stratosphere and is primarily driven by breaking of tropospheric generated waves (e.g Rossby waves) in the mid-latitude stratosphere. The influence of the planetary wave activity on the stratospheric circulation is generally explained in terms of the "downward control principle" [*Haynes et al.*, 1991], which means that the ascent or descent of air-masses at certain altitudes is determined by the momentum (as expressed by the convergence of the Eliassen-Palm flux) deposited above it. Mass balance requires that the descent of air from the stratosphere down to the troposphere at high latitudes and ascent of tropospheric air into the tropical stratosphere is accompanied by horizontal mixing. Descending airmasses at high latitudes undergo adiabatic compression thereby increasing polar stratospheric temperatures away from the radiative equilibrium [*Newman et al.*, 2001], while the ascent at low latitudes lowers stratospheric temperatures by adiabatic expansion [*Yulaeva et al.*, 1994]. The eddy heat flux which is directly proportional to the vertical component of EP flux and, approximately, proportional to the EP flux convergence, is a good measure of the magnitude of mid- to high latitude wave driving and the strength of the BD circulation. It has been linked to changes in stratospheric ozone and temperatures at high latitudes and tropics and chlorine activation inside the polar vortex [*Yulaeva et al.*, 1994; *Fusco and Salby*, 1999;

Newman et al., 2001; *Weber et al.*, 2003].

Using trajectory calculations and a cold point based dehydration mechanism, *Füglisthaler et al.* [2005] showed good agreement between modeled and observed stratospheric water vapor VMRs in the TTL. They concluded that an 1 K change in cold point temperatures lead to about 0.5 ppm change in water vapor VMRs. On long term scale, *Füglisthaler and Haynes* [2005] concluded that most of the inter-annual variability in the 1990s is dominated by QBO and to some extent by El Niño. *Randel et al.* [2006] showed that the seasonal variations in water vapor VMRs in TLS show a correlation ($r = 0.73$) with changes in cold point temperatures (with lag of 2 months). *Randel et al.* [2004b, 2006] showed that the observed decreases in stratospheric water vapor VMRs since 2000 are consistent with decreases in tropical cold point temperatures and enhanced tropical upwelling between 20°N-20°S. They also showed that temperature changes in the TTL can be explained by a radiative feedback from tropical ozone decrease near the tropical tropopause [*Randel et al.*, 2006].

Randel et al. [2006] demonstrated the significant correlation between tropical upwelling and cold point temperature in the TTL as well as water vapor VMRs in the tropical lower stratosphere, despite the fact that ascent velocities are associated with high uncertainties since it is a highly derived quantity from the meteorological analyses. They also showed that the period after 2000 with lower water vapor concentrations [*Randel et al.*, 2004b; *Nedoluha et al.*, 2002] can be linked to an increase in the average strength of the Brewer-Dobson circulation after 2000 as compared to a five year period before. The relationship between cold point temperature and tropical upwelling [*Randel et al.*, 2006], on one hand, and the expected correlation between tropical upwelling and mid-latitude eddy heat flux (both frequently used as a measure for the BD circulation strength), on the other hand, suggest a close relationship between the inter-annual variablity of TLS water vapor and eddy heat flux similar to that observed for stratospheric ozone [*Randel et al.*, 2002b; *Weber et al.*, 2003]. In this paper we are interested in the question how well the year-to-year variability in the tropical stratospheric water vapor can be associated with variations in the BD circulation strength (here expressed by the extratropical eddy heat flux) since the start of the satellite records in 1984 (SAGE II, HALOE). Also, can we quantify the potential contribution of the BD circulation to TLS and cold point temperature changes after 2000 from a regression analysis covering 27 years of temperature data.

After a brief introduction on the used water vapor data sets and meteorological analyses (Section 2), we look at the inter-annual variability in tropical water vapor and BD circulation strength (Section 3). The drop in stratospheric water vapor after 2000 [*Randel et al.*, 2004b, 2006] in connection with the enhanced planetary wave activity and TLS temperature changes is discussed in Section 4.

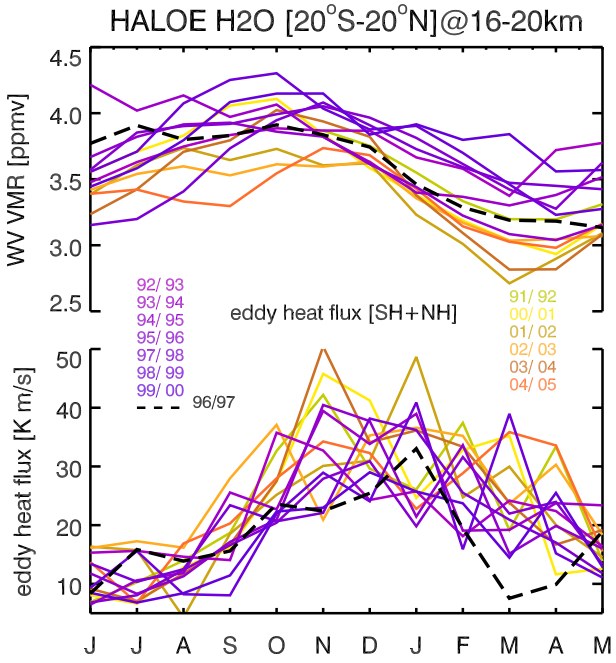

Figure 6.1: Annual cycle of monthly mean tropical water vapor VMRs from HALOE V19 data averaged between 16 km and 20 km and between 20°S and 20°N (top) and monthly mean mid-latitude eddy heat flux at 50 hPa averaged from 45° to 75° with area weights and added from both hemispheres (bottom). Years with higher and lower wave activity are shown in yellow–red and blue–violet lines, respectively.

6.3 Data

6.3.1 Water vapor data

Currently only few good quality stratospheric water vapor data sets are available for long term analysis. Near global water vapor measurements are provided by the Stratospheric Aerosol and Gas Experiment II (SAGE II, 1984-2005) and the Halogen Occultation Experiment (HALOE, 1992-2005). Both instruments and POAM III (1998-2005, see below) ceased operating by the end of 2005. All three instruments use the solar occultation technique to measure attenuated solar radiation through Earth's limb at discrete wavelengths, which is then inverted to retrieve concentrations of various trace gases in the atmosphere. For water vapor retrieval the primary channel used in SAGE II is near 935 nm [*Thomason et al.*, 2004], while HALOE uses radiances near 6.61 μm [*Russell et al.*, 1993]. Both instruments provide approximately 15 sunrise and 15 sunset measurements per day. For the retrieval below 35 km, both HALOE and SAGE II use temperature profiles from NCEP. For complete global coverage (except for the highest latitudes) both

instruments need about 1 to 1.5 months.

In this study SAGE II V6.2 data were analyzed that has been obtained from www-sage2.larc.nasa.gov/data/v6_data/. The vertical sampling of the SAGE II water vapor profile is about 0.5 km with a vertical resolution of 1 km. Although there are significant improvements compared to earlier version of the WV data, there are still some problems during years with high stratospheric aerosol loading [*Thomason et al.*, 2004]. *Taha et al.* [2004], suggested that water vapor profiles with aerosol extinction coefficient at 1020 nm greater than 2×10^{-4} km^{-1} are not reliable and they were removed from our analysis, thus excluding the periods 1984-1985 and 1992-1994. HALOE V19 data were obtained from haloedata.larc.nasa.gov/. HALOE has an instantaneous field of view of about 1.6 km and a vertical resolution varying between 2 and 3 km. However, the data were interpolated to a 0.3 km grid for retrieval purposes. It should be noted that both SAGE II and HALOE measurements show largest uncertainties near the TTL region due to measurement geometry [*SPARC*, 2000]. The water vapor profiles have been weighted with the inverse of square of measurement errors when calculating monthly zonal means.

In addition to SAGE II and HALOE, the Polar Ozone and Aerosol Measurement (POAM III, 1998–2005) water vapor version 4 data set has been used in this study [*Nedoluha et al.*, 2002]. POAM III also measures in solar occultation, but water vapor profiles are only available for higher latitudes. Data have been obtained from www.cpi.com/ and the vertical resolution is about one km.

In this study, monthly mean zonal mean water vapor values from the satellite data were calculated when at least five observed profiles in a given latitude band were available. Data gaps in months with less than five profiles were filled by values obtained from a harmonic analyses of the time series containing annual and semi-annual terms.

6.3.2 Meteorological data

Meteorological data used here are primarily from the National Centers for Environmental Prediction (NCEP)/ National Center for Atmospheric Research (NCAR) reanalysis model [*Kalnay et al.*, 1996]. Data at six hour intervals on a $2.5^\circ \times 2.5^\circ$ grid were obtained from www.cdc.noaa.gov/cdc/data.ncep.reanalysis.pressure.html. The major advantage of NCEP reanalysis data is that the assimilation system remains unchanged, although changes in the quality of data assimilated and their availability strongly influence the analyses (for detailed discussion see *Randel et al.* [2004a]). The eddy heat flux are calculated using daily temperature and wind data as described in *Randel et al.* [2002b]. The monthly mean eddy heat flux data have been derived from daily values. In addition to the available isobaric analysis fields, cold point temperatures have been derived from NCEP.

Another meteorological data are the 40-year re-analysis (ERA-40) [*Uppala et al.*, 2005] and operational analysis from ECMWF. Data from ERA40 are available

for the period September 1957–August 2002, operational data are available from January 2001 until present. Daily data at six hour intervals were obtained from www.ecmwf.int/ on a $2.5^\circ \times 2.5^\circ$ grid. For comparisons with the meteorological analyses in the tropics, we also use gridded radiosonde temperature (HadAT2) data from UK Met. Office [*Thorne et al.*, 2005]. They were obtained from hadobs.metoffice.com/hadat/hadat2.html and in the stratosphere they are available only at three pressure levels, 100 hPa, 50 hPa, and 30 hPa.

6.4 Extra-tropical wave forcing and stratospheric water vapor

Extra-tropical wave forcing and stratospheric water vapor The seasonal cycle of HALOE water vapor VMRs averaged between 16-20 km altitude and 20°S- 20°N together with the global 50 hPa eddy heat flux with contributions from both hemispheres are shown in Figure 6.1. These variations are consistent with earlier studies, [*SPARC*, 2000] which showed that the water vapor VMRs starts decreasing in November and reaches minimum in January-February and starts increasing afterwards with a seasonal cycle of about ± 0.5 ppmv near 18 km. This annual minimum in water vapor reaches 22 km altitude in summer depending on the speed of ascending motion [*Niwano et al.*, 2003]. These seasonal variations in water vapor are primarily due to changes in the tropical cold point temperatures and advection of air from TTL into TLS [*Niwano et al.*, 2003; *Randel et al.*, 2004b]. Cold point temperatures control the dehydration mechanism while ascending motion control the amount of dehydrated air entering into the stratosphere [*Randel et al.*, 2002a; *Seol and Yamazaki*, 1999]. Ascending motion in TLS is maximum during northern hemispheric winter which can be explained by a superposition of wave activity (or eddy heat flux) from both hemispheres [*Rosenlof and Holton*, 1993a; *Randel et al.*, 2002a; *Salby et al.*, 2003]. The maximum of the eddy heat flux is observed from November to March during NH winter and in the southern hemisphere (SH) from September to November, so that the total flux from both hemispheres shows large values from September to March [*Randel et al.*, 2002a]. This produces a seasonal variation in TLS temperatures [*Yulaeva et al.*, 1994; *Randel et al.*, 2002b] and also explains the so-called tape recorder effect in tropical stratospheric water vapor with low (high) WV when tropical stratospheric temperatures are minimum (maximum) during the seasonal cycle [*Mote et al.*, 1996].

In Fig. 6.1, we selected mean water vapor profiles averaged between 16 and 20 km in order to reduce the large uncertainties associated with the solar occultation data closer to the lowest retrieval altitudes. The speed of upward propagation of the WV anomalies is generally about 8 km/year (upper limit derived from a tape recorder plot, not shown here) or 6 km/year assuming a mean ascent velocity of 0.2 mm/sec [*Randel et al.*, 2006, Fig. 9], so that the vertical averaging leads to some smearing

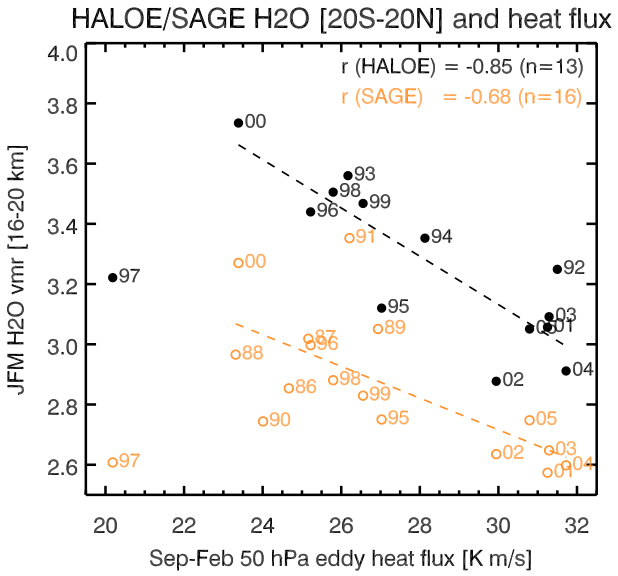

Figure 6.2: Anti-correlation between JFM TLS water vapor VMRs (16–20 km, 20°S-20°N) from SAGE II (open orange circles) and HALOE (filled black circles) and 50 hPa eddy heat flux added from both hemispheres and averaged over the period September-February. The correlation coefficients as indicated in the plot have been derived by excluding the year 1997 (see main text for discussions). The two digit indicate the year, for instance, 97 indicates 1996/97.

of the tape recorder signal. Since water vapor is quite a good tracer, the mean water vapor in the range 16–20 km, therefore, represents roughly the cumulative amount of air transported into the stratosphere from the previous half year. Therefore, the observed water vapor minima as shown in Fig. 6.1 are shifted towards March-April. The strong inter-annual variability in mid-latitude wave driving, here represented by the average eddy heat flux between 45°-75° at 50 hPa and added from both hemispheres, is shown in Fig. 6.1. The color coding indicates years with high wave activity (yellow-red) and low wave activity (violet-blue lines), when TLS water vapor VMRs are generally lower and higher, respectively. This is more emphasized in the scatter plot of tropical JFM water vapor VMRs and 50 hPa eddy heat flux integrated from September to February that shows a distinct anti-correlation between both quantities. Figure 6.2 shows average water vapor VMRs from HALOE (black solid symbols) and SAGE II (orange light symbols).

After filtering out the aerosol contaminated data from SAGE II data, 17 years of SAGE II data since 1984 and 14 years of HALOE data (1992-2005) remained in this analysis. Lower stratospheric water vapor VMRs from SAGE II are systematically lower than HALOE in agreement with *Taha et al.* [2004]. For all HALOE years

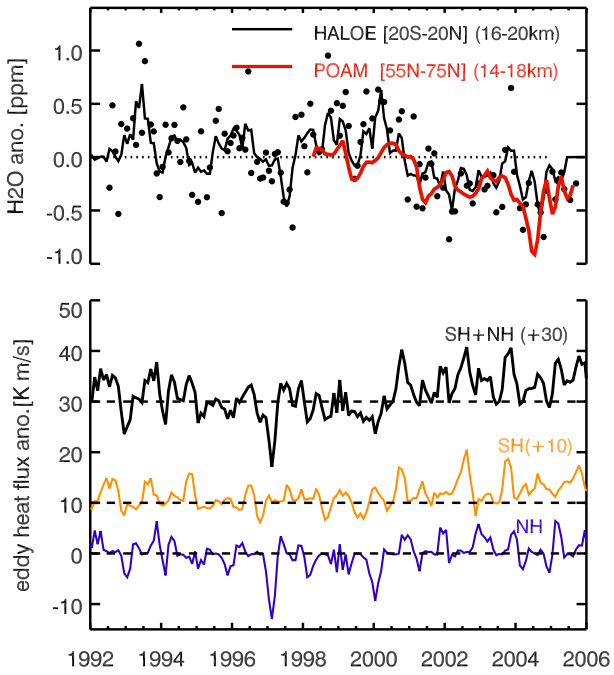

Figure 6.3: Top panel: monthly mean H_2O vapor anomalies from HALOE (16-20 km, 20°S-20°N) in the tropics (black line) and POAM III (14-18 km) at middle to high NH latitudes (red line). Both lines represent three month mean water vapor VMRs, while black circles are monthly mean HALOE values (Update from *Randel et al.* [2006]). Bottom panel: Time series of monthly mean 50 hPa eddy heat flux anomalies in each hemisphere and globally (added from both hemispheres).

the correlation between JFM TLS water vapor VMRs between 16 and 20 km and eddy heat flux is about -0.61 and excluding data from 1997 (here standing for 1996/1997), it improves to -0.85 (significant above 99% confidence interval). For SAGE II the correlation changes from -0.42 (including all years) to -0.68 after excluding 1997. Removing in addition the year 1991, the anti-correlation for SAGE II improves to -0.77 (significant above 99% confidence level). As expected higher global wave activity in a given year leads to lower water vapor VMRs in the tropical stratosphere at the end of the NH winter for most years. The period September-February for eddy heat flux and January-March for water vapor were selected for the highest anti-correlation between both quantities. The length of the September-February period roughly corresponds to the water vapor cumulation time in the 16-20 km column based upon typical ascent velocities discussed before. It should be kept in mind that the near global sampling of the solar occultation instruments like SAGE II and HALOE requires more than a month. This leads to rather low sampling of the tropical stratosphere when zonal monthly means are

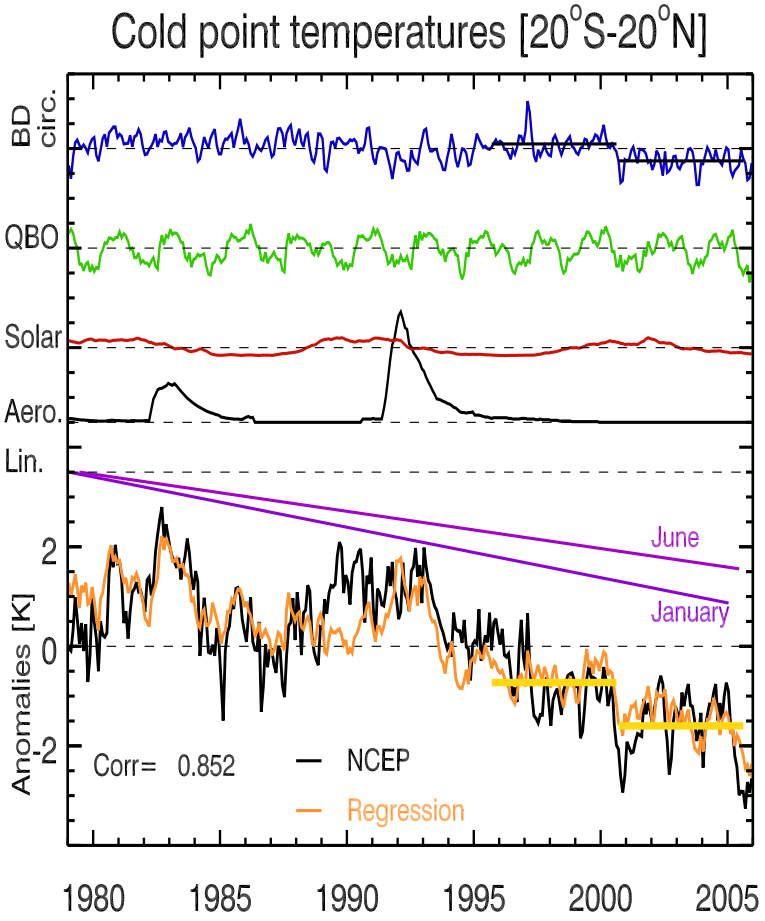

Figure 6.4: Temperature anomalies of the zonal mean cold point temperature from NCEP (20°S-20°N) and fitting results from a regression with contributions from QBO, monthly linear trends, solar variability, stratospheric aerosols, and BD circulation strength (as expressed by the extratropical 50hPa eddy heat flux). Linear trends are only shown January and June. The strengthening of the BD circulation after 2000 resulted in a cooling of about 0.4 K at this level compared to the late 1990s (see horizontal bars in the BD circulation panel). The NCEP data shows a mean cooling of nearly 1 K after 2000 (horizontal bars in the bottom panel).

derived and this may (in part) influence the correlation between both data sets.

We also find that by using eddy heat flux only from the NH the correlation coefficient is about -0.73 for HALOE data (without 1997) but for SAGE II data, it reduces significantly to -0.4 even without the years 1990/1991 and 1996/1997. Using eddy heat flux at 100 hPa or 70 hPa also reduces the correlation coefficients. A possible explanation are differences in the mid-latitude wave driving between both hemispheres. The stationary planetary waves (wavenumber 1-3) and transient synoptic scale waves (wavenumber 4-7) play an important role in driving the BD circulation in the NH while in the SH most of the contribution comes from the transient waves [*Tanaka et al.*, 2004]. The contribution of these high frequency waves to the total eddy heat flux at 100 hPa is quite small but at higher altitudes, they play an important role.

For some years like 1990/1991 (91 in Fig. 6.2) and 1996/97 (97 in Fig. 6.2) larger deviations from the linear relationship between extratropical wave driving and water vapor are noticeable. The year 1997 shows very low TLS water vapor VMRs (both SAGE II and HALOE measurements), despite the fact that the winter eddy heat flux is quite low. The opposite is true for 1990/1991 (SAGE II only), where both the cumulative eddy heat flux and water vapor VMRs are high. An explanation for the extreme departure from the linear relationship for both satellite data is not known. The increase in water vapor at the TTL have been related to El Niño events [*Gettelman et al.*, 2002; *Hatsushika and Yamazaki*, 2000; *Scaife et al.*, 2003]. In early 1997 the Southern Oscillation Index (SOI) shows very low values indicating the beginning of a strong El Niño event, however, in JFM of 1998 the TLS water vapor VMRs appears to be normal, although the Southern Oscillation Index (SOI) remained very low. Such exceptions highlight that the expected relationship between the BD circulation strength and tropical stratospheric water vapor does not hold for all years. Cold point temperature modeled water vapor VMRs (see Figure 2 from *Füglisthaler and Haynes* [2005]) are in agreement with HALOE and SAGE II in 1997, however, they differ significantly for years 1990 and 1993 (due to Mount Pinatubo eruption) from observations. *Randel et al.* [2004b] also noted that even though tropical cold point temperatures show a strong correlation with observed water vapor VMRs at 82 hPa, the years 1997/98, 1999/2000, and 2001/2002 show some unusual behavior (see Figure 13 from *Randel et al.* [2004b]).

Some studies argue that the tropical upwelling is not only driven by extratropical wave driving, but may be linked to the non-linear interaction between various physical processes in the tropical atmosphere such as equatorial Rossby waves and associated adiabatic heating [*Plumb and Eluszkiewicz*, 1999; *Semeniuk and Shepherd*, 2001]. Temperatures in the tropical tropopause layer (TTL) that control the water vapor entry into the stratosphere can also be associated with tropospheric processes related to convection and tropical waves [*Kerr-Munslow and Norton*, 2006; *Norton*, 2006]. Another issue here is the rather low sampling rate of solar occultation instruments

as discussed before, however, it can not explain the obvious outliers in the expected relationship between extratropical wave forcing and stratospheric water vapor in selected years as seen by both satellite instruments.

6.5 Decrease in TLS H_2O vapor after 2000

Decrease in TLS H_2O vapor after 2000 As seen in Figures 6.1 and 6.2 and reported in other studies [*Randel et al.*, 2004b, 2006], lower water vapor VMRs have been observed in the TLS since 2001 indicating that the stratosphere has become drier in recent years. Lower water vapor VMRs are also found in NH mid- to high latitudes with a time lag of a few months due to isentropic transport in the lowermost stratosphere as confirmed by POAM III data [*Randel et al.*, 2006]. Figure 6.3 shows the water vapor VMR anomaly time series from HALOE in the tropics and POAM III at NH mid- to high latitudes [*Nedoluha et al.*, 2002] in the lowermost stratosphere. Anomalies are calculated by subtracting the long-term monthly means (1965-1995) from the time series. Both data sets show a clear drop in the anomalies after 2000. At the same time a sudden increase in the monthly mean global eddy heat flux is evident as shown in Fig. 6.3. The enhancement of the BD circulation as indicated by the increased eddy heat flux is consistent with increased tropical upwelling velocities during the same time period and a weak average enhancement in the subtropical convergence of the EP fluxes during the period 2001-2004 in comparison with the late 1990s [*Randel et al.*, 2006]. From the global eddy heat flux time series separated by hemispheres (Figure 6.3) it can be concluded that each hemisphere contributed roughly equally (NH being slightly larger) to the BD circulation anomaly after 2000.

The strengthening of the BD circulation in the NH in recent years has been associated with increased Arctic stratospheric winter temperatures and rapid increases in NH total ozone since the middle 1990s [*Dhomse et al.*, 2006]. An anti-correlation between tropical and mid- to high latitude lower stratospheric temperatures exists on seasonal and inter-annual time scales [*Yulaeva et al.*, 1994; *Salby and Callaghan*, 2002b] so that a corresponding recent cooling of the TLS and cold point temperature are expected. Figure 6.4 shows a time series of the tropical monthly mean temperature anomaly of the thermal tropopause from NCEP and a regression analysis that quantifies the contributions from QBO, solar cycle variability, stratospheric aerosols, BD circulation strength (global eddy heat flux), and linear trend terms. The linear trend terms account for changes that are not accounted for by other factors and terms. For each month of the year two QBO terms (50 and 30 hPa, 24 fitting constants), one eddy heat flux term (12 fitting constants, no time lag), and a linear trend term (12 fitting constants) are included. One fitting constant for each major volcanic eruption and solar term are also included (for details on regression see *Dhomse et al.* [2006]). The regression analysis has been applied to several pressure levels (100, 70, 50, 30, and 10 hPa,

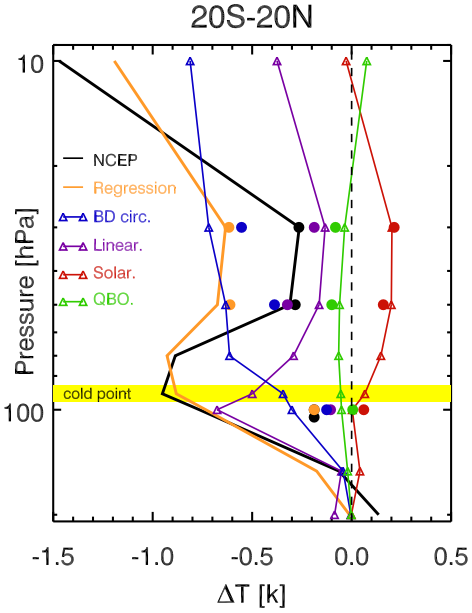

Figure 6.5: Average tropical temperature profile change between the periods 7/2000-6/2005 and 7/1996-6/2000. Thick solid lines: NCEP re-analysis (black) and regression analysis (orange). Other lines with small symbols: individual contributions from solar activity, QBO, and linear trend as derived from 27 years of NCEP data. Large solid circle are the same results, but derived from the HadAT2 radio sonde data. The results for the mean cold point temperatures from NCEP are displayed at the approximate mean cold point altitude of 93hPa.

and cold point altitude) as well to isobaric ERA40 data (up to August 2002) and HadAT2 data (100, 50, 30 hPa). The regression coefficients (for various terms) are similar for both NCEP and ERA40, except for HadAT2 data, where long term linear trends are lower than either ERA40 and NCEP data. In general the eddy heat flux contribution to the temperature change is statistically significant (2σ) from the cold point altitude up to 30 hPa. With radiative lifetime ranging from about 100 days (100 hPa) to 50 days at 50 to 30 hPa [*Randel et al.*, 2002a; *Niwano et al.*, 2003], the diabatic warming relaxation after the adiabatic expansion from the extratropical wave driving is sufficiently slow to detect a temperature change with no time lag in the eddy heat flux. Our regression analysis indicates that the strengthening of the BD circulation contributed nearly 0.4 K cooling to the total changes in the zonal mean cold point temperature when comparing a five year period before and after the drop in water vapor anomalies in 2000 (see the horizontal bars in the BD circulation contribution to the temperature trend in Figure 6.4).

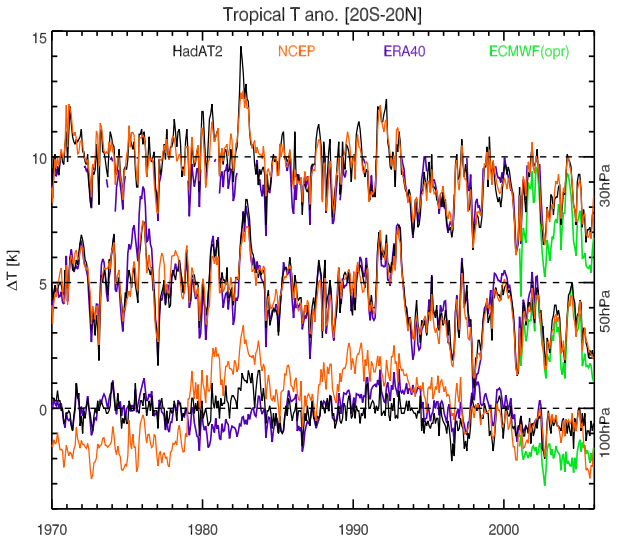

Figure 6.6: Temperature anomalies in the TLS (20°S-20°N) from different meteorological analyses. Temperature anomalies from ERA40 [*Uppala et al.*, 2005] are shown in blue and from ECMWF operational data in green. NCEP [*Kalnay et al.*, 1996] and HadAT2 [*Thorne et al.*, 2005] are shown in orange and black, respectively. Monthly mean anomalies are calculated by subtracting the long-term monthly means (1965-1995) from the time series. Temperature anomalies at 50 hPa and 30 hPa are shifted by 5 K and 10 K respectively, for clarity. The temperature anomalies from ECMWF operational data show a cold bias (1-2 K) with respect to ERA40.

The change in the vertical tropical temperature profile from NCEP and HadAT2 and the 25 year regression applied to both datasets between the period 7/2000-6/2005 and 7/1996-6/2000 is shown in Figure 6.5. From the NCEP data an overall temperature change after 2000 is evident at 100 hPa (-0.8 K), cold point altitude (-0.9 K), and 70 hPa (-1.0 K), while at 50 hPa and 30 hPa the total temperature change is smaller. The increase in the strength of BD circulation after 2000 may have contributed a cooling of 0.2 K at 100 hPa, nearly 0.4 K at the cold point altitude, and 0.7 K at 50 hPa and 30 hPa to the NCEP temperatures, compared to a range of 0.1 K (100 hPa) to 0.7 K (30 hPa) to the HadAT2 radio sonde data. The regression analyses tend to overestimate the overall cooling (including all contributions) above 70 hPa. A stronger cooling in the TLS compared to the cold point temperature would require enhanced adiabatic expansion and upwelling velocities increasing with altitude. According to Fig. 4 in *Niwano et al.* [2003] an increasing upwelling velocity with altitude is observed in the HALOE methane and water vapor data.

As mentioned earlier, *Füglisthaler and Haynes* [2005] found that a 1 K cooling in the cold point temperature roughly corresponds to a decrease of 0.5 ppm in TLS water vapor. This is consistent with cold point temperature changes from extratropical wave forcing of about -0.4 K and an average water vapor decrease of 0.2 to 0.3 ppm after 2000 (see Fig. 6.3). The contribution from the extratropical wave forcing to 100 hPa temperature is negligible, which is an indication that the 100 hPa level is mostly well inside the TTL layer, where the stratospheric influence becomes negligible. In contrast to NCEP data HadAT2 radiosonde data shows almost no changes in 100 hPa temperatures between the five year periods before and after 2000; the cooling seen in the NCEP data primarily has its main contribution from an apparent decadal linear trend that is absent in the radio sonde data. There is some considerable debate on the significance of these linear trends near the tropical tropopause, since changes in radiosonde operations (cooling bias) and changes in the assimilation scheme may strongly impact such long-term trends particularly near the tropical tropopause (see discussion in *Randel et al.* [2004b, 2006] and references therein).

The larger uncertainties associated with the temperature data sets are more evident when looking at different meteorological analyses that are currently avaliable. Figure 6.6 shows temperature anomalies in the TLS derived from various analyses, ERA40 (1958–2002), ECMWF operational analysis data set (2001–present), NCEP (1948–present), and the HadAT2 radiosonde data set. Shown are monthly mean temperature anomalies over the tropics (20°S-20°N) at 100 hPa (bottom), 50 hPa (middle) and 30 hPa (top). Anomalies were calculated by subtracting the climatological monthly means over the period 1965-1995 period from the timeseries. At 50 hPa and 30 hPa no significant bias in the NCEP data is noticeable with respect to the homogenized radiosonde data especially after NCEP switched from TOVS to ATOVS data [*Randel et al.*, 2004b] in July 2001. The ERA40 reanalysis from ECMWF that ended in 2002 shows a bias with respect to the ECMWF operational analysis that ranges from $+1$ K to $+2$ K at all altitudes during the overlapping period (January 2001 – August 2002). This is an indication of uncertainties in temperatures from differences in the assimilation schemes.

There are significant differences among these analyses at 100 hPa. The NCEP data show a larger linear cooling trend after the middle 1990s than either the radio sonde data or ERA40 as discussed before, nevertheless a jump of about of about -0.5 to -1 K during 2000 is noticeable in all data sets (this difference nearly vanishes when averaging over five year periods before and after 2000). The temperature variability apart from spurious linear trends is strongly reduced at 100 hPa (below ± 1 K), which is an indication of a weakening of the stratospheric influence as one goes deeper into the TTL region, while the higher altitudes (above and including the cold point temperature altitude) show larger variations in the anomalies mainly influenced by the QBO and extratropical wave-driving as shown as an example in Fig. 6.5. The NH winter 1996/1997 that was regarded as an

outlier in the TLS water vapor - eddy heat flux anti-correlation (marked 1997 in Fig. 6.2) shows good agreement in the regression analysis of TLS temperatures (positive anomalies in eddy heat flux and temperatures, while at 100 hPa and cold point altitude the negative temperature anomaly (Fig. 6.4) appears to be more consistent with observations of low water vapor observations in that year. One year later (1997/98) the modeled temperature at 70 hPa and 50 hPa are higher than the observed temperature, which makes the five year period before 2000 warmer and the difference to the late period as shown in 6.5 larger (more cooling) in the regression.

While the cooling contribution from BD circulation changes to the NCEP cold point temperature (-0.4 K) after 2000 agree quite well with the observed water vapor change, the total temperature change of nearly -1 K should have doubled the reduction in water vapor in the lowermost tropical stratosphere. The observed long-term downward trends apart from the sudden jump during 2000 is not evident in the water vapor observations. As the homogenized HadAT2 radio sonde data show in contrast to NCEP no linear trend at 100 hPa, it is very likely that the spurious long-term trends are rather artefacts from the larger uncertainties in the radio sonde data that are assimilated into the meteorological analysis.

In summary we have shown that satellite data from HALOE and SAGE show interannual variability in LS WV anomalies that are anti-correlated with the strength of the BD circulation with exception of few years (1991, 1997) with extreme departure from that relationship which is currently not understood. In addition, this relationship also explains the widely reported increasing trends in stratospheric WV until 2000 are most probably due to decrease in planetary wave driving during that period. There is now clear evidence that the drop in the lower stratospheric WV anomalies after 2000 that has persisted until present can be directly related to raising planetary wave forcing with nearly equal contribution to the increase from both hemispheres. From a regression analysis of tropical temperature data a cooling of about 0.7 K in TLS was estimated in connection with the recent enhancement in BD circulation strength. A coherent picture of changes in mid- to high latitude ozone [*Dhomse et al.*, 2006] and lower stratospheric WV in connection with BD circulation changes emerges that may have important implications in a future changing climate.

7 Overall summary and conclusions

This thesis is an assessment of changes in stratospheric ozone and water vapor using updated satellite and climate data sets. Long term observations, improvements in the measurement techniques and data quality in the last two to three decades allows a better attribution of various processes to long term changes in the atmospheric composition in a changing climate. In particular changes in atmospheric dynamics, halogen loading, solar cycle, stratospheric aerosol loading and QBO have been assessed in a number of ways. Some of the key finding of this thesis are summarised as follows:

- A compact relationship between tropospheric generated planetary wave driving and winter ozone gain has been demonstrated. It has been found that the accumulated winter-time eddy heat flux is a very useful proxy in determining the strength of tropospheric generated wave activity, which drives the stratospheric circulation. In Chapter 3, it has been shown that mid-latitude wave activity not only controls the ozone transport from tropical latitudes to higher latitudes but also heterogenous chemical ozone loss by influencing the temperatures inside the polar vortex. A strong anti-correlation between tropical total ozone and mid-latitude eddy heat flux confirms the role of wave activity on ozone transport (dynamics) and chemistry. Using these results, accumulated winter-time eddy heat flux has been proposed as a new proxy for the attribution of dynamical influence of stratospheric ozone. Analysis of long term data records shows significant clustering of data points as well as changes in eddy heat flux- ozone relationship in last two decades, which can undermine the validity of the proposed proxy. These discrepancies can also arise from changes in stratospheric aerosol loading due to large volcanic eruptions, changes in stratospheric halogen loading as well as changes in the quality of meteorological data sets.

- In Chapter 4, influence of solar variability on the stratospheric temperatures has been studied using meteorological data sets from NCEP and ECMWF (ERA40). Correlation analysis shows that solar cycle influence is largest in NH stratosphere during west phase of QBO. This phase dependent relationship is well represented in both ECMWF and NCEP. Multivariate regression analysis of the temperature data for time period of 1979-2005, confirm these results. The regression model shows that during solar maxima mid-winter SSWs are more frequent while during solar minima early winter SSWs are more common. Downward propagation of solar response is significant in both the data sets. Although in NH, solar response for satellite era data period is similar to that for longer period of data starting from 1958, significant differences are observed in SH. Cold temperature bias during 1970s has a significant influence in determining solar response from ECMWF.

In the troposphere, NCEP wind data clearly shows movement of subtropical jet associated with solar variability. This response is absent in ECMWF, probably due to inhomogeneities in ECMWF assimilation scheme. Comparison with HadAT2 radiosonde temperature data however, shows large uncertainties near the tropical tropopause region in NCEP data.

- In Chapter 5, multivariate regression analysis of zonally averaged total ozone data from various satellite instruments (1979–2005) is used to attribute the influence of various atmospheric processes on total ozone variability. Regression analysis shows that solar cycle contributes up to 12 DU (NH) and up to 16 DU (SH) to ozone variability at high latitudes. Stratospheric aerosol loading due to Mt. Pinatubo contributed $\sim$60 DU ozone loss at higher latitudes in the NH but its effect is quite insignificant in SH. Using accumulated winter-time eddy heat flux (Chapter 3) as a dynamical proxy, it has been shown that wave driving contributes up to 12 DU in NH and up to 8 DU ozone variability in SH. Replacing linear trend term with stratospheric halogen loading (or EESC) term shows that regression fit does not change significantly. Detailed analysis of regression fits shows that detection of ozone recovery in total ozone data due to a decrease in halogen loading can not be confirmed for 27 years of ozone data. These two models (linear vs. EESC) predict nearly 4 DU/decade and 8 DU/decade increase in total ozone since middle 1990s in NH and SH respectively. The major contribution to the high-latitude total ozone increases mid-nineties is most probably through increase in planetary wave activity and solar cycle.

- Interannual variability in stratospheric water vapor (WV) is presented in Chapter 6. Updated HALOE V19 and SAGE 6.2 confirms that most of the WV variability in lower stratosphere is controlled by the strength of Brewer-Dobson circulation. Lower temperatures leads to decreases in WV throughout the lower stratosphere through rapid isentropic transport. A compact relationship between wave activity and tropical lower stratospheric WV confirms results from earlier studies. Some years such as 1991, 1997, however show a deviation from the these relationship, indicating that WV variability in the tropical lower stratosphere can not be solely attributed to the strength of the BD circulation. The sudden decrease in stratospheric WV since 2001 as reported in other studies and is uniquely reflected in sudden increases in wave driving in both hemispheres. It is shown that this is due to increase in wave driving in both hemispheres which led to decreases in TTL temperature. Regression analysis shows that recent increase in wave activity in both hemispheres may have contributed a 0.7 K cooling in the tropical lower stratosphere.

Acknowledgement

This thesis is the result of four and half years of work whereby I have been accompanied and supported by many people. It is a great feeling that I have now the opportunity to express my gratitude for all of them.

First of all I would like to thank my research advisors, Dr. Mark Weber and Prof. John Burrows for entrusting me to work on this interesting project. Both of them are not only a great scientists with visions but also and most importantly kind persons. I sincerely thank Mark for his scientific excitement which inspired me throughout this work and at the same time for being critical about my results. Now I know that it was not in vain to develop TEN different regression models to make sure that none of the important process is missing or misleading.

I would like to take this opportunity to express my thanks to "CANDIDOZ" team specially Ingo Wohltman, Markus Rex, Esko Kyrö, Johanes Stahelin, Neil Harris for useful scientific discussions.

I wish to express my debt to all present and former colleagues at Institute of Environmental Physics and Remote Sensing (IUP/IFE), University of Bremen, who have so generously shared their knowledge and technical expertise with me. Many thanks to Bjoern-Martin Sinnhuber for evaluating my papers and interesting discussions. I am also very grateful to Viju O. John, Oliver Lemke, Lok Nath Lamsal and Julian Meyer-Arnek for teaching me some of the important aspects of the programming and data handling.

Thanks to the many friends, T.R. Sreerekha, Leonard Amekudzi, Aveek Sarkar, Ninad Sheode, Sarang Limaye, Ketan Thakar, Parag Narvekar, Mukul Moholkar, Amol Pargaonkar and many others, with whom I enjoyed a number of fun and intellectual exchanges during my stay in Bremen. I appreciate the co-operation of Stefanie Bühler. My special thanks to Sarah Ervenich, Janika Ots, Rudy Eid, Sorin Grigorescu, Nassar Albunni, Daniel Daraban for making Lilienthal house into pleasant place to live in.

I wish to thank the secretaries, especially Sabine Packeiser, and other members of IUP for their assistance. I would like to express my deepest thanks to my parents, brothers, sisters, and their families for their constant love and supports.

Bibliography

Andersen, S. B., and B. Knudsen, The influence of vortex ozone depletion on Arctic ozone trends, *Geophys. Res. Lett.*, *29*, 2013, doi:10.1029/2001GL014595, 2002.

Anderson, J., J. M. Russel III, S. Solomon, and L. E. Deaver, Halogen Occultation Experiment confirmation of stratospheric chlorine decreases in accordance with the Montreal Protocol, *J. Geophys. Res.*, *105*, 4483–4490, 2000.

Andrews, D. G., and M. McIntyre, Planetary waves in horizontal and vertical shear: The generalized Eliassen-Palm relation and the mean zonal acceleration, *J. Atmos. Sci.*, *33*, 2031–2048, 1976.

Andrews, D. G., J. R. Holton, and C. B. Leovy, *Middle Atmosphere Dynamics*, Academic Press, 1987.

Austin, J., N. Butchart, and K. P. Shine, Possibility of an Arctic ozone hole in a doubled-CO_2 climate, *Nature*, *360*, 221–225, 1992.

Baldwin, M. P., and T. J. Dunkerton, Propagation of the Arctic Oscillation from the stratosphere to the troposphere, *J. Geophys. Res.*, *104*, 30,937–30,946, 1999.

Baldwin, M. P., , D. B. Stephenson, D. Thompson, D. J. Dunkerton, A. J. Charlton, and A. O'Neill, Stratospheric memory and extended-range weather forecasts, *Science*, *301*, 636–640, 2003a.

Baldwin, M. P., D. Thompson, E. F. Shuckburgh, W. A. Norton, and N. P. Gillet, Weather from the stratosphere?, *Science*, *301*, 317–318, 2003b.

Baldwin, M. P., et al., The Quasi-Biennial Oscillation, *Geophy. Rev.*, *39*, 179–229, 2001.

Barthia, P. K., C. G. Wellemeyer, S. L. Taylor, N. Nath, and A. Gopolan, Solar backscatter (SBUV) Version 8 profile algorithm, in *Proceedings of the Quadrennial Ozone Symposium-2004*, edited by C. Zerefos, pp. 295–296, Athens, Greece, ISBN 960–630–103–6, 2004.

Bates, D., and M. Nicolet, The photochemistry of the atmospheric water vapor, *J. Geophys. Res.*, *55*, 301–327, 1950.

Bodeker, G. E., I. S. Boyd, and W. A. Matthews, Trends and variability in vertical ozone and temperature profiles measured by ozone sondes at Lauder, New Zealand: 1986-1996, *J. Geophys. Res.*, *103*, 28,661–28,681, 1998.

Bodeker, G. E., J. C. Scott, K. Kreher, and R. L. McKenzie, Global ozone trends in potential vorticity coordinates using TOMS and GOME intercompared against the Dobson network: 1978 - 1998, *J. Geophys. Res.*, *106*, 23,029–23,042, 2001.

Bowman, K. P., Global patterns of the Quasi-Biennial Oscillation in total ozone, *J. Atmos. Sci.*, *46*, 3328–3343, 1989.

Braesicke, P., and J. A. Pyle, Changing ozone and changing circulation: Possible feedbacks?, *Geophys. Res. Lett.*, *30(2)*, 1059, doi:10.1029/2002GL015973, 2003.

Braesicke, P., and J. A. Pyle, Sensitivity of dynamics and ozone to different representations of SSTs in the Unified Model, *Q. J. R. Meteorol. Soc.*, *130*, 2033–2046, 2004.

Bramstedt, K., Comparison of total ozone from the satellite instruments GOME and TOMS with measurements from the Dobson network 1996-2000, *Atmos. Chem. Phys Discuss.*, *2*, 1131–1157, 2002.

Brasseur, G., The response of the middle atmosphere to long-term and short-term solar variability: A two-dimensional model, *J. Geophys. Res.*, *98*, 23,079–23,090, 1993.

Brewer, A. W., Evidence for a world circulation provided by the measurements of helium and water vapour distribution in the stratosphere, *Q. J. R. Meteorol. Soc.*, *75*, 351–363, 1949.

Brühl, C., P. J. Crutzen, and J. Grooss, High-latitude, summertime NO_x activation and seasonal ozone decline in the lower stratosphere: Model calculations based upon HALOE on UARS, *J. Geophys. Res.*, *103*, 3587–3597, 1998.

Burrows, J., et al., The Global Ozone Monitoring Experiment (GOME): Mission concept and first scientific results, *J. Atmos. Sci.*, *56*, 151–171, 1999.

Butchart, N., and A. A. Scaife, Removal of chlorofluorocarbons by increased mass exchange between the stratosphere and troposphere in a changing climate, *Nature*, *410*, 799–802, 2001.

Cebula, R. P., and M. T. DeLand, Comparisons of the NOAA11 SBUV/2, UARS SOLSTICE, and UARS SUSIM MgII solar activity proxy indices, *Sol. Phys.*, *177*, 117–132, 1998.

Chandra, S., and R. S. Stolarski, Recent trends in stratospheric total ozone: Implications of dynamical and El Chichón perturbations, *Geophys. Res. Lett.*, *18*, 2277–2280, 1991.

Charney, J., and P. Drazin, Propagation of planetary scale disturbances from the lower into the upper atmosphere, *J. Geophys. Res.*, *66*, 83–109, 1961.

Chipperfield, M. P., and R. L. Jones, Relative influences of atmospheric chemistry and transport on arctic ozone trends, *Nature*, *400*, 551–554, 1999.

Cochrane, D., and G. H. Orcutt, Application of least squares regression to relationships containing autocorrelated error terms, *J. Am. Stat. Assoc.*, *44*, 32–61, 1949.

Coldewey-Egbers, M., M. Weber, L. N. Lamsal, R. de Beek, M. Buchwitz, and J. P. Burrows, Total ozone retrieval from GOME UV spectral data using the weighting function DOAS approach, *Atmos. Chem. Phys.*, *5*, 5015–5025, 2005.

Collimore, C. C., D. W. Martin, M. H. Hitchman, A. Huesmann, and D. E. Waliser, On the relatioship between the QBO and tropical deep convection, *J. Climate*, *16*, 2552–2568, 2003.

Crooks, S. A., and L. J. Gray, Characterization of the 11-year solar signal using a multiple regression analysis of the ERA-40 dataset, *J. Climate*, *18*, 996–1015, 2005.

Crutzen, P. J., The influence of nitrogen oxide on the atmospheric ozone content, *Q. J. R. Meteorol. Soc.*, *96*, 320–325, 1970.

Crutzen, P. J., Photochemical reaction initiated by and influencing ozone in unpolluted tropospheric air, *Tellus*, *26*, 45–55, 1974.

Dethof, A., and E. Holm, Ozone assimilation in the ERA-40 reanalysis project, *Q. J. R. Meteorol. Soc.*, *130*(603), 2851–2872, 2004.

Dhomse, S., M. Weber, J. Burrows, I. Wohltmann, and M. Rex, On the possible causes of recent increases in NH total ozone from a statistical analysis of satellite data from 1979 to 2003, *Atmos. Chem. Phys.*, *6*, 1165–1180, 2006.

DLR2000, GOME Level 1 to 2 Algorithms Description, *Tech. Rep. ER-TN-DLR-GO-0025*, DLR Oberpfaffenhofen, Wessling, Germany, 2000.

Dobson, G., "Forty years" research on atmospheric ozone at Oxford: A history, *Appl. Opt.*, *7*, 387–402, 1968.

Dobson, G. M., Measurements of the amount of ozone in the earth's atmosphere and its relations to other geophysical conditions, Part IV, *Proc. Roy. Soc.*, *A129*, 411–433, 1930.

Eichmann, K. U., M. Weber, and J. Burrows, Ozone depletion in Northern hemisphere winter/spring 1999/2000 as measured by the Global Ozone Monitoring Experiment on ERS-2, *J. Geophys. Res.*, *107(D20)*, 8280, doi:10.1029/2001JD001148, 2002.

Eyring, V., et al., A strategy for process-oriented validation of coupled chemistry-climate models, *Bull. Amer. Met. Soc.*, *86*, 1117, doi:10.1175/BAMS-86-8-1117, 2005.

Farman, J. C., B. G. Gardiner, and J. D. Shanklin, Large losses of total ozone in Antarctica reveal seasonal ClO_x/NO_x interaction, *Nature*, *315*, 207–210, 1985.

Fioletov, V. E., and T. G. Shepherd, Seasonal persistence of midlatitude total ozone anomalies, *Geophys. Res. Lett.*, *30*, doi:10.1029/2002GL016,739, 2003.

Fioletov, V. E., and T. G. Shepherd, Summertime total ozone variations over middle and polar latitudes, *Geophys. Res. Lett.*, *32*, L04,807, doi:10.1029/2004GL022,080, 2005.

Fleming, E. L., S. Chandra, M. Schoeberl, and J. Barnett, Monthly mean global climatology of temperature, wind, geopotential height, and pressure for 0-120 km, *Tech. rep.*, NASA Tech. Memo. NASA TM-100697, 1988.

Fleming, E. L., S. Chandra, C. Jackman, D. Considine, and A.R.Douglass, The middle atmosphere response to short and long term UV variations: An analysis of observations and 2D model results., *J. Atmos. Terr. Phys.*, *57*, 333–365, 1995.

Frederick, J. E., R. P. Cebula, and D. F. Heath, Instrument characterization for the detection of long-term changes in stratospheric ozone: An analysis of the SBUV/2 radiometer, *J. Atmos. Ocean Tech.*, *3*, 472–480, 1986.

Frith, S., R. Stolarski, and P. K. Barthia, Implications of Version 8 TOMS and SBUV data for long-term trend, in *Proceedings of the Quadrennial Ozone Symposium-2004*, edited by C. Zerefos, pp. 65–66, Athens, Greece, 2004.

Fritts, D. C., and M. J. Alexander, Gravity wave dynamics and effects in the middle atmosphere, *Geophy. Rev.*, *44*(1), 1003, doi:10.1029/2001RG000106, 2003.

Füglisthaler, S., and P. Haynes, Control of interannual and longer-term variability of stratospheric water vapor, *J. Geophys. Res.*, *110*(D24108), doi:10.1029/2005JD006019, 2005.

Füglisthaler, S., M. Bonazzola, P. Haynes, and T. Peter, Stratospheric water vapor predicted from the Lagrangian temperature history of air entering the stratosphere in the tropics, *J. Geophys. Res.*, *110*(D08107), doi:10.1029/2004JD005516, 2005.

Fusco, A. C., and M. L. Salby, Interannual variations of total ozone and their relationship to variations of planetary wave activity, *J. Climate*, *12*, 1619–1629, 1999.

Gettelman, A., W. J. Randel, S. Massie, F. Wu, W. G. Read, and J. M. Russell III, Elnino as a natural experiment for studying the tropical tropopause region, *J. Climate*, *14*, 3375–3392, 2001.

Gettelman, A., W. J. Randel, F. Wu, and S. T. Massie, Transport of water vapor in the tropical tropopause layer, *Geophys. Res. Lett.*, *29*(01), 1009, doi:10.1029/2001GL013818, 2002.

Gillett, N. P., M. R. Allen, and K. D. Williams, Modelling the atmospheric response to doubled CO_2 and depleted stratospheric ozone using a stratosphere- resolving coupled GCM, *Q. J. R. Meteorol. Soc.*, *129*, 947–966, 2003.

Gray, L. J., The influence of the equatorial upper stratosphere on stratospheric sudden warmings, *Geophys. Res. Lett.*, *30*, 1166, doi:10.1029/2002GL016430, 2003.

Gray, L. J., S. Crooks, C. Pascoe, S. Sparrow, and M. Palmer, Solar and QBO influences on the timing of stratospheric sudden warmings, *J. Atmos. Sci.*, *61*, 2777–2796, 2003.

Hadjinicolaou, P., J. A. Pyle, and N. R. P. Harris, The recent turnaround in stratospheric ozone over Northern middle latitudes: A dynamical modeling perspective, *Geophys. Res. Lett.*, *32*, L12,821, doi:10.1029/2005GL022,476, 2005.

Haigh, J., The impact of solar variability on climate., *Science*, *272*, 981–984, 1996.

Haigh, J. D., A GCM study of climate change in response to the 11-year solar cycle., *Q. J. R. Meteorol. Soc.*, *125*, 871,892, 1999.

Hamilton, K., R. J. Wilson, and R. S. Hemler, Middle atmosphere simulated with high vertical and horizontal resolution versions of a GCM: improvements in the cold pole bias and generation of a QBO-like oscillation in the tropics, *J. Atmos. Sci.*, *56*, 3829–3846, 1999.

Hansen, J., and M. Sato, Greenhouse gas growth rates, *Proc. Natl. Acad. Sci.*, *101*, 16,109–16,114, doi:10.1073/pnas.0406982101, 2004.

Hansen, J., et al., Earth's energy imbalance: Confirmation and implications, *Science*, *308*, 1431–1435, doi:10.1126/science.1110252, 2005.

Hanson, D., and K. Mauersberger, Laboratory studies of nitric acid tryhydrate: Implications for the South polar stratosphere, *Geophys. Res. Lett.*, *15*, 855–858, 1988.

Harris, N. R., M. Rex, F. Goutail, B. M. Knudsen, G. L. Manney, R. Müller, and P. Gathen, Comparison of empirically derived ozone losses in the Arctic vortex, *J. Geophys. Res.*, *107(D20)*, 8264, doi:10.1029/2001JD000482, 2002.

Hartmann, D. L., J. M.Wallace, V. Limpasuvan, D. Thompson, and J. R. Holton, Can ozone depletion and global warming interact to produce rapid climate change?, *Proc. Nat. Acad. Sci.*, *97*, 1412–1417, 2000.

Hatsushika, H., and K. Yamazaki, Interannual variations of temperature and vertical motion at the tropical tropopause associated with enso, *Geophys. Res. Lett.*, *28(15)*, 2891–2894, 2000.

Haynes, P. H., C. J. Marks, M. E. McIntyre, T. G. Shepherd, and K. P. Shine, On the "downward control" of extratropical diabatic circulations by eddy-induced mean zonal forces, *J. Atmos. Sci.*, *48*, 651–678, 1991.

Heath, D. F., A. Krueger, H. Roeder, and B. Henderson, The solar backscatter ultraviolet and total ozone spectrometer (TOMS/SBUV) for Nimbus G., *Opt. Eng.*, *14*, 323–331, 1975.

Hilsenrath, E., R. P. Cebula, M. T. DeLand, K. Laamann, S. Taylor, C. Wellemeyer, and P. K. Bhartia, Calibration of the NOAA-11 SBUV/2 ozone data set from 1989 to 1993 using in-flight calibration data and SSBUV, *J. Geophys. Res.*, *100*, 1351–1366, 1995.

Hofmann, D. J., and S. Solomon, Ozone destruction through heterogeneous chemistry following the eruption of El Chichon, *J. Geophys. Res.*, *94*, 5029–5041, 1989.

Holton, J., and H.-C. Tan, The influence of the equatorial Quasi-Biennial Oscillation on the global circulation at 50 mb, *J. Atmos. Sci.*, *37*, 2200–2208, 1980.

Holton, J., P. Haynes, M. McIntyre, A. Douglass, R. Rood, and L. Pfister, Stratosphere-troposphere exchange, *Geophy. Rev.*, *33*, 403–439, 1995.

Holton, J. R., *An introduction to dynamic meteorology*, 3rd ed., Academic Press Inc., London, 1992.

Hood, L. L., Thermal response of the tropical tropopause region to solar ultraviolet variations, *Geophys. Res. Lett.*, *30*(23), 2215, doi:10.1029/2003GL018364, 2003.

Hood, L. L., and B. E. Soukharev, Interannual variations of total ozone at Northern midlatitudes correlated with EP flux and potential vorticity, *J. Atmos. Sci.*, *62*, 3724–3740, 2005.

Hood, L. L., and S. Zhou, Stratospheric effects of 27-day solar ultraviolet variations: The column ozone response and comparisons of solar cycles 21 and 22, *J. Geophys. Res.*, *104(D21)*, 26,473–26,480, doi:10.1029/1999JD900466, 1999.

Hood, L. L., J. P. McCormick, and K. Labitzke, An investigation of dynamical contributions to midlatitude ozone trends in winter, *J. Geophys. Res.*, *102*, 13,079–13,093, 1997.

Hoskins, B. J., M. E. McIntyre, and A. Robertson, On the use and significance of isentropic potential vorticity maps, *Q. J. R. Meteorol. Soc.*, *111*, 877–946, 1985.

IPCC, Climate Change 2001: The Scientific Basis, *Tech. rep.*, Intergovernmental Panel on Climate Change, IPCC/WMO/UNEP, 2001.

Jackman, C., E. Fleming, and F. Vitt, Influence of extremely large solar proton events in a changing stratosphere, *J. Geophys. Res.*, *105*, 11,659–11,670, 2000.

Jackman, C. H., E. L. Fleming, S. Chandra, D. B. Considine, and J. E. Rosenfield, Past, present, and future modeled ozone trends with comparisons to observed trends, *J. Geophys. Res.*, *101*, 28,753–28,768, 1996.

Kalnay, E., et al., The NCEP/NCAR 40-year reanalysis project, *Bullet. Amer. Meteorol. Soc.*, *77*, 437–471, 1996.

Kerr-Munslow, A. M., and W. A. Norton, Tropical wave driving of the annual cycle in tropical tropopause temperatures Part I: EMCWF analyses, *J. Atmos. Sci.*, *63(5)*, 1410–1419, 2006.

Kleinböhl, A., et al., Vortexwide denitrification of the Arctic polar stratosphere in winter 1999/2000 determined by remote observations, *J. Geophys. Res.*, *108*(D5), doi:10.1029/2001JD001042, 2003.

Knudsen, B. M., and J. Grooss, Northern midlatitude stratospheric ozone dilution in spring modeled with simulated mixing, *J. Geophys. Res.*, *105*, 6885–6890, 2000.

Kodera, K., On the origin and nature of the interannual variability of the winter stratospheric circulation in the Northern hemisphere, *J. Geophys. Res.*, *100*, 14,077–14,087, 1995.

Kodera, K., and Y. Kuroda, Dynamical response to the solar cycle: Winter stratopause and lower stratosphere, *J. Geophys. Res.*, *107*, 4749, doi:310.1029/2002JD002,224, 2002.

Labitzke, K., Some aspects of a probable association between atmospheric variabiblity and the 11-year solar cycle, *Geophys. Res. Lett.*, *14*, 535–537, 1987.

Labitzke, K., On the solar cycle-QBO-relationship: A summary, *J.A.S.-T.P*, *67*, 45–54, 2005.

Labitzke, K., and H. Loon, Association between the 11-year solar cycle, the QBO and the atmosphere. Part I: The troposphere and stratosphere in the Northern hemisphere in winter, *J. Atmos. Terr. Phys.*, *50*, 197–206, 1988.

Labitzke, K., and H. van Loon, Some recent studies of probable connections between solar and atmospheric variability, *Ann. Geophysicae*, *11*, 1084–1094, 1993.

Labitzke, K., J. Austin, N. Butchart, J. Knight, M. Takahashi, M. Nakamoto, T. Nagashima, J. Haigh, and V. Williams, The global signal of the 11-year solar cycle in the stratosphere: Observations and models., *J. Atmos. Solar-Terr. Phys.*, *64*, 203–210, 2002.

Labow, G. J., R. D. McPeters, and P. K. Barthia, A comparison of TOMS & SBUV Version 8 total column ozone data with data from ground, in *Proceedings of the Quadrennial Ozone Symposium-2004*, edited by C. Zerefos, pp. 123–124, Athens, Greece, ISBN 960–630–103–6, 2004.

Lait, L. R., M. Schoeberl, and P. Newman, Quasi–Biennial modulation of the Antarctic ozone depletion, *J. Geophys. Res*, *94*, 11,559–11,571, 1989.

Lamsal, L. N., *Advanced total column ozone retrieval from hyperspectral UV satellite instruments*, Berichte aus dem Institut für Umweltphysik, Logos Verlag Berlin, PhD thesis, University of Bremen, ISBN X-XXXX-XXXX-X, 2006.

Langematz, U., M. Kunze, K. Krüger, K. Labitzke, and G. L. Roff, Thermal and dynamical changes of the stratosphere since 1979 and their link to ozone and CO_2 changes, *J. Geophys. Res.*, *108(D1)*, 4027, doi:doi:10.1029/2002JD002069, 2003.

Lanzante, J. R., S. Klein, and D. Seidel, Temporal homogenization of monthly radiosonde temperature data. Part I: Methodology, *J. Climate*, *16*, 224–240, 2003.

Larkin, A., J. D. Haigh, and S. Djavidnia, The effect of solar UV radiation variations on the earth's atmosphere, *Space Sci. Rev.*, *94*, 199–214, 2000.

Lee, H., and A. K. Smith, Simulation of the combined effects of solar cycle, Quasi-Biennial Oscillation, and volcanic forcing on stratospheric ozone changes in recent decades, *J. Geophys. Res.*, *108(D2)*, 4049, doi:10.1029/2001JD001503, 2003.

Limpasuvan, V., and D. Hartmann, Wave-maintained annular modes of climate variability, *J. Climate*, *13*, 4414–4429, 2000.

Logan, J. A., D. B. A. Jones, I. A. Megretskaia, S. J. Oltmans, B. J. Johnson, H. Voemel, W. J. Randel, W. Kimani, and F. J. Schmidlin, Quasibiennial oscillation in tropical ozone as revealed by ozonesonde and satellite data, *J. Geophys. Res.*, *108*, doi:4244,doi:10.1029/2002JD002170, 2003.

Lumpe, J. D., R. M. Beviacqua, K. W. Hoppel, and C. E. Randell, POAM III retreival algorithm and error analysis, *J. Geophys. Res.*, *107*(4575), doi:10.1029/2002JD002137, 2002.

Manney, G. L., K. Krueger, J. L. Sabutis, S. A. Sena, and S. Pawson, The remarkable 2003/2004 winter and other recent warm winters in the Arctic stratosphere since the late 1990s, *J. Geophys. Res.*, *110*, D04,107, doi:10.1029/2004JD005,367, 2005.

McCormack, J. P., The influence of the 11-year solar cycle on the Quasi-Biennial Oscillation, *Geophys. Res. Lett.*, *30(22)*, 2162, doi:10.1029/2003GL018314, 2003.

McCormack, J. P. ., and L. L. Hood, Apparent solar cycle variations of upper stratospheric ozone and temperature, *J. Geophys. Res.*, *101*, 20,933–20,944, 1996.

McCormack, J. P., L. L. Hood, R. Nagatani, A. J. Miller, W. G. Planet, and R. D. McPeters, Approximate separation of volcanic and 11-year signals in the SBUV-SBUV/2 total ozone record over the 1979-1995 period, *Geophys. Res. Lett.*, *24*, 2,729–2,732, 1997.

McLinden, C. A., S. C. Olsen, B. Hannegan, O. Wild, M. J. Prather, and J. Sundet, Stratospheric ozone in 3-D models: a simple chemistry and the cross-tropopause flux, *J. Geophys. Res.*, *105*, 14,653–14,665, 2000.

Miller, A. J., et al., Comparisons of observed ozone trends and solar effects in the stratosphere through examination of ground-based umkehr and combined solar backscattered ultraviolet (SBUV) and SBUV 2 satellite data, *J. Geophys. Res.*, *101*, 9017–9021, 1996.

Molina, M. J., and F. S. Rowland, Stratospheric sink for chlorofluoromethanes: chlorine atom catalysed destruction of ozone, *Nature*, *249*, 810–812, 1974.

Montzka, S. A., J. H. Butler, R. C. Myers, T. M. Thompson, T. H. Swanson, A. D. Clark, L. T. Lock, and J. W. Elkins, A decline in the tropospheric abundance of halogen from halocarbons, *Science*, *272*, 1318–1322, 1996.

Montzka, S. A., J. H. Butler, J. W. Elkins, T. M. T. A. D. Clarke, and L. T. Lock, Present and future trends in the atmospheric burden of ozone- depleting halogens, *Nature*, *398*, 690–694, 1999.

Mote, P., K. H. Rosenlof, J. R. Holton, R. S. Harwood, and J. W. Waters, An atmospheric tape recorder: The imprint of tropical tropopause temperatures on stratospheric warter vapor, *J. Geophys. Res.*, *101*, 3989–4006, 1996.

Nedoluha, G. E., R. M. Bevilacqua, K. W. Hoppel, J. D. Lumpe, and H. Smit, Polar Ozone and Aerosol Measurement III measurments of water vapor in the upper troposphere and lower stratosphere, *J. Geophys. Res.*, *108*, 4391, doi:10.1029/2002JD003332, 2002.

Newman, P. A., E. R. Nash, and J. E. Rosenfield, What controls the temperature of the Arctic stratosphere during the spring?, *J. Geophys. Res.*, *106*, 19,999–20,010, 2001.

Niwano, M., K. Yamazaki, and M. Shiotani, Seasonal and QBO variations of ascent rate in the tropical lower stratosphere as inferred from UARS HALOE trace gas data, *J. Geophys. Res.*, *108(D24)*(4794), doi:10.1029/2003JD003871, 2003.

Norton, W. A., Tropical wave driving of the annual cycle in tropical tropopause temperatures, Part II: Model results, *J. Atmos. Sci.*, *63(5)*, 1420–1431, 2006.

Oltmans, S. J., H. Voemel, D. J. Hofmann, K. H. Rosenlof, and D. Kley, The increase in stratospheric water vapor from balloonborne, frostpoint hygrometer measurements at Washington, D.C., and Boulder, Colorado, *Geophys. Res. Lett.*, *27(21)*, 3453–3456, 2000.

Parrish, A., B. J. Connor, J. J. Tsou, G. Beyerle, I. S. McDermid, and S. M. Hollandsworth, Microwave ozone and lidar aerosol profile observations at Table Mountain, California, following the Pinatubo eruption, *J. Geophys. Res.*, *208*, 20,201–22,208, 1998.

Parrish, D. F., and J. C. Derber, The National Meteorological Center's spectral statistical interpolation analysis system, *Mon. Wea. Rev.*, *120*, 1747–1763, 1992.

Pawson, S., and B. Naujokat, The cold winters of the middle 1990s in the Northern lower stratosphere, *J. Geophys. Res.*, *104*, 14,209–14,222, 1999.

Perlwitz, J., and N. Harnik, Downward coupling between the stratosphere and troposphere: The relative roles of wave and zonal mean processes, *J. Climate*, *17*, 4902–4909, doi:10.1175/JCLI-3247.1, 2004.

Platt, U., Differential optical absorption spectroscopy (DOAS), *Chem. Anal. Series*, *127*, 27–83, 1994.

Plets, H., and C. Vynckier, A comparative study of statistical total column ozone forecasting model, *J. Geophys. Res.*, *105*, 26,503–26,517, 2000.

Plumb, A. R., and J. Eluszkiewicz, The Brewer-Dobson circulation: Dynamics of the tropical upwelling, *J. Atmos. Sci.*, *56(6)*, 868–890, 1999.

Plumb, R. A., and A. Semeniuk, Downward migration of extratropical zonal wind anomalies, *J. Geophys. Res.*, *108*, 4223, doi:10.1029/2002JD002,773, 2003.

Ramaswamy, V., et al., Stratospheric temperature trends: observations and model simulations, *Geophy. Rev.*, *391*, 71–122, 2001.

Randel, W., et al., The SPARC intercomparison of middle atmosphere climatologies, *J. Climate*, *17*, 986–1003, 2004a.

Randel, W. J., and J. B. Cobb, Coherent variations of monthly mean column ozone and lower stratospheric temperature, *J. Geophys. Res.*, *99*, 5433–5447, 1994.

Randel, W. J., F. Wu, J. R. III, J. W. Waters, and L. Froidevaux, Ozone and temperature changes in the stratosphere following the eruption of Mt. Pinatubo, *J. Geophys. Res.*, *100*, 16,753–16,764, 1995.

Randel, W. J., R. S. Stolarski, D. M. Cunnold, J. A. Logan, M. J. Newchurch, and J. M. Zawodny, Trends in the vertical distribution of ozone, *Science*, *285*, 1689–1692, 1999.

Randel, W. J., F. Wu, A. Gettelman, J. M. Russel III, J. M. Zawodny, and S. J. Oltmans, Seasonal variation of water vapor in the lower stratosphere observed in Halogen Occultation Experiment data, *J. Geophys. Res.*, *106*(D13), 14,313–14,325, 2001.

Randel, W. J., F. Wu, and R. S. Stolarski, Changes in column ozone correlated with the stratospheric EP flux, *J. Meteor. Soc. Jpn.*, *80*, 849–862, 2002a.

Randel, W. J., F. Wu, and R. S. Stolarski, Changes in column ozone correlated with the stratospheric EP flux, *J. Meteor. Soc. Jpn.*, *80*, 849–862, 2002b.

Randel, W. J., F. Wu, S. J. Oltmans, K. Rosenlof, and G. E. Nedoluha, Interannual changes of stratospheric water vapor and correlations with tropical tropopause temperatures, *J. Atmos. Sci.*, *61*, 2133–2148, 2004b.

Randel, W. J., F. Wu, H. Voemel, G. E. Nedoluha, and P. Forster, Decreases in stratospheric water vapor after 2001: links to changes in the tropical tropopause and the Brewer-Dobson circulation, *J. Geophys. Res.*, *111*, 12,312, doi:10.1029/2005JD006744, 2006.

Reed, R. J., A tentative model of the 26–month oscillation in tropical latitudes, *Q. J. R. Meteorol. Soc.*, *90*, 441–466, 1964.

Reinsel, G. C., E. C. Weatherhead, G. C. Tiao, A. J. Miller, R. M. Nagatani, D. J. Wuebbles, and L. E. Flynn, On detection of turnaround and recovery in trend for ozone, *J. Geophys. Res.*, *107*, 4078, doi:10.1029/2001JD000,500, 2002.

Reinsel, G. C., A. J. Miller, E. C. Weatherhead, L. E. Flynn, R. M. Nagatani, G. C. Tiao, and D. J. Wuebbles, Trend analysis of total ozone data for turnaround and dynamical contributions, *J. Geophys. Res.*, *110*, D16,306, doi:10.1029/2004JD004,662, 2005.

Rex, M., R. J. Salawitch, P. von der Gathen, N. R. P. Harris, M. P. Chipperfield, and B. Naujokat, Arctic ozone loss and climate change, *Geophys. Res. Lett.*, *31*, L04,116, doi:10.1029/2003GL018,844, 2004.

Richter, A., F. Wittrock, . Eisinger, and J. P. Burrows, GOME observations of tropospheric BrO in Northern hemispheric spring and summer 1997, *Geophys. Res. Lett.*, *25*, 2683–2686, 1998.

Rind, D., The sun's role in climate variations, *Science*, *296*, 673–677, 2002.

Rind, D., and N. K. Balachandran, Modeling the effects of UV variability and the QBO on the troposphere-stratosphere system., *J. Climate*, *8*, 2080–2095, 1995.

Rind, D., R. Suozzo, N. Balachandran, and M. Prather, Climate change and the middle atmosphere Part I : The doubled CO_2 climate, *J. Atmos. Sci.*, *47*, 475–494, 1990.

Robock, A., Volcanic eruptions and climate, *Rev. Geophys.*, *38*(2), 191–219, 2000.

Rosenlof, K., and J. R. Holton, Estimates of the stratospheric residual circulation using the downward control principle, *J. Geophys. Res.*, *98*, 10,465–10,479, 1993a.

Rosenlof, K. H., Seasonal cycle of the residual mean meridional circulation in the stratosphere, *J. Geophys. Res.*, *100*(D3), 5173–5191, 1995.

Rosenlof, K. H., How water enters the stratosphere, *Science*, *302*, 1691–1692, 2003.

Rosenlof, K. H., and J. R. Holton, Estimates of stratospheric residual circulation using the downward principle, *J. Geophys. Res.*, *98*, 10,465–10,479, 1993b.

Rozanov, V., D. Diebel, R. Spurr, and J. P. Burrows, GOMETRAN: A radiative transfer model for the satellite project GOME- the plane parallel version, *J. Geophys. Res.*, *102*, 16,683–16,695, 1997.

Russell, J. M., et al., The Halogen Occultation Experiment, *J. Geophys. Res.*, *98*(D6), 10,777–10,797, 1993.

Salby, M., F. Sassi, P. Callaghan, W. Read, and H. Pumphrey, Fluctuations of cloud, humidity and thermal structure near tropical tropopause, *J. Climate*, *16*, 3428–3446, 2003.

Salby, M. L., and P. F. Callaghan, Interannual changes of the stratospheric circulation: Relationship to ozone and tropospheric structure, *J. Climate*, *15*, 3673–3685, 2002a.

Salby, M. L., and P. F. Callaghan, Interannual changes of the stratospheric circulation: Relationship to ozone and tropospheric structure, *J. Climate*, *15*, 3673–3685, 2002b.

Sato, M., J. E. Hansen, M. P. McCormack, and J. B. Pollack, Stratospheric aerosol optical depth, *J. Geophys. Res.*, *98*, 1850–1990, 1993.

Scaife, A. A., J. Austin, N. Butchart, S. Pawson, M. Keil, and J. Nash, Seasonal and interannual variability of the stratosphere diagnosed from UKMO TOVS analyses, *Q. J. R. Meteorol. Soc.*, *126*, 2585–2604, 2000.

Scaife, A. A., N. Buchart, D. R. Jackson, and R. Swinbank, Can changes in ENSO activity help to explain increasing stratospheric water vapor?, *Geophys. Res. Lett.*, *30*(1880), doi:10.1029/2003GL017591, 2003.

Schnadt, C., M. Dameris, M. Ponater, R. Hein, V. Grewe, and B. Steil, Interaction of atmospheric chemistry and climate and its impact on stratospheric ozone, *Clim. Dyn.*, *18*, 501–518, 2002.

Semeniuk, K., and T. G. Shepherd, Mechanisms for tropical upwelling in the stratosphere, *J. Atmos. Sci.*, *58(21)*, 3097–3115, 2001.

Seol, D., and K. Yamazaki, Residual mean meridional circulation in the stratosphere and upper troposphere: Climatological aspects, *J. Meteor. Soc. Jpn.*, *77(5)*, 985–996, 1999.

Shindell, D., D. Rind, N. Balachandran, J. Lean, and P. Lonergan, Solar cycle variability, ozone, and climate, *Science*, *284*, 305–308, 1999a.

Shindell, D. T., Climate and ozone response to increased stratospheric water vapor, *Geophys. Res. Lett.*, *28*, 1551, doi:doi:10.1029/1999GL011197, 2001.

Shindell, D. T., D. Rind, and P. Lonergren, Increased polar stratospheric ozone losses and delayed eventual recovery due to increasing greenhouse gas concentrations, *Nature*, *392*, 589–592, 1998.

Shindell, D. T., R. L. Miller, G. A. Schmidt, and L. Pandolfo, Simulation of recent Northern winter climate trends by greenhouse-gas forcing, *Nature*, *399*, 452–455, 1999b.

Shindell, D. T., G. Schmidt, R. Miller, and D. Rind, Northern hemisphere winter climate response to greenhouse gas, ozone, solar, and volcanic forcing, *J. Geophys. Res.*, *106*, 7193–7210, 2001.

Shiotani, M., Annual Quasi-Biennial, and El Nino-Southern Oscillation (ENSO) time-scale variations in equatorial ozone, *J. Geophys. Res.*, *97*, 7625–7633, 1992.

Simmons, A. J., and J. K. Gibson, The ERA-40 project plan, *Tech. rep.*, ECMWF, Reading UK, ERA-40 project report series no. 1, 2000.

Sinnhuber, B., M. Weber, A. Amankwah, and J. P. Burrows, Total ozone during the unusual antarctic winter of 2002, *Geophys. Res. Lett.*, *30*, 1580, doi:10.1029/2002GL016,798, 2003a.

Sinnhuber, M., J. Burrows, M. P. Chipperfield, C. H. Jackman, M.-B. Kallenrode, K. F. Künzi, and M. Quack, A model study of the impact of magnetic field structure on atmospheric composition during solar proton events, *Geophys. Res. Lett.*, *30*, 1818, doi:10.1029/2003GL017,625, 2003b.

Solomon, S., Stratospheric ozone depletion: A review of concepts and history, *Geophy. Rev.*, *101*, 275–316, 1999.

Solomon, S., R. W. Portman, R. R. Garcia, L. W. Thomason, L. R. Poole, and M. P. McCormack, The role of aerosol variations in anthropogenic ozone depletion at Northern midlatitudes, *J. Geophys. Res.*, *101*, 6713–6727, 1996.

SPARC, *Assessment of trends in the vertical distribution of ozone, in WMO Ozone Research and Monitoring Project Report No. 34*, pp. 3413–3418, World Climate Research Programme, WCRP-113,WMO/TD-No.1043, 1998.

SPARC, *Assesment of upper tropospheric and stratospheric water vapour*, chap. Conclusions, pp. 261–264, World Climate Research Programme, WCRP-113,WMO/TD-No.1043, 2000.

Staehelin, J., N. Harris, C. Appenzeller, and J. Eberhard, Ozone trends: A review, *Rev. Geophys.*, *39*, 231–290, 2001.

Staehelin, J., J. Kerr, R. Evans, and K. Vanicek, Comparison of total ozone measurements 25 of Dobson and Brewer spectrophotometers and recommended transfer functions, *Tech. Rep. 149*, World Meteorological Organization Global Atmosphere Watch (WMO-GAW), Geneva, 2003.

Steinbrecht, W., B. Hassler, H. Claude, P. Winkler, and R. S. Stolarski, Global distribution of total ozone and lower stratospheric temperature variations, *Atmos. Chem. Phys.*, *3*, 3411–3449, 2003.

Steinbrecht, W., H. Claude, and P. Winkler, Enhanced upper stratospheric ozone: Sign of recovery or solar cycle effect?, *J. Geophys. Res.*, *109*, 6713–6727, 2004.

Stenke, A., and V. Grewe, Simulation of stratospheric water vapor trends: Impact on stratospheric ozone chemistry, *Atmos. Chem. Phys.*, *5*, 1257–1272, 2005.

Stolarski, R. S., and R. J. Cicerone, Stratospheric chlorine: a possible sink for ozone, *Can. J. Chem.*, *52*, 1610–1615, 1974.

Swinbank, R., and A. O'Neill, A stratosphere-troposphere data assimilation system, *Mon. Weather Rev.*, *122*, 686–702, 1994.

Tabzadeh, A., M. L. Santee, M. Y. Danilin, H. C. Pumphrey, P. A. Newman, P. J. Hamill, and J. L. Mergenthaler, Quantifying denitrification and its effect on ozone recovery, *Science*, *288*, 1407–1411, 2000.

Tabzadeh, A., K. Drdla, M. R. Schoeberl, P. Hamil, and O. B. Toon, Arctic "ozone hole" in a cold volcanic stratosphere, *Proc. Nat. Acad. Sci.*, *106*, 2609–2612, 2002.

Taha, G., L. W. Thomason, and S. P. Burton, Comparison of Stratospheric Aerosol and Gas Experiment (SAGE) II version 6.2 water vapor with balloon-borne and space-based instruments, *J. Geophys. Res.*, *109*(D18313), doi:310.1029/2004JD004859, 2004.

Tanaka, D., T. Iwasaki, S. Uno, M. Ujiie, and K. Miyazaki, Eliassen Palm flux diagnosis based on isentropic representation., *J. Atmos. Sci.*, *61*, 2370–2383, 2004.

Thomason, L. W., S. P. Burton, N. Iyer, J. M. Zawodny, and J. Anderson, A revised water vapor product for the Stratospheric Aerosol and Gas Experiment (SAGE) II version 6.2 data set, *J. Geophys. Res.*, *109*(D06312), doi:10.1029/2003JD004465, 2004.

Thompson, D., and J. M. Wallace, The Arctic Oscillation signature in the wintertime geopotential height and temperature fields, *Geophys. Res. Lett.*, *25*, 1297–1300, 1998.

Thorne, P. W., D. E. Parker, S. Tett, P. D. Jones, M. McCarthy, H. Coleman, and P. Brohan, Revisiting radiosonde upper air temperatures from 1958 to 2002, *J. Geophys. Res.*, *110*(D18105), doi:10.1029/2004JD005753, 2005.

Tiao, G., G. Reinsel, D. Xu, J. H. Frederick, X. Zhu, A. J. Miller, J. J. DeLuisi, C. L. Mateer, and D. J. Wuebbles, Effects of auto-correlation and temporal sampling schemes on estimates of trends and spatial correlation, *J. Geophys. Res.*, *95*, 20,507–20,517, 1990.

Tung, K. K., and H. Yang, Global QBO in circulation and ozone. Part I: Reexamination of observational evidence, *J. Atmos. Sci.*, *51*, 2699–2707, 1994.

Uppala, S. M., et al., The ERA40 analysis, *Q. J. R. Meteorol. Soc.*, *131*(612), 2961–3012, doi:10.1256/qj.04.176, 2005.

Viereck, R., L. Puga, D. McMullin, D. Judge, M. Weber, and W. K. Tobiska, The Mg II index: A proxy for solar EUV, *Geophys. Res. Lett.*, *28*, 1343–1346, 2001.

Viereck, R. A., L. Floyd, P. Crane, T. Woods, B. Knapp, G. Rottman, M. Weber, L. Puga, and M. DeLand, A composite Mg II index spanning from 1978 to 2003, *Space Weather*, *30*, S10,005, doi:10.1029/2002GL016,008, 2004.

Wagner, T., C. Leue, K. Pfeilsticker, and U. Platt, Monitoring of the stratospheric chlorine activation by GOME OClO measurements in the austral and boreal winters 1995 through 1999, *J. Geophys. Res.*, *106*, 4971–4996, 2001.

Waugh, W. D., Persistence of the lower stratospheric vortices, *J. Geophys. Res.*, *104*, 27,191–27,201, 1999.

Weatherhead, E. C., and S. B. Anderson, The search for signs of recovery of the ozone layer, *Nature*, *441*, 39–45, 2006.

Weatherhead, E. C., et al., Factors affecting the detection of trends: Statistical considerations and applications to environmental data, *J. Geophys. Res.*, *103*, 17,149–17,162, 1998.

Weber, M., The cold arctic winter 1995/96 as observed by the Global Ozone Monitoring Experiment GOME and HALOE: Tropospheric wave activity and chemical ozone loss, *Q. J. R. Meteorol. Soc.*, *128*, 1293–1319, 2002.

Weber, M., S. Dhomse, F. Wittrock, A. Richter, B. Sinnhuber, and J. P. Burrows, Dynamical control of NH and SH winter/spring total ozone from GOME observations in 1995-2002, *Geophys. Res. Lett.*, *30*, 1583, doi:10.1029/2002GL016,008, 2003.

Weber, M., L. N. Lamsal, M. Coldewey-Egbers, K. Bramstedt, and J. P. Burrows, Pole-to-pole validation of GOME WFDOAS total ozone with groundbased data, *Atmos. Chem. Phys.*, *5*, 1341–1355, 2005.

WHO, Protection against exposure to ultraviolet radiation, *Tech. Rep. WHO/EHG/95.17*, World Health Organization, Geneva, 1995.

WMO, Scientific assessment of ozone depletion: 1994, *Global Ozone Research and Monitoring Project Report 37*, World Meteorological Organization, Geneva, 1995.

WMO, Scientific assessment of ozone depletion: 1998, *Global Ozone Research and Monitoring Project Rport 44*, World Meteorological Organization, Geneva, 1999.

WMO, Scientific assessment of ozone depletion: 2002, *Global Ozone Research and Monitoring Project Rport 47*, World Meteorological Organization, Geneva, 2003.

Wohltmann, I., M. Rex, D. Brunner, and J. Mäder, Integrated equivalent latitude as a proxy for dynamical changes in ozone column, *Geophys. Res. Lett.*, *32*, L09,811, doi:10.1029/2005GL022,497, 2005.

Yulaeva, E., J. R. Holton, and J. M. Wallace, On the cause of the annual cycle in the tropical lower stratospheric temperature, *J. Atmos. Sci.*, *51*, 169–174, 1994.

Zerefos, C. S., K. Tourpali, R. Bojkov, D. Balis, B. Rognerund, and I. Isaksen, Solar acticity - total ozone relationships: observations and model studies with heterogeneous chemistry, *J. Geophys. Res.*, *102*, 1561–1569, 1997.

Ziemke, J. R., S. Chandra, R. D. McPeters, and P. A. Newman, Dynamical proxies of column ozone with applications to global trend models, *J. Geophys. Res.*, *102*, 6117–6129, 1997.

Zimov, S. A., E. Schuur, and F. S. III, Permafrost and global warming, *Science*, *312*, 1612–1613, 2006.